NTNU – Trondheim
Norwegian University of
Science and Technology

Electrical Excitation of Water Drops in Oil

Torstein Eidsnes Penne

Master of Science in Physics and Mathematics
Submission date: June 2015
Supervisor: Jon Otto Fossum, IFY

Norwegian University of Science and Technology
Department of Physics

Abstract

The purpose of this master's thesis is studying the behavior of salt water droplets subjected to electrical fields, while falling through different types of oils. Different factors are expected to affect this behavior. These factors come from the water/oil combination, such as interfacial tension, elasticity, temperature and viscosity, or come from parameters of the electrical fields such as amplitude, waveform and frequency. In this thesis a total of five oils have been studied, one reference oil (Marcol 52 with 0.005wt% Span80) and four crude oils where one has an added demulsifier. Each oil is subjected to five different voltage forms each and two different temperatures, for a total of ten different experiments for each oil. At least five drops were tested for each experiment. Two other oils were also tested with fewer different voltage forms. These experiments are being used in a yet to be published paper[1], but are not analyzed here. An estimated 400 droplet experiments are the basis of the discussion in this study. These droplets were all in the size range of 1 mm, and subjected to electric fields with intensities around 1 MV/m, with a typical time scale of 10 ms. The experiments have given results making possible the calculation of the drops' surface tensions, oscillation frequencies, oscillation damping coefficient, phase shifts and how these parameters depend on time and temperature. The results show varying degrees of effect from time and temperature. The deformation of the droplets shows the greatest effect from time and temperature, but depending on the oil, the effect can be stabilizing or destabilizing. Temperature shows some effect on oscillation frequencies and damping coefficients, but no great effects have been seen from time. Phase shifts act as expected for most oils, but show signs of surface rheology effects. From the following results it is evident that the effect on drop behavior from drop aging, and previous electrical excitations can not be ignored.

Sammendrag

Hensikten med denne masteroppgaven er å studere oppførselen til dråper av saltvann under påvirkning av elektriske felt, mens de faller gjennom forskjellige typer olje. Forskjellige faktorer er forventet å påvirke denne oppførselen. Disse faktorene kommer fra vann/olje-kombinasjonen, som overflatespenning, elastisitet, temperatur og viskositet, eller kommer fra parametre fra det elektriske feltet, som amplitude, bølgeform og frekvens. I denne oppgaven har totalt fem oljer blitt studert, en referanseolje (Marcol 52 med 0.005 wt% Span 80) og fire råoljer hvor en har blitt tilsatt emulsjonsbryter. Hver olje har blitt utsatt for fem forskjellige spenningsformer hver og to forskjellige temperaturer, hvilket gir totalt ti eksperimenter for hver olje. Minst fem dråper har blitt testet for hvert eksperiment. To andre oljer ble også testet med færre spenningsformer. Disse eksperimentene skal brukes i en ikke ennå utgitt publikasjon[1], men blir ikke analysert her. Et anslått antall på 400 dråpeeksperimenter er grunnlaget for diskusjonen i denne oppgaven. Disse dråpene var alle i størrelsesområdet 1 mm, og ble utsatt for elektriske felt med intensitet i området 1 MV/m, med en typisk tidsskala på 10 ms. Disse eksperimentene har gitt resultater som gjør det mulig å beregne dråpenes overflatespenning, svingefrekvenser, dempingskoeffisienter, faseforskyvninger og hvordan disse påvirkes av tid og temperatur. Resultatene viser varierende grad av effekt fra tid og temperatur. Deformasjonen av dråpene viser størst effekt fra tid og temperatur, men avhengig av olje, kan denne effekten være stabiliserende eller destabiliserende. Temperatur viser noe effekt på svingefrekvenser og dempingskoeffisienter, men ingen stor effekt har blitt sett fra tid. Faseforskyvning oppfører seg som forventet for de fleste oljer, men viser tegn til effekter fra overflatereologi. Fra de følgende resultatene er det klart at effekten på dråpeoppførsel fra dråpealdring og tidligere elektriske eksitasjoner ikke kan ignoreres.

Preface

This thesis concludes my master's degree in Applied Physics at the Norwegian University of Science and Technology (NTNU) in Trondheim, Norway. The thesis is a conclusion of a summer internship and a year long project in cooperation with SINTEF Energy Research. Experimental work was done in a high voltage laboratory in SINTEF's NTNU Gløshaugen facilities.

I would like to thank SINTEF Energy Research in general for the opportunity to be a part of their project and using their facilities and equipment for my thesis. I would also like to thank Gunnar Berg and Lars Lundgaard for their help and guidance throughout the project. The lab work conducted for this thesis would not have been possible without the help and expertise of Svein Magne Hellesø, without which I would surely still be trying to turn on the camera. Cedric Lesaint helped by measuring permittivities and preparing the demulsifier-added oil and it is much appreciated.

Thank you, to Jon Otto Fossum at the NTNU department of physics for being my supervisor.

I would also like to say thank you to Åsmund Ervik for his helpful comments and for providing experimental work. In addition to him I would like to thank Svend Tollak Munkejord, Svein Magne Hellesø and Bernhard Müller for the opportunity of cooperating on a scientific paper, an experience I greatly appreciate.

Final thanks to Hege Westvold Johansen for keeping me fed and caffeinated during the final stages of this work, and for suffering through a year of my endless ramblings on broken glass needles and image analysis software.

Torstein Eidsnes Penne
June 11, 2015

Contents

1 Introduction

During the initial extraction of crude oil, the natural pressure of the reservoir is used to push oil to the surface through a single extraction well. Over time the reservoir pressure decreases to a level which is not sufficient to force more oil to the surface, and the oil stops flowing. At this point, the reservoir is however far from empty. The amount of oil recovered after this phase, called primary oil extraction, is often in the range of 5-15%[2]. One possible way of increasing the oil recovery rate is to increase the reservoir pressure again to force more oil to the surface. This can be done by drilling injection wells where another liquid is forced down to increase the pressure and force the remaining oil to the extraction well, or wells. For offshore platforms in the North sea, salt water is the natural choice for this liquid, as it is naturally abundant. This phase of oil extraction is called secondary oil extraction, and using water this usually recovers 30% of the reservoir's total amount of oil[2].

Due to the viscosity of salt water being considerably lower than that of most crude oils, the water/oil interface will exhibit viscous fingering[3] where "fingers" of water cut through the oil phase and reach the extraction well before all the oil is extracted. This causes an oil/water mixture to be extracted rather than pure oil. Variations in the porosity of the reservoir will only add to this effect. This mixture needs to be separated before it can be sold or used. The problem is made worse by the fact that the mixture is run through choke valves and pipelines that cause the oil and water to be partly mixed to an oil/water emulsion. This causes tiny droplets of oil in water and water in oil to be created. The gravitational forces acting on these droplets are very small compared to the viscous forces (Galilei number $Ga \ll 1$), and therefore settle slowly. The oil/water mixture is traditionally kept in large separation tanks for quite some time while the oil and water droplets respectively rise or sink to the oil/water interface due to differences in density. Due to impurities in the oil, these droplets may even become stable, and not merge when they reach the interface. Asphaltenes are believed to be a major component behind the effect of emulsion stabilization[4]. In any case, this separation method is very time consuming. As the percentage of water in the mixture increases, the separation time increases and the profitability of the well decreases. Perhaps more than elsewhere, in the oil industry, time is money. Speeding up this process is very much in the interest of oil producers. There are ways to decrease this settling time. One way is to decrease the viscosity by increasing the temperature. This requires large amounts of energy, which is a problem economically.

A water droplet subjected to an electric field will be affected by an electrostatic pressure which will elongate the droplet in the direction of the applied electric field, possibly to the point of disintegration.[5] Two droplets in close proximity will be attracted as dipoles and merge. From Stokes flow it can be shown that the settling speed increases with the square of their radii. Removing the smaller droplets, or merging them to larger ones can improve the settling time of the mixture. This process is already in use and is called electrocoalescence, and the machines utilizing this technique are

called electrocoalescers. Although there is much research and development behind these electrocoalescers, the process is still not fully understood, and electrocoalescers will sometimes be less effective or completely ineffective seemingly with no explanation. There are many factors that affect the behavior of these water drops in oil. Drop diameter, surface tension, water conductivity, as well as the form and strength of applied electric fields are some of these factors.

2 Theory

2.1 Viscosity

The viscosity of a fluid is a measure of its resistance to deformation by shear stress. Dynamic viscosity is measured in kg/ms and is denoted by the greek letter μ. Viscosity comes from the collisions of particles in a fluid that have different velocities. The force acting on an area A of e.g. a pipe wall, or a falling drop's surface from viscous forces is

$$F = \mu A \frac{u}{y}, \tag{1}$$

where $\frac{u}{y}$ is called the rate of shear deformation or shear velocity, and is the derivative of the fluid speed in the direction perpendicular to the surface. Isaac Newton expressed this as a differential equation using the shear stress, $\tau = F/A$, and the local shear velocity

$$\tau = \mu \frac{\partial u}{\partial y}. \tag{2}$$

Kinematic viscosity is defined as the ratio between dynamic viscosity and mass density ρ

$$\nu = \frac{\mu}{\rho}. \tag{3}$$

Using the flow speed U, and the system's natural length scale L, another useful relation is the dimensionless Reynold's number

$$Re = \frac{\rho U L}{\mu} = \frac{U L}{\nu}, \tag{4}$$

which is the ratio of a flow's inertial forces to viscous forces, and indicates whether a flow can be considered laminar or turbulent. At low Reynolds numbers, where viscous forces are dominant, the motion of the fluid is smooth and constant. This is called laminar flow. When inertial forces dominate the flow, vortices and other flow instabilities appear. This is called turbulent flow.

2.2 Bulk viscosity

When compressed or expanded, a compressible fluid can exhibit an internal friction that will resist this motion. The force is related to the rate of

compression or expansion and is called the bulk viscosity. The bulk viscosity is only important in cases where there is a rapid expansion or compression, and is the explanation for the energy loss in sound waves.

2.3 Stokes' flow and Stokes' law

Stokes' flow is flow where the viscous forces are much larger than the inertial forces, making $Re \ll 1$. The dimensionless Navier-Stokes's equation for a velocity field $\mathbf{u}$ is

$$\mathrm{Re}\frac{\mathrm{D}\mathbf{u}}{\mathrm{D}t} = -\nabla p + \nabla^2\mathbf{u}. \tag{5}$$

Due to $\mathrm{Re} \ll 1$, inertia (left hand side) is neglected, and the Stokes flow assumption is reached,

$$\nabla p \approx \mu\nabla^2\mathbf{u}. \tag{6}$$

This is combined with the incompressible continuity relation,

$$\nabla \cdot \mathbf{u} = 0. \tag{7}$$

The total drag force on a sphere of radius r moving through a liquid at a speed U is found by integrating pressure and shear around its surface,[6, p. 165-170]

$$F_d = 6\pi\mu r U. \tag{8}$$

For a sphere falling or rising due to differences in mass densities of sphere and surrounding fluid, respectively ρ_s and ρ_f, subjected to a gravitational acceleration g the buoyancy will be

$$F_g = \frac{4}{3}\pi(\rho_s - \rho_f)gr^3. \tag{9}$$

A sphere obtaining terminal velocity will do this when these forces are equal $F_d = F_g$, which gives the terminal velocity

$$U = \frac{2}{9}\frac{(\rho_s - \rho_f)}{\mu}gr^2. \tag{10}$$

The following proportionalities concerning drop volume V and settling speed U

$$\begin{aligned} V &\propto r^3 \\ U &\propto r^2 \end{aligned}$$

give the result

$$U \propto V^{2/3} \tag{11}$$

This shows the motivation for increasing the drop diameter for separation as merging two identical drops will increase their settling speed by a factor of $2^{2/3} = 1.59$.

2.4 Surface tension

Surface tension is the contractive tendency of the surface of a liquid that allows it to resist expansion by an external force. In terms of energy it is defined as the energy needed to expand a surface a unit area ($\mathrm{J/m^2}$). The units (N/m) are equivalent, and are commonly used. Surface tension is usually written as γ. It is caused by the attractive force of the equal molecules of a liquid, cohesion, being greater than their attractive force to different molecules in the bordering medium, adhesion. This force will try to pull the surface molecules into the liquid, and will for a free flowing fluid drop make it spherical. Due to the forces pulling in from all sides, the internal pressure will be greater than that of the surrounding medium. The pressure difference can be expressed by Laplace's law

$$\Delta p = \gamma \left(\frac{1}{R_x} + \frac{1}{R_y} \right), \tag{12}$$

where R_x and R_y are the radii of curvature. At any given point these are the radii of circles with the same curvature as the surface at that point. x and y indicate two perpendicular directions on the surface the curvature is calculated for. For a sphere these are of course equal to the sphere's own radius R_0, and the Laplace pressure simplifies to

$$\Delta p = \frac{2\gamma}{R_0}. \tag{13}$$

2.5 Diffusion

Diffusion is the spontaneous mixing of the particles of two or more substances as a result of random thermal motion. The diffusion flux J, is the amount of substance that will flow through a small area in a small time interval. This is proportional to the diffusion coefficient D and the gradient of substance concentration ϕ. This is described in Fick's law:

$$J = -D\nabla\phi. \tag{14}$$

The diffusion constant in liquids is given by the Einstein–Smoluchowski relation:

$$D = c_m k_B T, \tag{15}$$

where c_m is the mobility of the dissolved substance, i.e. the ratio between its terminal drift velocity and an applied force, k_B is Boltzmann's constant and T is the absolute temperature. In the limit of low Reynold's number the mobility c_m can be replaced with the inverse of the drag, which is given by Eq. (8). The Stokes radius of a substance is the radius of a hard sphere that diffuses at the same rate as that substance. Replacing the mobility with the inverse Stokes drag from Eq. (8), with r_s as the diffusing substance's Stokes radius, the diffusion constant is given as:

$$D = \frac{k_B T}{6\pi\mu r_s}. \tag{16}$$

From these equations it is clear that the diffusion effect is larger at higher temperatures. Assuming lower viscosity at higher temperature increases this effect.

2.6 Damped harmonic oscillator

An ideal mass-spring-damper system with mass m, spring constant k, and viscous damping constant c follows the differential equation

$$m\ddot{x} + c\dot{x} + kx = 0. \tag{17}$$

Assuming a solution of the form

$$x = e^{-\sigma t}, \tag{18}$$

and inserting Eq. (18) into Eq. (17), we get

$$m\sigma^2 - c\sigma + k = 0. \tag{19}$$

The roots of this equation are on the form

$$\sigma = \frac{c \pm \sqrt{c^2 - 4mk}}{2m} \tag{20}$$

Different value combinations of m, c and k give different results:

$$\begin{aligned} c^2 > 4mk &\Rightarrow \sigma = \frac{c}{2m} \pm \frac{\sqrt{c^2 - 4mk}}{2m} \\ c^2 = 4mk &\Rightarrow \sigma = \frac{c}{2m} \\ c^2 < 4mk &\Rightarrow \sigma = \frac{c}{2m} \pm i\frac{\sqrt{4mk - c^2}}{2m} \end{aligned}$$

These three cases are known as over-, critical and underdamping respectively. Defining the damping coefficient $\lambda = \mathrm{Re}(\sigma)$ and eigenfrequency $\omega_0 = \mathrm{Im}(\sigma)$, and ignoring the overdamped case for now, these give two different solutions to Eq. (17):

$$x_1(t) = (C_1 + C_2 t)e^{-\lambda t} \tag{21}$$

$$x_2(t) = C_3 e^{-\lambda t}\cos(\omega_0(t + \phi)) = C_3 e^{-\lambda t}\cos(2\pi f_0(t + \phi)) \tag{22}$$

for three arbitrary constants C_1, C_2 and C_3. Any further discussions of damping coefficient or frequency concern λ and f_0 as they are defined here. For the sake of brevity, it is stated without proof that for an oscillation driven by a force with frequency f_d:

$$F = F_0 \sin(2\pi f_d t) \tag{23}$$

the phase shift in time for the solution for underdamped oscillations is:

$$\phi = \frac{1}{2\pi f_0}\arctan\left(\frac{f_d c}{m(f_d^2 - f_0^2)}\right) \tag{24}$$

2.7 Taylor model

Laplace's law Eq. (12) gives the pressure difference, Δp, between two immiscible fluids such as oil and water. The force of the drop's surface tension will try to keep the drop spherical while an electric field will elongate it in the direction of the field. G.I. Taylor[7] developed a model for describing the deformation of a drop. The Taylor model assumes an electrically neutral drop subjected only to the forces arising from surface tension and the electric field. The drop is assumed to be perfectly conductive, and the surrounding medium is assumed to be a dielectric. The surface tension γ is assumed constant. The following derivation is based on Taylor's paper. It is assumed

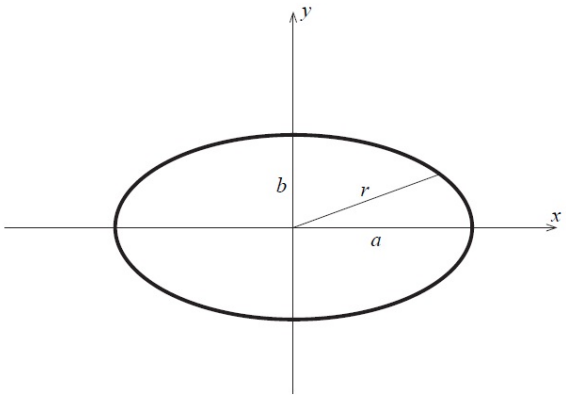

Figure 1: A 2-dimensional cross section of a prolate spheroid. a,b are the radii of the prolate spheroid. The radius c perpendicular to the xy-plane is equal to b.

that the combination of forces will elongate the drop to the form of a prolate spheroid, which can be described as the result of stretching just one radius of a sphere, $r_x > r_y = r_z$, or in this case $a > b = c$. Because of the rotational symmetry about the x-axis, only the xy-plane will be considered, $z = 0$. The radii of curvature of an ellipse are defined as:

$$r_1 = a^2 b^2 \left(\frac{x^2}{a^4} + \frac{y^2}{b^4} \right)^{\frac{3}{2}}, \tag{25}$$

$$r_2 = b^2 \left(\frac{x^2}{a^4} + \frac{y^2}{b^4} \right)^{\frac{1}{2}}. \tag{26}$$

Calculating the radii of curvature for $(x, y) = (a, 0)$:

$$r_{1a} = a^2 b^2 \left(\frac{1}{a^2} \right)^{\frac{3}{2}} = \frac{b^2}{a} \tag{27}$$

$$r_{2a} = b^2 \left(\frac{1}{a^2} \right)^{\frac{1}{2}} = \frac{b^2}{a}, \tag{28}$$

and for $(x, y) = (0, b)$:

$$r_{1b} = a^2 b^2 \left(\frac{1}{b^2}\right)^{\frac{3}{2}} = \frac{a^2}{b} \tag{29}$$

$$r_{2b} = b^2 \left(\frac{1}{b^2}\right)^{\frac{1}{2}} = b. \tag{30}$$

The eccentricity e_{cc} of the spheroid is defined as:

$$e_{cc}^2 = 1 - \frac{b^2}{a^2}. \tag{31}$$

The pressure difference is the same over the drop's surface, and is the sum of the interfacial tension pressure difference from Laplace's law and the electrostatic pressure $\frac{1}{2}\varepsilon E^2$. It is worth noting that the electrostatic pressure is proportional to the square of the field strength, making the sign of the electric field irrelevant. The difference lies in which side of the drop is positive or negative, but the deformation remains the same. The electric field strength at the surface is:

$$E(x) = \frac{E_0 x}{b\sqrt{\left(1 - \frac{x^2 e_{cc}^2}{a^2}\right) I_2}}, \tag{32}$$

where E_0 is the applied electric field strength, and

$$I_2 = \frac{1}{2e_{cc}^3} \ln\left(\frac{1 + e_{cc}}{1 - e_{cc}}\right) - \frac{1}{e_{cc}^2}. \tag{33}$$

The Laplace pressures at $(a, 0)$ and $(0, b)$ are, respectively.

$$\Delta P_a = \gamma\left(\frac{1}{r_{1a}} + \frac{1}{r_{2a}}\right) - \frac{1}{2}\varepsilon E_a^2 = 2\gamma\frac{a}{b^2} - \frac{1}{2}\varepsilon E_0^2 \left(\frac{a^2/b^2}{I_2}\right)^2 \tag{34}$$

and

$$\Delta P_b = \gamma\left(\frac{1}{r_{1b}} + \frac{1}{r_{2b}}\right) - \frac{1}{2}\varepsilon E_b^2 = 2\gamma\left(\frac{b}{a^2} + \frac{1}{b}\right). \tag{35}$$

Requiring that

$$\Delta P_a = \Delta P_b, \tag{36}$$

implies that

$$2\gamma\frac{a}{b^2} - \frac{1}{2}\varepsilon E_0^2 \left(\frac{a^2/b^2}{I_2}\right)^2 = 2\gamma\left(\frac{b}{a^2} + \frac{1}{b}\right), \tag{37}$$

$$\frac{\varepsilon}{\gamma} E_0^2 = 2\frac{1}{a}\left(\frac{b}{a}\right)^2 \left(2 - \frac{b}{a} - \left(\frac{b}{a}\right)^3\right) I_2^2. \tag{38}$$

To get an expression using the drop's aspect ratio, $\frac{a}{b}$, or AR, and not the actual lengths, conservation of volume can be used. The volume and surface of a prolate spheroid are

$$V = \frac{4}{3}\pi a b^2, \tag{39}$$

and

$$S = 2\pi b^2, \left(1 + \frac{a}{be_{cc}} \arcsin(e_{cc})\right) \tag{40}$$

and in the case of a sphere where $a = b = r_0$ the volume is

$$V = \frac{4}{3}\pi r_0^3. \tag{41}$$

Conservation of volume gives

$$\frac{4}{3}\pi r_0^3 = \frac{4}{3}\pi a b^2, \tag{42}$$

$$\frac{1}{a} = \frac{1}{r_0}\left(\frac{b}{a}\right)^{\frac{2}{3}}. \tag{43}$$

Putting this into Eq. (38) gives

$$\frac{\varepsilon}{\gamma}E_0^2 = 2\frac{1}{r_0}\left(\frac{b}{a}\right)^{\frac{2}{3}}\left(\frac{b}{a}\right)^2\left(2 - \frac{b}{a} - \left(\frac{b}{a}\right)^3\right)I_2^2, \tag{44}$$

$$\frac{\varepsilon}{\gamma}E_0^2 = 2\frac{1}{r_0}\left(\frac{b}{a}\right)^{\frac{8}{3}}\left(2 - \frac{b}{a} - \left(\frac{b}{a}\right)^3\right)I_2^2, \tag{45}$$

$$\sqrt{\frac{2r_0\varepsilon}{\gamma}}E_0 = 2\left(\frac{b}{a}\right)^{\frac{4}{3}}\left(2 - \frac{b}{a} - \left(\frac{b}{a}\right)^3\right)^{\frac{1}{2}}I_2. \tag{46}$$

Substituting twice the radius $2r_0$ with the initial drop diameter d_0 and the permittivity of the continuous phase with its relative permittivity, ε_r, and the vacuum permittivity, ε_0, this can be written as:

$$\zeta = E_0\sqrt{\frac{d_0\varepsilon_0\varepsilon_r}{\gamma}} = 2\left(\frac{a}{b}\right)^{-\frac{4}{3}}\left(2 - \left(\frac{a}{b}\right)^{-1} - \left(\frac{a}{b}\right)^{-3}\right)^{\frac{1}{2}}I_2, \tag{47}$$

Where ζ is a dimensionless variable. This equation gives an implicit equation that gives $\frac{a}{b}$ for a value of ζ. It is worth noting that the theoretical model has a turning point at around $E_0 = 0.648\sqrt{\frac{\gamma}{d_0\varepsilon_0\varepsilon_r}}$. This is the maximal field strength before drop break up. The model also predicts two possible elongations for each field strength value. In this study, only the lower part of the graph in Figure 2 is observed.

2.8 Improvement of the Taylor model

The Taylor model assumes the drop to be a perfect conductor with an infinite electric permittivity, which would be an appropriate approximation if the conductivity of the drop is substantially higher than the surrounding medium. For a real system the drop will have a finite permittivity, and this will affect the deformation.[8] For a dielectric drop there will be an internal electric

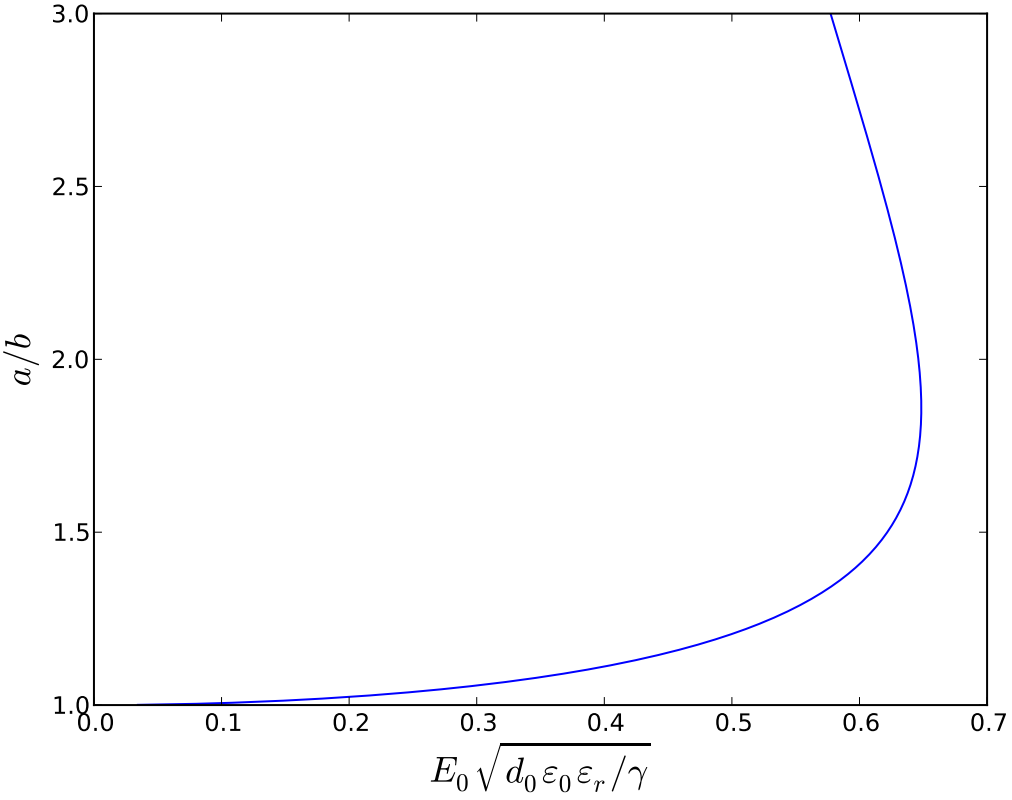

Figure 2: The theoretical aspect ratio of a water drop as a function of electric field, drop size, and sample parameters.

field. By solving Laplace's equation for the prolate spheroids geometry the internal field can be expressed as:

$$E_i = \frac{E_0}{1 - \left(1 - \frac{\varepsilon_d}{\varepsilon_r}\right) I_2 (1 - e_{cc}^2)} \tag{48}$$

where ε_d is the drop's relative electric permittivity. The expressions for the electrostatic pressures at points a and b are given as [8]:

$$P_a = \frac{1}{2}\varepsilon_0 \frac{\varepsilon_d}{\varepsilon_r}(\varepsilon_r - \varepsilon_d) E_i^2 = \frac{1}{2}\varepsilon_0 \frac{\varepsilon_d}{\varepsilon_r}(\varepsilon_r - \varepsilon_d) \left[\frac{\varepsilon_r E_0}{\varepsilon_r - (\varepsilon_r - \varepsilon_d)(1 - e_{cc}^2) I_2}\right]^2 \tag{49}$$

$$P_b = \frac{1}{2}\varepsilon_0 (\varepsilon_r - \varepsilon_d) E_i^2 = \frac{1}{2}\varepsilon_0 (\varepsilon_r - \varepsilon_d) \left[\frac{\varepsilon_r E_0}{\varepsilon_r - (\varepsilon_r - \varepsilon_d)(1 - e_{cc}^2) I_2}\right]^2 \tag{50}$$

By using Eq. (34) and Eq. (35) with these new field strengths:

$$\Delta P_a = 2\gamma \frac{a}{b^2} + \frac{1}{2}\varepsilon_0 \frac{\varepsilon_d}{\varepsilon_r}(\varepsilon_r - \varepsilon_d) \left[\frac{\varepsilon_r E_0}{\varepsilon_r - (\varepsilon_r - \varepsilon_d)(1 - e_{cc}^2) I_2}\right]^2 \tag{51}$$

$$\Delta P_b = \gamma \left(\frac{b}{a^2} + \frac{1}{b}\right) + \frac{1}{2}\varepsilon_0 (\varepsilon_r - \varepsilon_d) \left[\frac{\varepsilon_r E_0}{\varepsilon_r - (\varepsilon_r - \varepsilon_d)(1 - e_{cc}^2) I_2}\right]^2 \tag{52}$$

and the requirement Eq. (36), the result is

$$\gamma\left(\frac{a}{b^2}-\frac{1}{b}-\frac{b}{a^2}\right)=\left(1-\frac{\varepsilon_d}{\varepsilon_r}\right)\frac{1}{2}\varepsilon_0\varepsilon_r(\varepsilon_r-\varepsilon_d)\left[\frac{E_0}{\varepsilon_r-(\varepsilon_r-\varepsilon_d)(1-e_{cc}^2)I_2}\right]^2 \tag{53}$$

$$\frac{\varepsilon_0\varepsilon_r}{\gamma}E_0^2=2\frac{1}{a}\left(\frac{a}{b}\right)^2\left(2-\frac{b}{a}-\left(\frac{b}{a}\right)^3\right)\left(\frac{1}{1-\frac{\varepsilon_d}{\varepsilon_r}}-\frac{b^2}{a^2}I_2\right)^2 \tag{54}$$

substituting a as in Eq. (43), the result is

$$\frac{r_0\varepsilon_0\varepsilon_r}{\gamma}E_0^2=2\left(\frac{a}{b}\right)^{\frac{4}{3}}\left(2-\frac{b}{a}-\left(\frac{b}{a}\right)^3\right)\left(\frac{1}{1-\frac{\varepsilon_d}{\varepsilon_r}}-\frac{b^2}{a^2}I_2\right)^2 \tag{55}$$

which can be rewritten as

$$E_0\sqrt{\frac{d_0\varepsilon_0\varepsilon_r}{\gamma}}=2\left(\frac{a}{b}\right)^{\frac{2}{3}}\left(2-\left(\frac{a}{b}\right)^{-1}-\left(\frac{a}{b}\right)^{-3}\right)^{\frac{1}{2}}\left|\frac{1}{1-\frac{\varepsilon_d}{\varepsilon_r}}-\left(\frac{a}{b}\right)^{-2}I_2\right| \tag{56}$$

This is the form used in any calculation of theoretical aspect ratio in this thesis. This simplifies to Eq. (47) in the limit $\frac{\varepsilon_d}{\varepsilon_r}\to\infty$. It is worth noting that below a certain permittivity ratio, there is no critical field strength. The droplet's aspect ratio will increase indefinitely with an increasing field strength.[8] The theoretical predictions of the model can be seen in Figure 3.

3 Previous research

There has been extensive research done on the field of electric field drop elongation and electrocoalescence. In 1964 two important works were published. These were by Sir Geoffrey Ingram Taylor [7], and by C.G. Garton and Z. Krasucki [8], both on the theoretical deformation of water droplets by application of electric fields. Although these theoretical models are over 50 years old, they still serve as the fundamental model for deformation used in this thesis. In recent years experimental and computational studies have been conducted on the deformation[9] and the coalescence[10] of droplets. Several studies have been performed on the effect of different voltage wave forms. These studies have shown the effectiveness of different forms for augmenting coalescence rates. This has been shown for DC fields[11], pulsed DC fields [12] and AC fields [13]. Studies have also shown that the shape of the applied voltage can affect the maximum field strength endured before drop breakup [14]. The prospect of using electric deformation of water droplets to study the surface tension has also been discussed previously [15].

4 Equipment and samples

4.1 Oil and water samples

The first oil used was Marcol 52 with added surfactant Span 80. Marcol 52 is an oil produced by ExxonMobil, and is a purified mixture of liquid saturated

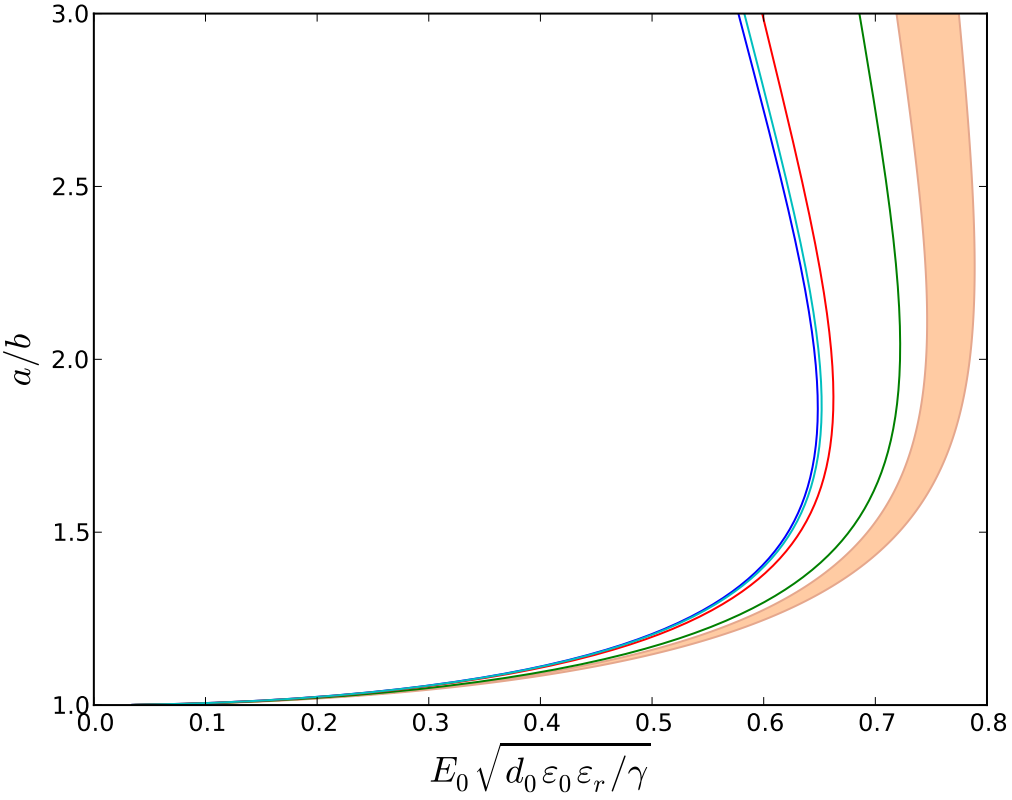

Figure 3: Comparison between the simple Taylor model, and improved model with different permittivity ratios. From left to right: Simple Taylor model, $\frac{\varepsilon_d}{\varepsilon_r}$ =1000, 250, 50. The theoretical curves for the oils tested, are within the shaded region.

hydrocarbons. It is a transparent and colourless oil that is both odourless and tasteless. The oil is produced through several refining stages of petroleum. This includes a final purification stage called catalytic hydrogenation. The density and dynamic viscosity of Marcol 52 at 20 °C are 825-834 kg/m^3 and 12 mPa s. Although the oil used was especially pure, some impurities were expected which could give unexpected or scattered results. To gain more control over the properties of the Marcol 52 some surfactant Span 80 was added. Span 80, also known as sorbitane monooleate, is an amber liquid with a viscosity of about 1 Pa s which acts as a nonionic surfactant on the interface between oil and water. The interfacial tension between water and oil decreases as a result of increased concentration of Span 80. This decrease is also dependent on the time the drop has been suspended in the oil before being dropped. This is due to more of the free flowing Span 80 molecules settling on the surface over time. This change in surface tension is biggest immediately after drop creation and slows down over time. This makes the difference between no aging and 10 s larger and more varied than between e.g. 60 s and 70 s. These effects become more pronounced with greater concentrations of Span 80.

In the experiments three different concentrations of Span 80 were used.

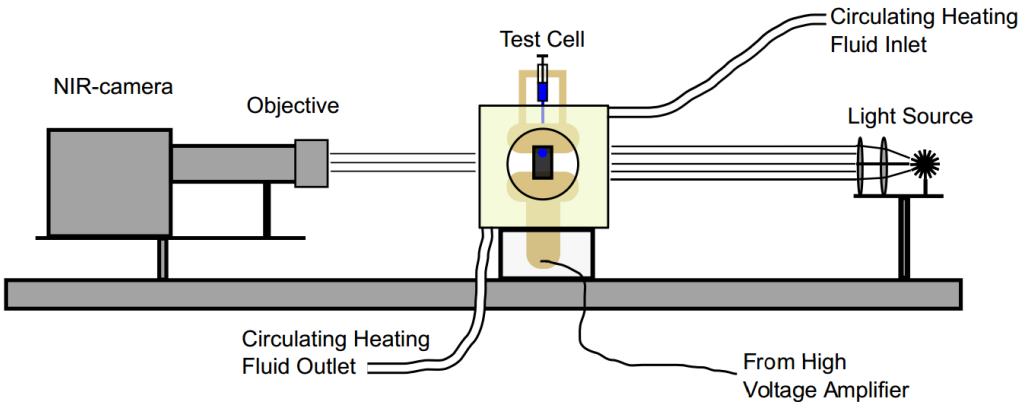

Figure 4: Experimental setup

These were 0.001wt%, 0.005wt% and 0.016wt%. 0.001wt% and 0.016wt% were only used in experiments which are discussed elsewhere[1].Unless otherwise specified the Marcol 52 used is with 0.005wt% of Span 80. Due to the high viscosity of Span 80 it was found to be impossible to get exact doses using a pipette. To precisely make concentrations of Span 80 it was necessary to first produce an oil sample using Marcol 52 and a drop of Span 80. This is referred to as the initial sample. The concentration of this sample depended on the uncontrolled size of the drop of Span 80, but could be precisely calculated by measuring the weight of the Span 80 and of the Marcol 52 used. A Sartorius CP225D weight was used for weighing, and the resulting initial sample obtained a concentration of 0.58wt%. This sample was mixed by a magnetic stirrer for at least an hour. This might be more than is necessary, but as the making of oil samples was done so rarely it was more important to be sure of complete mixing rather than saving time. This sample had a lower viscosity, and precise amounts of it could be measured. By mixing this sample with precisely measured amounts of pure Marcol 52 it was possible to achieve precise concentrations of Span 80.

In addition to Marcol 52 with added Span 80, there were 4 other oils used in the experiments presented in this thesis. Five crude oils were initially provided. These oils were known only as oils A, B, C, D and E. No other information was given, or was needed to conduct the experiments. While conducting experiments it was revealed that oils B and E were not viscous enough at 21.5 °C to gather any results. The water droplets would simply fall through the oils so quickly as to make recording them practically impossible. It was suggested to try these experiments after cooling these oils to around 0 °C. This was never done, as the oils were still far from viscous enough, even after staying in the lab refrigerator at around 4 °C. It was also discovered that the circulation fluid keeping the sample temperatures constant during experiments would be too viscous at these temperatures. Later, it was revealed that oil D, was a “pure” crude oil, without any chemicals added from the time of extraction. This made it interesting to see if the effect of controlled addition of a demulsifier could be studied. A small bottle of oil

D was prepared with 1000ppm of the demulsifier EB-8228 added. The crude oils that ended up being tested were: A, C, D and D with demulsifier, also referred to as oil DE. The relative electrical permittivities of oils A, C and D were eventually provided, and were respectively 2.43, 2.88 and 2.94. The surface tensions were not provided or measured for the crude oils. The value used in the plotting of aspect ratios for comparisons between oils was the surface tension of Marcol 52 with 0.005 wt% Span 80, i.e. 24.5 mN/m.

When changing oils between experiments, the test cuvette, and any parts in contact with the oil was rinsed thoroughly with toluene and left to dry for at least 30 min.

The water used in the experiments was purified water with 3.35-3.36wt% salt (NaCl), with an estimated relative permittivity of $\varepsilon_r = 82$.

4.2 Test cell

The oil samples were contained in a transparent cuvette held in a test cell. This test cell consisted of a watertight cube with round windows on three walls and electrodes through its top and bottom. The last side was fastened to a linear stage with the ability of raising and lowering the test cell. The bottom electrode was the one given the voltage signal being generated in each experiment. The top electrode was hollow, with a hole through the center. Through this, the glass needles used for producing the drops were inserted. The test cell needed to be water tight to contain the fluid used to maintain a constant temperature during the experiments. The top electrode could be removed, as was necessary when the sample cuvette was replaced. The glass needle holder could also be removed. This was necessary if the needle was to be replaced, or it needed to be refilled with water. This glass needle holder contained a screw-in plunger and a small electromagnet as described in the next section. The experimental setup can be seen in Figure 4.

4.3 Glass needles and drop production

For the making of submillimeter water drops, glass needles were used. These were made in the lab from hollow glass tubes with internal and external diameter of respectively 1.5 mm and 2.5 mm. By placing the middle of a tube in a heated metal coil and pulling from each side it was possible to thin the tube and thus produce two glass needles from each tube. To be able to hang the water drops from the tip of the glass needle it was necessary to prevent the water drops from clinging to the side of the needle's tip. The glass needle tips were made hydrophobic by coating them in the siliconizing reagent Sigmacote and left in a heating cabinet. The time and temperature needed to properly apply the coating was not fully investigated. No discernible difference in hydrophobicity was found in drying the needles for 15 minutes or an hour, so any needles produced were subjected to a minimum of 15 minutes drying. Any minimum temperature was not found as the temperatures used by others using the cabinet proved sufficient, and was typically 80 °C. When preparing the needles for use, the tips were scratched by a small glass cutter and broken

by hand to ensure that the needle had the proper hole thickness to allow water to exit the needle tip. The same was done to the unstretched back of the needle to ensure an appropriate needle length.

After filling the glass needle with water, a screw-in plunger could be twisted to force a small amount of water out of the needle tip. If the needle was properly coated with Sigmacote and the outside of the needle was hydrophobic the water would only cling to the broken absolute tip. This water would form a stable drop hanging from the tip of the needle. To release the drop, a small electromagnet surrounding the glass needle was given a short pulse of electricity. This jerked the needle and its metal holder quickly straight up. If the drop was not too small, the drop's inertia ensured it could not keep up with the needle, and was released.

4.4 Parameter control and calibration

Being able to maintain controlled experimental parameters is essential to getting consistent results. The electrode distance affects the electric field generated by the voltage applied. The distance is maintained at 15 mm by placing a piece of teflon between the electrodes. Teflon has been chosen due its relative permittivity being similar to the oil, making its interference with the electric field minimal. For the crude oils it was necessary to insert glass squares inside the cuvette in order for the camera to receive sufficient light. In these cases the glass pieces with a length of 14 mm were used for controlling the electrode distance.

The temperature in each experiment series was held constant by the use of a circulating transformer fluid (MIDEL 7131 synthetic ester oil) surrounding the cuvette holding the oil sample. An Ismatec MCP-Z gear pump circulates the fluid maintaining a steady flow around the cuvette. The circulation fluid is circulated through plastic and metal tubing, where the metal tubing is placed in a Jalabo F25 Refrigerated/Heating Circulator maintaining a stable temperature throughout each experiment series. Due to what is most likely frictional heating and heat dissipation in the circulation tubing, the temperature set on the circulator is not the same as the temperature in the fluid surrounding the sample cuvette. The temperature of the surrounding fluid is measured by a Fluke 54 IIB thermometer, and a set temperature of 18.9 °C corresponds to a sample temperature of 21.5 °C, while a set temperature of 58 °C gives a sample temperature of 50 °C. Due to the sealing of the sample container during experiments it is not possible to measure temperature while the experiments are running. The measurements must be done before or after running a series of experiments.

For accurate measurements of length, a calibration of the length scale was needed. This was achieved by placing a tungsten wire with a diameter of 0.3 mm in the oil cuvette. A photo of this could be used for calibration.

4.5 Generating signal and electric field

The electric field signal was generated by a Stanford Research Systems Model DS340 Function Generator with a maximum amplitude of 10 V. The function generator has several built-in signal generation capabilities such as sine waves and square pulses. It is also possible to create arbitrary signals that can be defined by the user. Of the built-in functions, only sine waves were used. All other signals were generated in MATLAB. Communication between a computer and the function generator was done through an RS-232 serial port using MATLAB. The MATLAB script, henceforth referred to as the signal script, was written specifically for these experiments and handled both the opening of and communication through the RS-232 serial port, but also created a list of numbers in the appropriate text-string format required by function generator. The function generator's arbitrary function generation works by taking a string of numbers from a computer and generating a signal which will jump instantaneously between the values, in the order they are given with a delay between jumps determined by the signal script. This is quite practical for the generation of square pulses as a single square pulse can be defined by just two numbers.

By pressing a trigger button, a signal is sent to a Stanford Research Systems Model DG535 Four channel digital delay/pulse generator. This sends a signal to the camera to start recording. After a delay of 10 ms another signal is sent to the LED to make it flash. The same signal is also sent to trigger the function generator, which sends the voltage signal to a TREK model 20/20B High voltage amplifier amplifying the signal by a factor of 2000. This signal is sent to the bottom electrode for generating the electric field. The electrodes are separated by a minimum of 14 mm which makes the maximum achievable voltage and electric field strength respectively 20 kV and 1.43 MV/m. After the camera has recorded for a complete second, the delay generator cuts the signals to both the camera and the function generator, shutting down their signals. In total this gives four different signals:

Table 1: Signals used in experiments

Signal	From	To	Form
Signal 1	Delay/pulse generator	Camera	Single square pulse
Signal 2	Delay/pulse generator	Function generator and LED	Single square pulse
Signal 3	Function generator	High voltage amplifier	From signal script
Signal 4	High voltage amplifier	Electrode	2000× signal 3

These signals are monitored with a Tektronix TPS2014 Four channel digital storage oscilloscope, where the form of the signals as well as their amplitudes can be viewed after each experiment.

4.6 Camera and film processing

The camera used for filming the drops was a Xenics Cheetah CL camera. This is a near infrared (NIR) high speed camera. The camera has the ability to be

record film with a resolution of 630 × 512 pixels at 1730 frames per second. Unless otherwise stated, this is the framerate used. To increase the contrast between the Marcol 52 and the water, the camera films in NIR, which means the oil is transparent while the water drop is not. This black/white contrast helps getting clear results during analysis of the film. For crude oils that are not transparent in visible light, the NIR range is essential for even being able to see the drop.

As regular room lighting does not contain enough intensity in the spectral range covered by the camera, a light source was needed. For the experiments a Newport Model 66884 housing with a light source including near infrared light was used. To be able to see the relatively weak LED flashing at the beginning of voltage application, two small holes were drilled in the side of the camera's objective. The LED was placed inside with its anode and cathode sticking out of the two holes, making it possible to connect to the pulse generator. The LED was pointed directly at the camera's image sensor.

For recording the film of the experiments, Streams 7 Scientific video recording software was used. This software was connected to the camera so it could start recording at the signal of the trigger from the delay generator. The software also recorded the voltage coming from from the function generator. The electrical signals in the experiments were captured using a National Instruments PCI-6052E DAQ board.

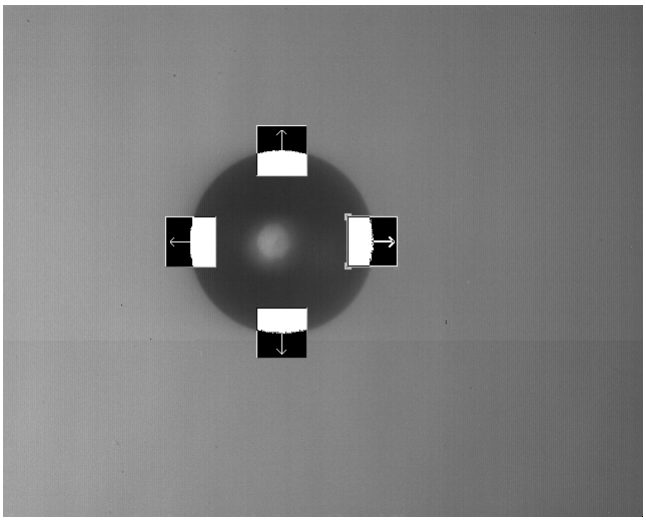

Figure 5: A typical frame from the Spotlight-8 image analysis software. Note the four Area-Of-Interest's with arrows indicating the directions being tracked

The measuring of drop size and deformation was done using Spotlight-8 image analysis software [16]. The first thing to do is calibrating the length scale of the film. This is done by using a picture of a 0.3 mm tungsten wire, and setting the wire's thickness in pixels to the real world size of the wire. This length calibration is then used to determine lengths. The software uses the contrast of the image to be able to track e.g an edge or the center of a shape in the film. For measuring the aspect ratio of the water drops it was

necessary to measure the length of the drop's long and short axes. This is how the values for a and b in Figure 1 are found. Spotlight edge tracing works by first being given an intensity value, in percentage of illumination of a pixel, 0% being a completely dark pixel, and 100% being a maximally illuminated white pixel. Within a selected Area Of Interest(AOI) anything over this value is made white, and anything under this value is made black. This can be inverted, as in Figure 5. The AOI has a selected direction, and from each frame to the next the AOI will center itself on the white pixel furthest in the direction it has been given. The position of the center of each AOI is written to a text file that can be used for further analysis. There are also functions for removing smaller objects in the picture, like dust, since these may change the results. Since the software relies on contrast, it is important that the drops are in focus in the image. This makes it easier to get a sharp clear border and will give smaller fluctuations in the lengths measured. Focusing on the drop is done while it hangs on the tip of the glass needle by moving the camera slightly closer or further away from the drop. This does not always result in the film being in focus as the jerking of the needle can move the drop in the direction of the camera and thus out of focus. This is usually just enough to make the drop edge slightly blurry and never enough to make the film unusable.

Due to Spotlight's way of processing the films, the program is very sensitive to certain things in the films, such as a smaller droplet passing by in the background. Getting results out of films like these, was very difficult and time consuming. Because of this and the overall low speed of Spotlight, the image analysis software was changed half way through the project and replaced with Fiji (Fiji Is Just ImageJ), which is an Open Source image processing package based on the image processing program ImageJ. With this program it was possible to use films that could not be properly analyzed with Spotlight, and also complete the analyses in a much shorter time. The images were divided in two, as with Spotlight, depending on whether the illumination of the pixel was above or below a selected threshold. This could result in many different droplets being found in one image. This program made it possible to only follow the droplets that satisfied certain parameters given by the user. These were the minimum and maximum values of droplet size and circularity of droplets. The circularity, C_{irc}, of a droplet was defined as:

$$C_{irc} = \frac{4\pi area}{perimeter^2}. \tag{57}$$

These requirements made it possible to ignore smaller droplets in the image, as well as shapes that were of a similar size, but not a similar shape. The program would find the longest and shortest axes of the droplet and write this to a text file which could be used in further processing.

4.7 Linear stage and motion control

Although the drops did not fall quickly ($\sim 1\,\mathrm{cm/s}$) the camera's field of view was small, so it was necessary to either lower the camera with the falling

drop, or lift the sample to make the drop stay in the camera's field of view. In this case the sample is lifted. This is done by using a Newport (M-)IMS-V High performance linear stage for vertical use. This was controlled by turning a dial that set the movement speed of the linear stage. The control was done through a Newport Motion controller/driver model XPS.

4.8 Result analysis scripts

The final step in the analysis of the experiment was turning the result text files from Spotlight and Fiji into more comprehensible information and illustrative plots. Quite a big part of the work was writing the scripts needed to transform the Spotlight and Fiji .txt-files from rows of numbers to actual values of E_0, d, $\frac{a}{b}$ etc. needed for the theoretical model in Eq. (56). Due to the different forms of the electric field the different experiments needed different scripts to be able to extract the required information.

The first issue was to make sense of the result files from Spotlight. The files contain row by row of the x and y positions of the centers of each of the four AOIs for each frame of film. Each row also contains some text and information that is not needed, so it was necessary to be able to separate the useful information from the rest. Since the text needing to be overlooked came from the name of the films, e.g. "Movie1_Scene15_1-Multiple Device Stitcher" it was possible to detect and skip them. The method is however vulnerable to different naming conventions, but as long as the names made automatically by Streams were kept, this was not a problem. When the x and y positions of all AOIs were found, the vertical and horizontal axes of the drop could be calculated. Using Fiji, there were more options for the generation of result files. This made it possible to only include the needed information, vastly simplifying the result analysis process. Measuring the initial drop diameter d_0 was done by averaging the vertical and horizontal diameters of the frames from before the electric field signal was initiated. When the two diameters are measured one is divided by the other and the drop's aspect ratio AR from Eq. (56) is determined. Most of the experiments only look at the stable deformation of the drops, meaning $\frac{a}{b}$ of every frame is not needed. For this it was necessary to detect the peaks of the drop's AR. For this objective a MATLAB to python translation of an openly available peak detection script was used [17]. This detected the maximum peaks well. The theoretical model however looks at the stable aspect ratio of the drops, while the peaks detected were the overshoot in aspect ratio expected when subjected to a sudden increase in field strength. The easiest way of finding the stable aspect ratio of the drops is reading them manually off the plots. This is however time consuming, inaccurate and inconsistent. This was solved for the square pulses by averaging the AR of the previous 25 ms, which was the length of a single square pulse. This assumed that the sum of over- and undershoot from the stable aspect ratio was small. This proved not to be accurate, as the values detected quite consistently gave a higher AR than the stable value. Because of this, the script was changed to detect the time position of stable AR as before, but calculating the average AR from only the

last half of the square wave. The electric field could be easily calculated from the maximum field displayed by the oscilloscope, the shape of the signal and the length between the electrodes. With this, all three experimental variables E_0, d_0 and $\frac{a}{b}$ were determined. The remaining γ and ε_r are dependent on the oil and surfactant concentration being used. All values needed for Eq. (56) were then found and it was possible to compare experimental values to those of the theoretical model.

5 Experiments

Following are explanations of experimental procedure, and in what way the experiments differ, and explanations as to which parameters are measured or calculated for each of the different experiments.

Experimental procedure

The differences between experiments are in the form of electric field and/or oil samples. The step by step experimental procedure for each experiment was the same:

(1) By using the linear controller, move the test cell so the needle tip is in the field of view of the camera.

(2) Produce a drop of desired size by using the screw-in plunger and wait one minute for drop aging.

(3) Arm the camera to be ready for filming, and if needed, the computer for recording voltages.

(4) Activate the electromagnet jerking the needle up to release the drop.

(5) Quickly match the drop's falling speed with the linear controller. Trigger the camera and the electric field.

(6) Save the film, and determine the drop deformation using proper software.

5.1 Sine wave voltage

By using a sinusoidal wave signal it is possible to oscillate the drop between a maximum and minimum deformation. Since the deformation of the drops only depend on the magnitude of the electric field, as shown in section 2.7, the drop will oscillate at twice the frequency of the signal. The resonance modes $n \geq 2$ have been calculated theoretically[18]. As the drop surface dynamics are dominated by viscous effects the mode $n = 2$ dominates. The experiments will determine the resonance frequency of the drop. The length of the longest axis is measured, its biggest (a_{max}) and smallest (a_{min}) values and their difference, or length span δ. The $n = 2$ theoretical resonance frequencies of inviscid droplets with density ρ_s suspended fluid with density ρ_f has been previously been found[19]

$$f = \frac{2}{\pi}\sqrt{\frac{3\gamma}{(\rho_s + \rho_f)d_0^3}}. \tag{58}$$

Table 2: Parameters studied for experiments with sine wave voltage

Parameter	Symbol	Unit
Minimum length	a_{min}	[mm]
Maximum length	a_{max}	[mm]
Length span	δ	[mm]

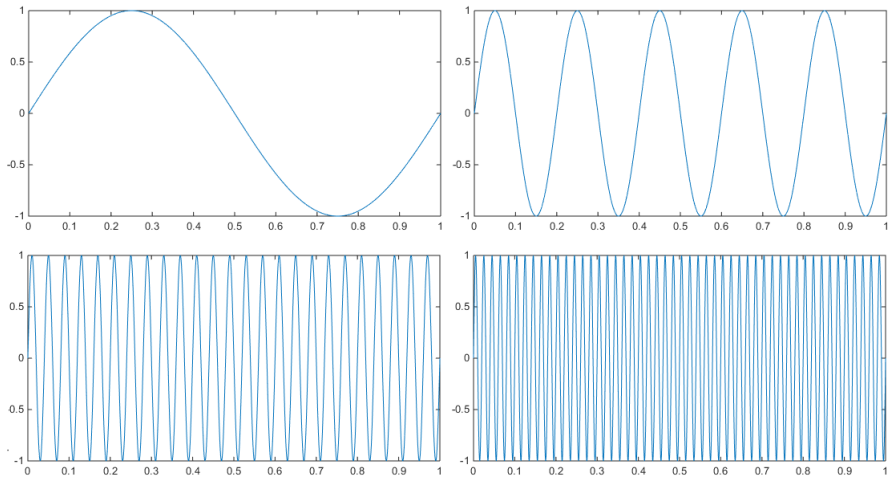

Figure 6: Examples of voltages applied across electrodes for experiments with sinusoidal wave signal

5.2 Square wave voltages with constant amplitude

In this experiment the drop is subjected to a series of bipolar square pulses with constant electric field strength. The drops are deformed repeatedly by the same electric field strength. Repeating the pulse multiple times in rapid succession makes it possible to make several repeated measurements per drop. The drops deformation in response to a square pulse signal is expected to behave like an under damped oscillation. The objective of this experiment is determining the deformation, oscillation frequency and damping coefficient. Multiple consecutive deformations might affect these parameters, so this potential change will be studied.

Table 3: Parameters studied for experiments with square wave voltages with constant amplitude

Parameter	Symbol	Unit
Aspect ratio	$\frac{a}{b}$	[-]
Oscillation frequency	f	Hz
Damping coefficient	λ	s^{-1}

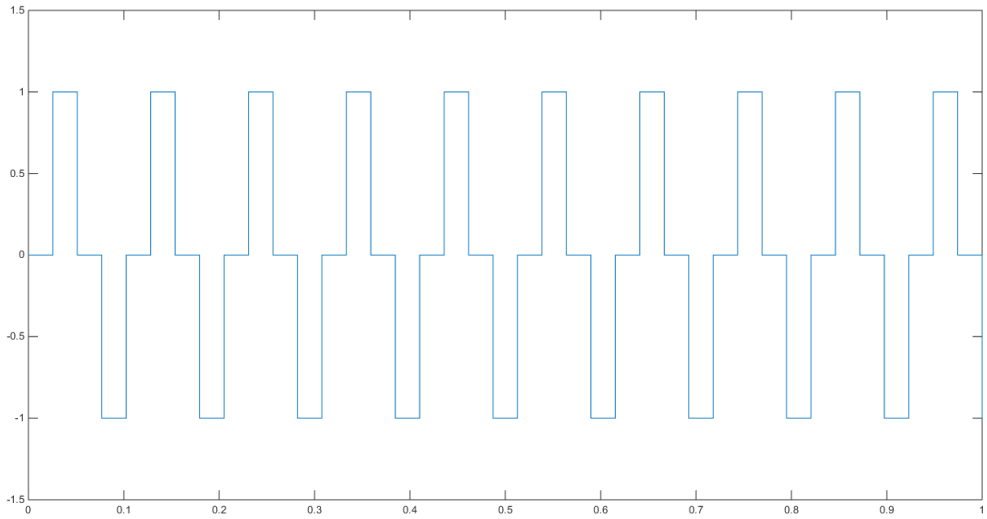

Figure 7: Shape of voltage applied across electrodes for experiments with square wave voltages with constant amplitude

5.3 Square wave voltages with increasing amplitude

This experiment uses square waves of increasing field strength for every second square pulse. The changing amplitude makes it possible to collect data points for the entire spectrum of amplitude and field strength available while keeping drop size exactly constant. The experiments will determine drop AR $\frac{a}{b}$, oscillation frequency f, damping coefficient λ and effective surface tension γ_{eff}. The effect of multiple consecutive deformations might affect these parameters, so any changes in these during an experiment will be studied. By adjusting the surface tension used in calculation ζ and selecting the value that gives the best fit to theory, it is possible to find the effective surface tension of the droplets, and thus use this experiment to test this technique as a way of measuring surface tension.

Table 4: Parameters studied for experiments with square wave voltages with increasing amplitude

Parameter	Symbol	Unit
Aspect ratio	$\frac{a}{b}$	[-]
Oscillation frequency	f	Hz
Damping coefficient	λ	s^{-1}
Effective surface tension	γ_{eff}	mN/m

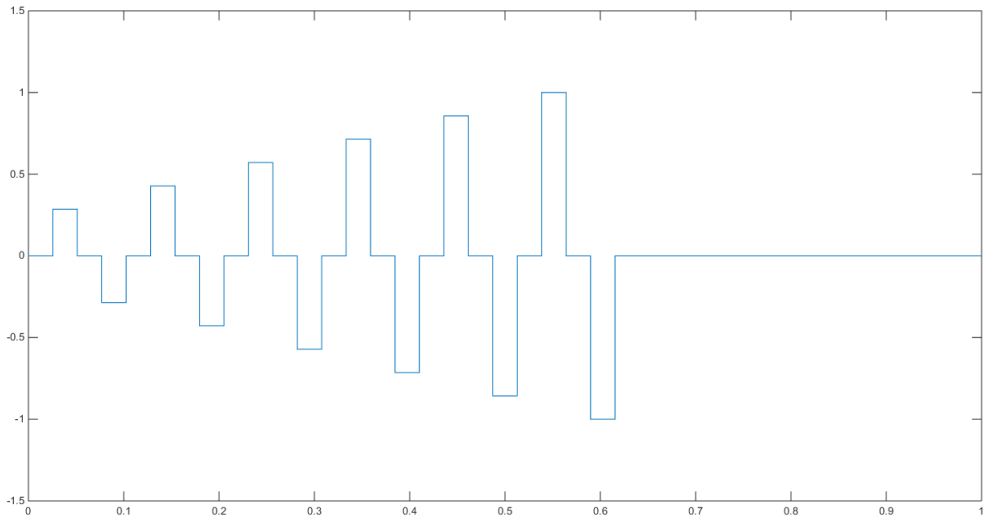

Figure 8: Shape of voltage applied across electrodes for experiments with square wave voltages with increasing amplitude

5.4 Square wave voltages with decreasing amplitude

This experiment is the same as in section 5.3, but with a decreasing field strength for every second square pulse. This experiment will determine drop AR $\frac{a}{b}$, oscillation frequency f, damping coefficient λ and effective surface tension γ_{eff}. The effect of multiple consecutive deformations might affect these parameters, so any changes in these during an experiment will be studied. Effective surface tension will be determined in the same way as the experiment with increasing square wave voltages.

Table 5: Parameters studied for experiments with square wave voltages with decreasing amplitude

Parameter	Symbol	Unit
Aspect ratio	$\frac{a}{b}$	[-]
Oscillations frequency	f	Hz
Damping coefficient	λ	s^{-1}
Effective surface tension	γ_{eff}	mN/m

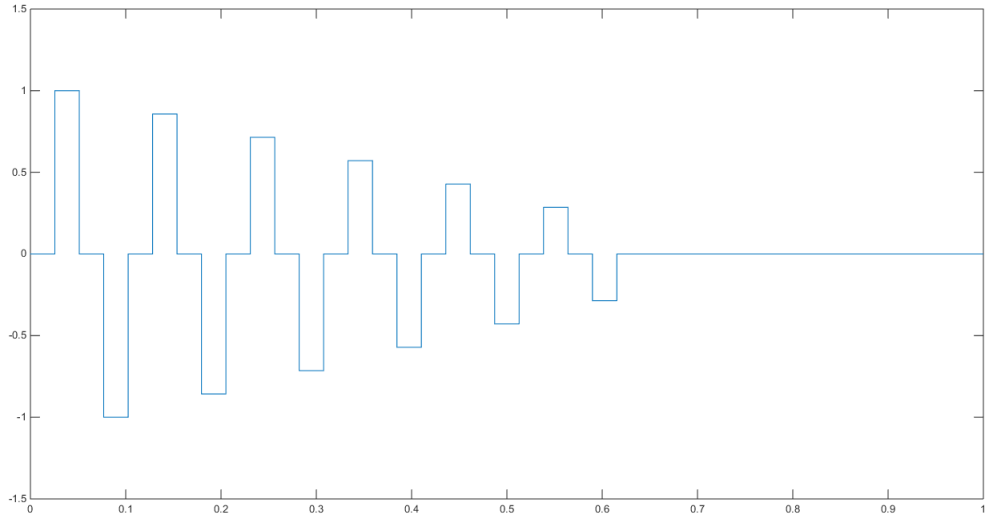

Figure 9: Shape of voltage applied across electrodes for experiments with square wave voltages with decreasing amplitude

5.5 Phase shift

This experiment uses sine waves and may therefore be done simultaneously with the experiment described in section 5.1. The focus of this experiment is finding the phase shift, in milliseconds, between drop deformation and electric field. To reduce the influence of bulk viscosity the signal's frequency should be kept as low as possible. In the following experiments the signal frequency used has been 5 Hz, giving an oscillation frequency of 10 Hz. This was done so it was possible to measure several deformations for each drop. By also recording the voltage supplied it is possible to synchronize this with the film, and determine the time shift between each peak.

Table 6: Parameters studied for experiments with phase shift/loss factor

Parameter	Symbol	Unit
Aspect ratio	$\frac{a}{b}$	[-]
Phase shift	Δt	ms

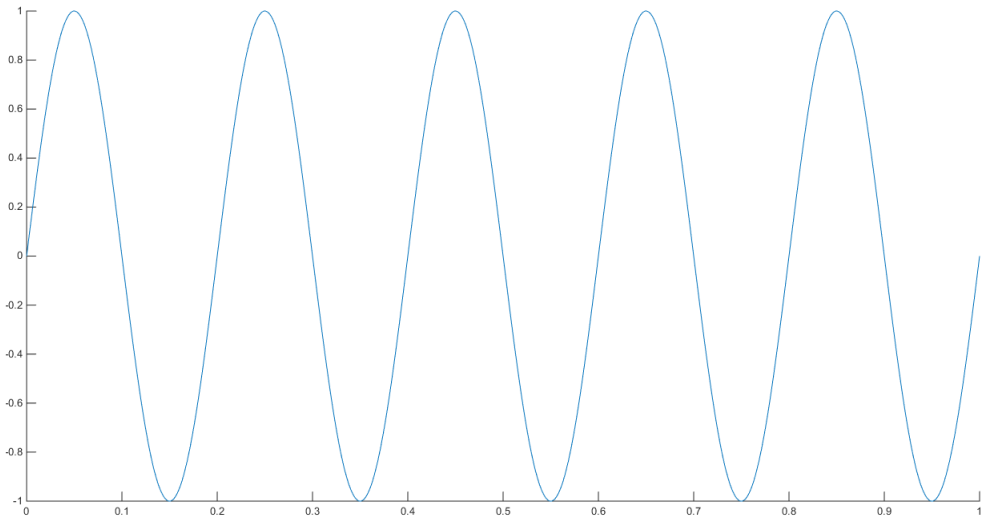

Figure 10: Shape of voltage applied across electrodes for experiments finding phase shift

6 Results and discussion

6.1 Sine wave voltage

For very low frequencies, the oscillation should behave about the same as for stable deformations during square pulse voltages. For higher signal frequencies the field can almost be considered constant, due to the drop's inability to react to the rapid changes in field strength, and the length span will tend to zero. This is observed in all oils tested.

Figure 11 and Figure 12 show the length span of the drops tested plotted against different values of drop oscillation frequency.

Figures 13-20 show the length span of the drops tested, relative to the drops' diameter, plotted against different values of drop oscillation frequency. These also include the standard deviation around the average length span found for each oscillation frequency tested.

Table 7: Approximate values of drop oscillation frequencies giving resonance peaks in Hz

Temp.\oil	Marcol	A	C	D	DE
21.5 °C	150	80	-	60	50
50 °C	240	120	-	80	50

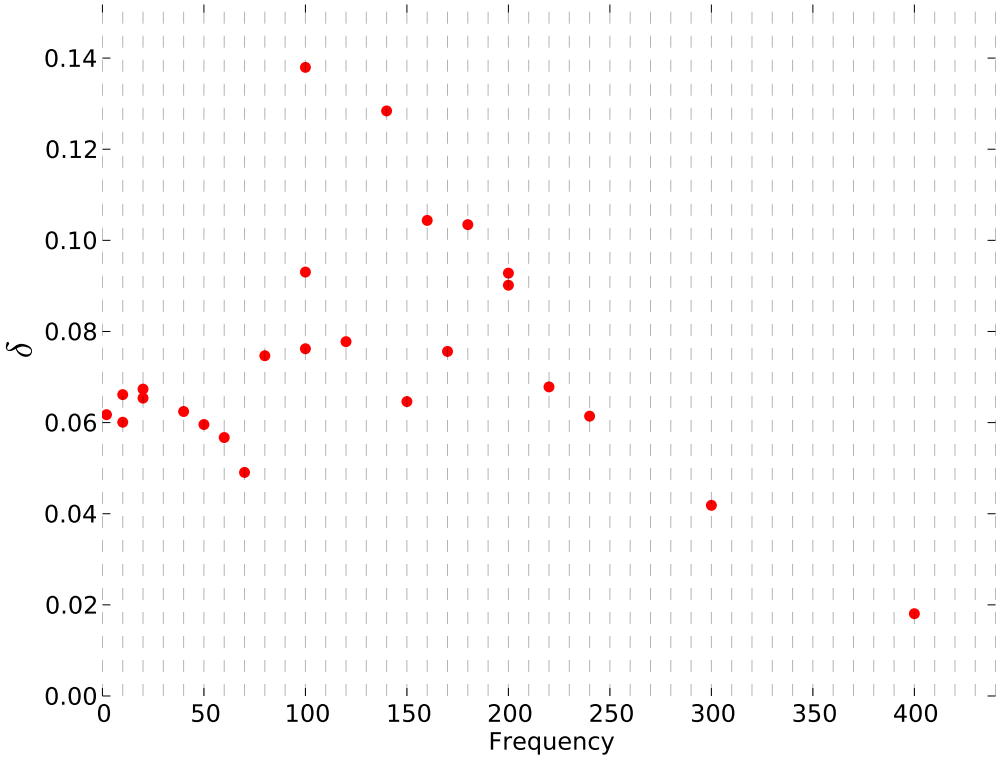

Figure 11: Oil: Marcol, Temperature: 21.5 °C.

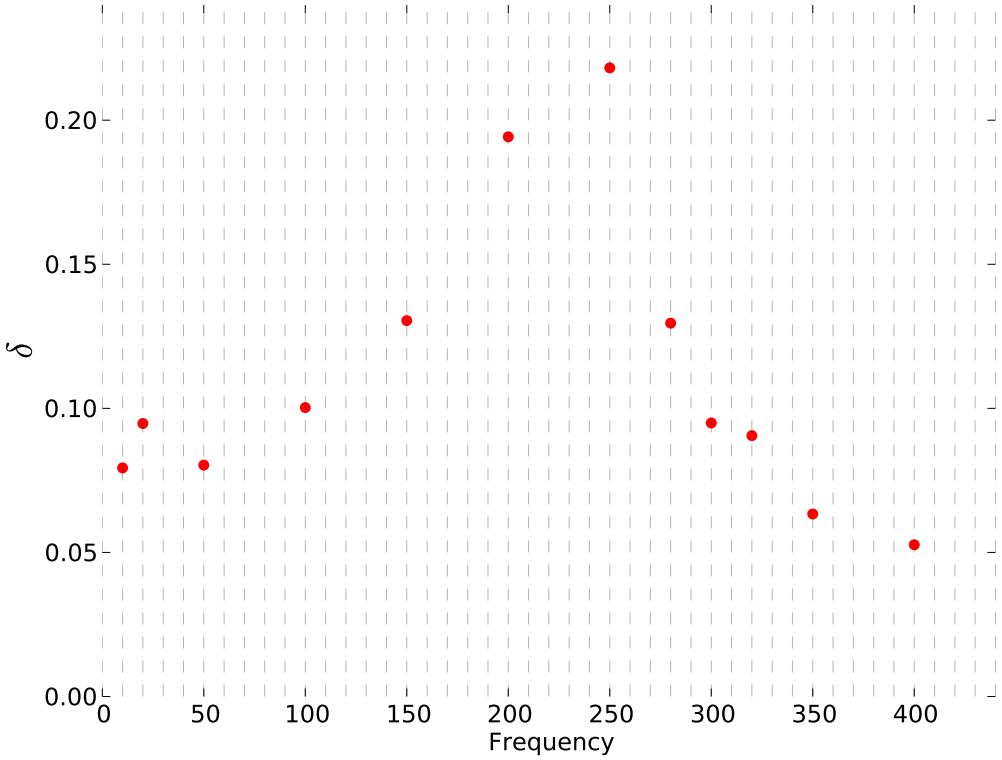

Figure 12: Oil: Marcol, Temperature: 50 °C.

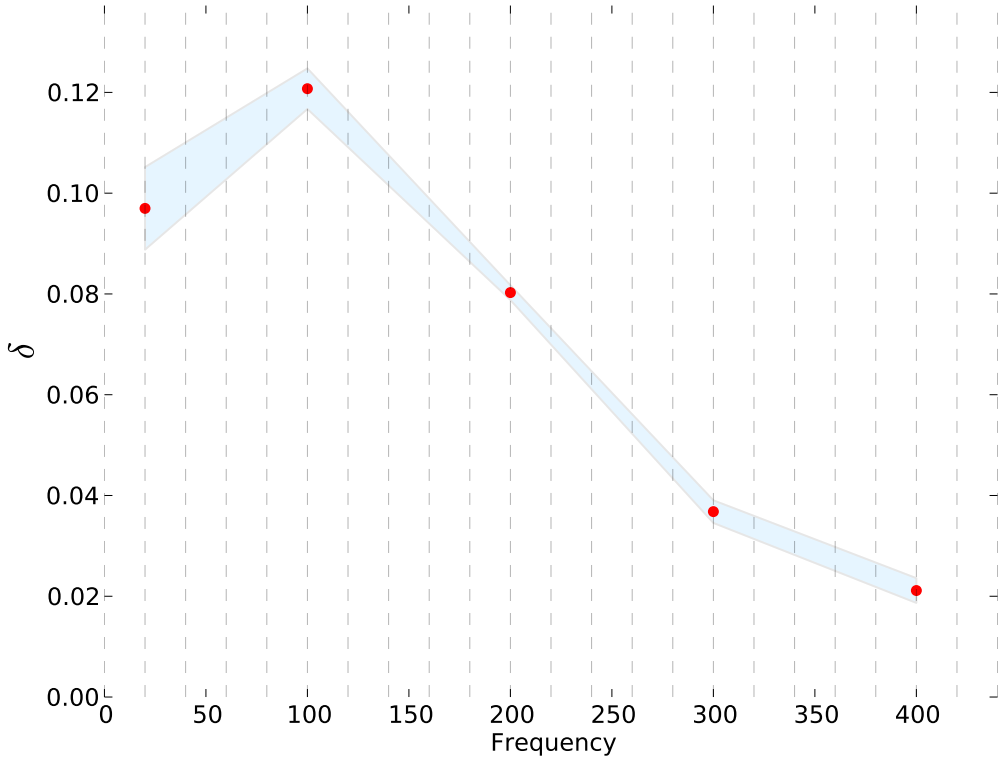

Figure 13: Oil: A, Temperature: 21.5 °C.

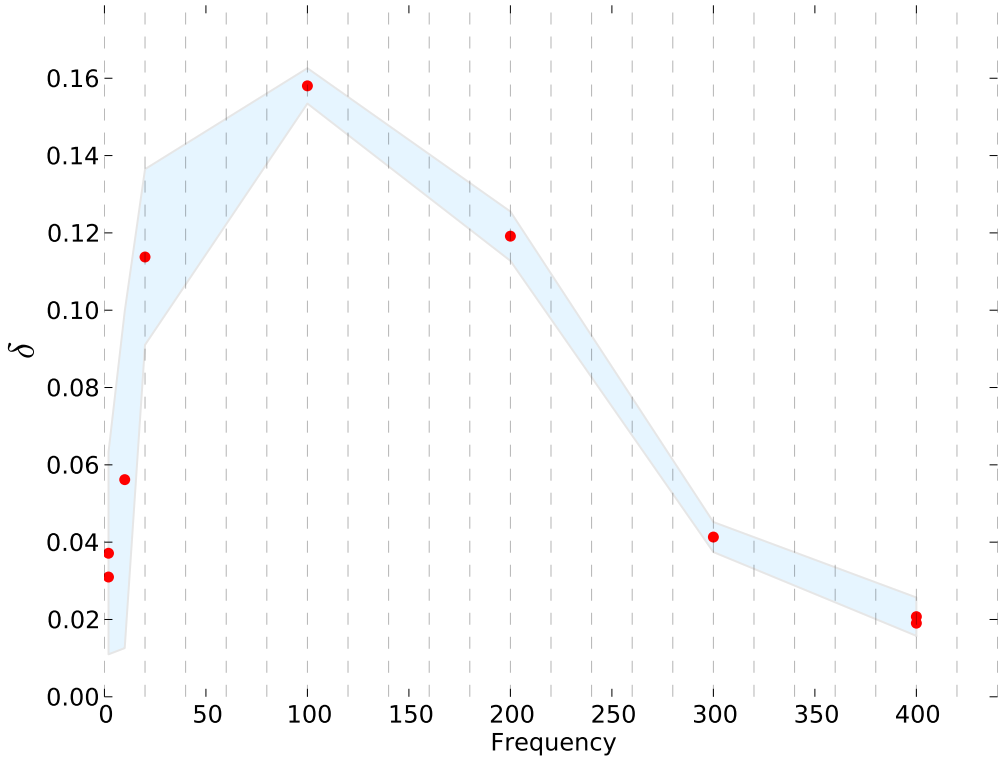

Figure 14: Oil: A, Temperature: 50 °C.

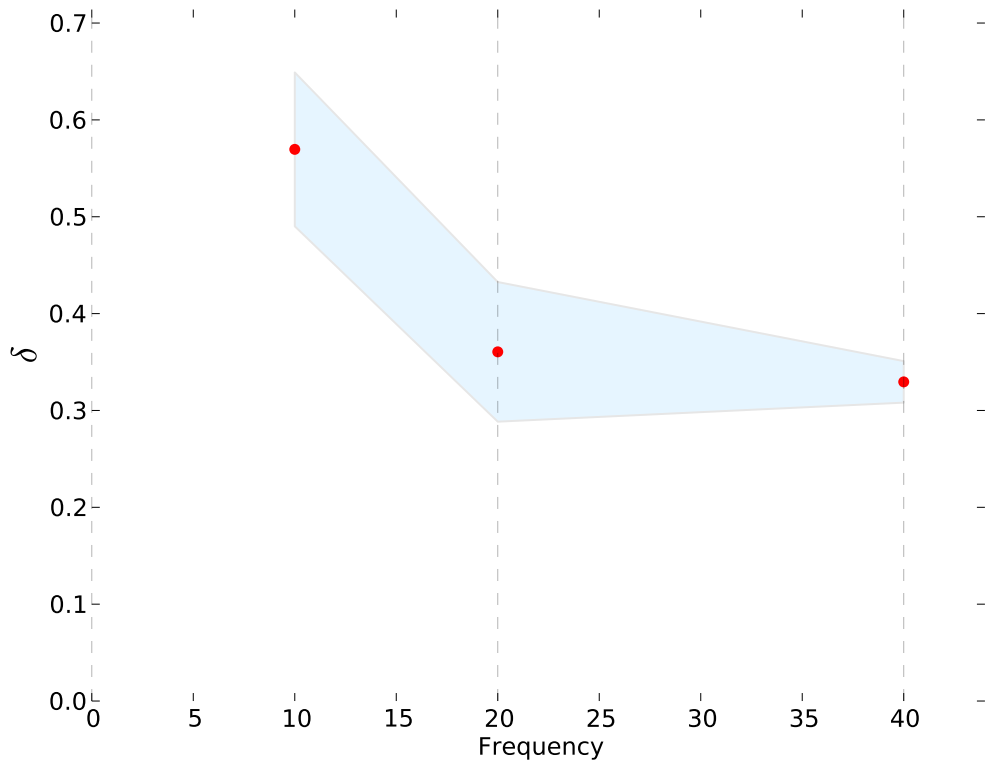

Figure 15: Oil: C, Temperature: 21.5 °C.

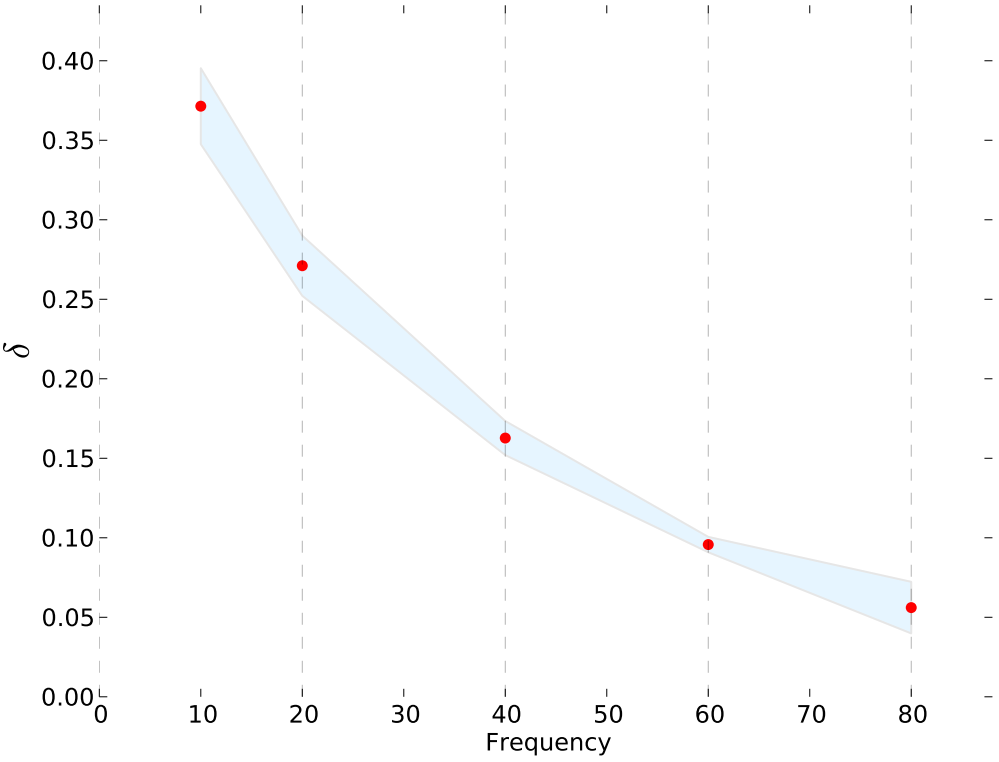

Figure 16: Oil: C, Temperature: 50 °C.

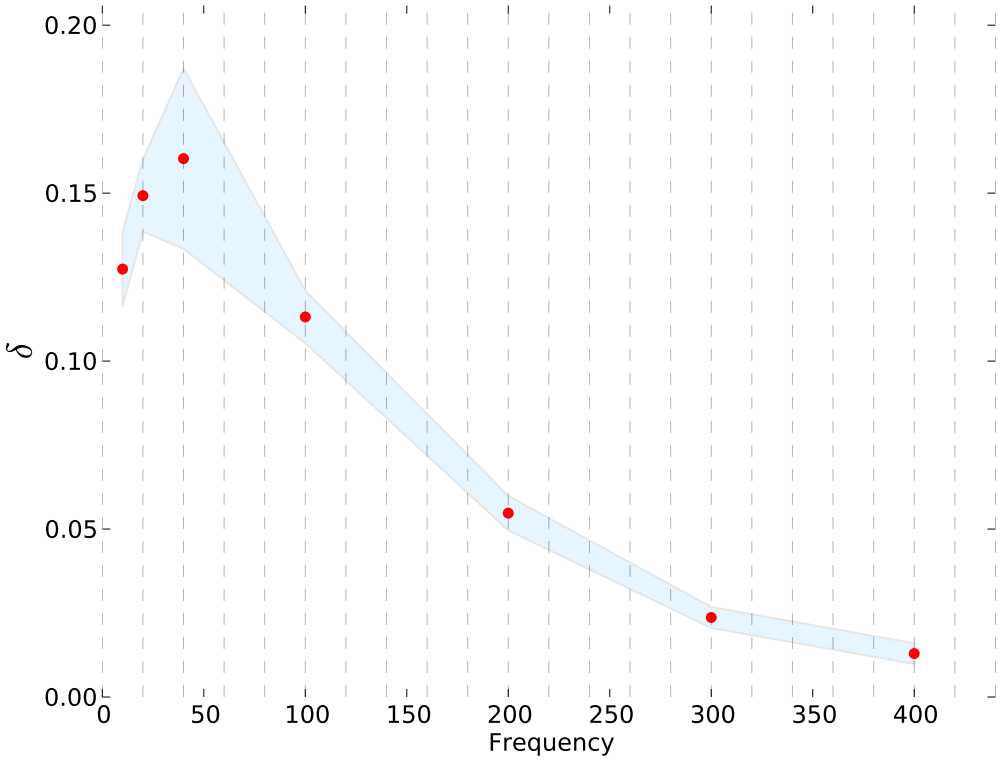

Figure 17: Oil: D, Temperature: 21.5 °C.

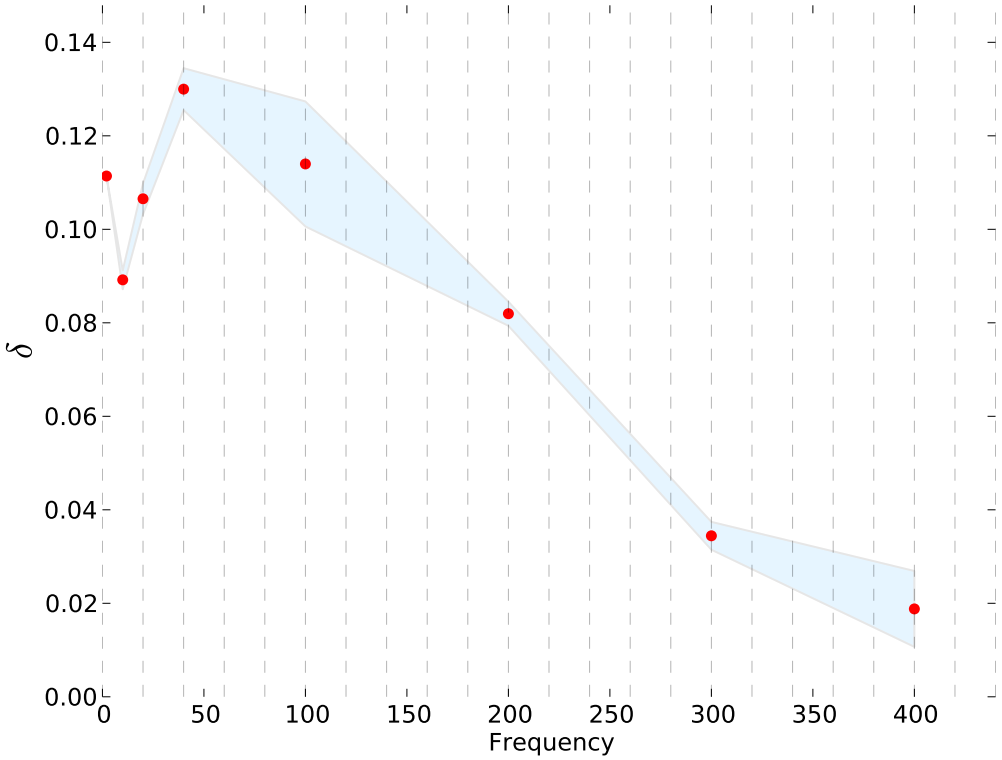

Figure 18: Oil: D, Temperature: 50 °C.

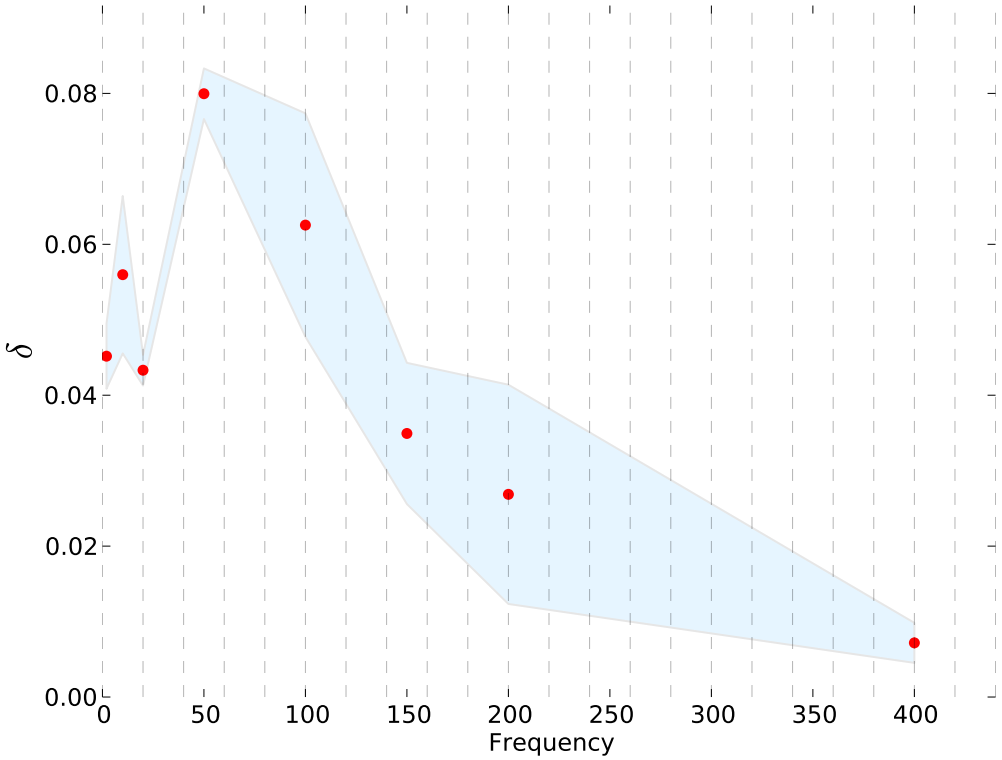

Figure 19: Oil: DE, Temperature: 21.5 °C.

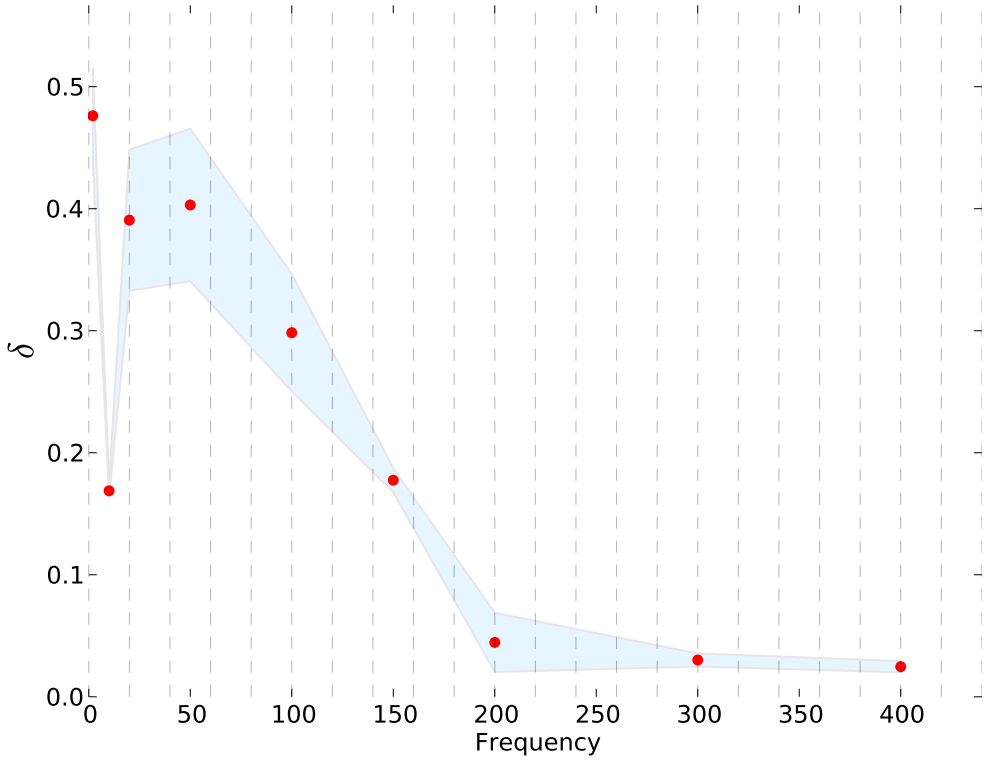

Figure 20: Oil: DE, Temperature: 50 °C.

Marcol

The length span of the longest axis under the influence of sine wave voltages acts somewhat as expected. The highest frequency gave the lowest length span, and both temperatures show signs of having a resonance frequency, with the resonance frequency being higher for the higher temperature. These frequencies are hard to pinpoint due to the scattered results, but seem to be around 150 Hz and 240 Hz for 21.5 °C and 50 °C respectively. The results can be seen in Figure 11 and Figure 12.

Oil A

The deformations of drops in oil A show similar behavior to that of the model oil Marcol. Both temperatures show a resonance peak where the highest length spans are found. The frequencies where these are located are different from Marcol. The resonance peaks seem to be located at around 80 Hz and 120 Hz, for 21.5 °C and 50 °C. These are quite a bit lower than for Marcol. This could suggest a more viscous oil, with higher damping. This fits well with the observed settling speed of droplets dropped in oil A compared to Marcol. The results can be seen in Figure 13 and Figure 14.

Oil C

The deformations of drops in oil C show a different behavior than the other oils. For oil C there is no sign of a resonance peak. The deformation only seems to increase with decreasing frequency. Observing the settling speed of the droplets, this seems appropriate. Of the oils studied, oil C appears to be the most viscous. Oil C was also the most opaque. To be able to get a good image the camera's frame rate needed to be kept low for oil C, as low as 179 fps. Only oscillation frequencies under 80 Hz were tested, as any higher oscillation frequencies would give rise to aliasing. The lack of a resonant peak indicates that the droplet deformation in oil C is overdamped. The results can be seen in Figure 15 and Figure 16.

Oil D

The deformations of drops in oil D show similar behavior to that of Marcol and oil A. Both temperatures show a resonance peak where the highest deformations are found. The frequencies where these are located are different from Marcol. The resonance peaks seem to be located at around 60 Hz and 80 Hz, for 21.5 °C and 50 °C. These are quite a bit lower than for Marcol. Oil D would seem to have a viscosity between that of oils A and C. The results can be seen in Figure 17 and Figure 18.

Oil D with demulsifier

The deformation of drops in oil D with demulsifier do not show a great difference between temperatures as far as resonance frequencies are concerned.

Both temperatures show a resonance peak at around 50 Hz. The results can be seen in Figure 19 and Figure 20.

6.2 Constant square waves

Figures 21-30 show the relative AR for each step for transient oscillations with constant voltage amplitude, relative to the average of the AR's of two initial square pulses. The top subplot represents stable deformations, while the bottom represents maximal deformations.

Figures 31-37 show the calculated damping coefficient for each square wave pulse with the closest linear fit.

Figures 38-42, and show the observed oscillation frequency for each square wave pulse with the closest linear fit.

Any reference to a "stiff" or "soft" droplet, refers to its ability to resist deformation, where a soft droplet will achieve a higher aspect ratio than a stiff droplet for equal values of field strength.

Table 8: Average increase in stable AR per step, compared to average of two first deformations

Temp.\oil	Marcol	A	C	D	DE
21.5 °C	0.06%	-0.14%	0.09%	0.16%	0.11%
50 °C	0.04%	-0.4%	0.07%	0.12%	1.25%

Table 9: Average increase in max AR per step, compared to average of two first deformations

Temp.\oil	Marcol	A	C	D	DE
21.5 °C	0.12%	-0.13%	0.11%	0.14%	0.12%
50 °C	0.1%	-0.65%	0.14%	0.19%	1.44%

Table 10: Damping coefficients for constant voltages in s^{-1}

Temp.\oil	Marcol	A	C	D	DE
21.5 °C	299	289	-	231	-
50 °C	357	387	-	326	356

Table 11: Oscillation frequencies for constant voltages in Hz

Temp.\oil	Marcol	A	C	D	DE
21.5 °C	164	-	-	-	-
50 °C	289	112	-	116	97

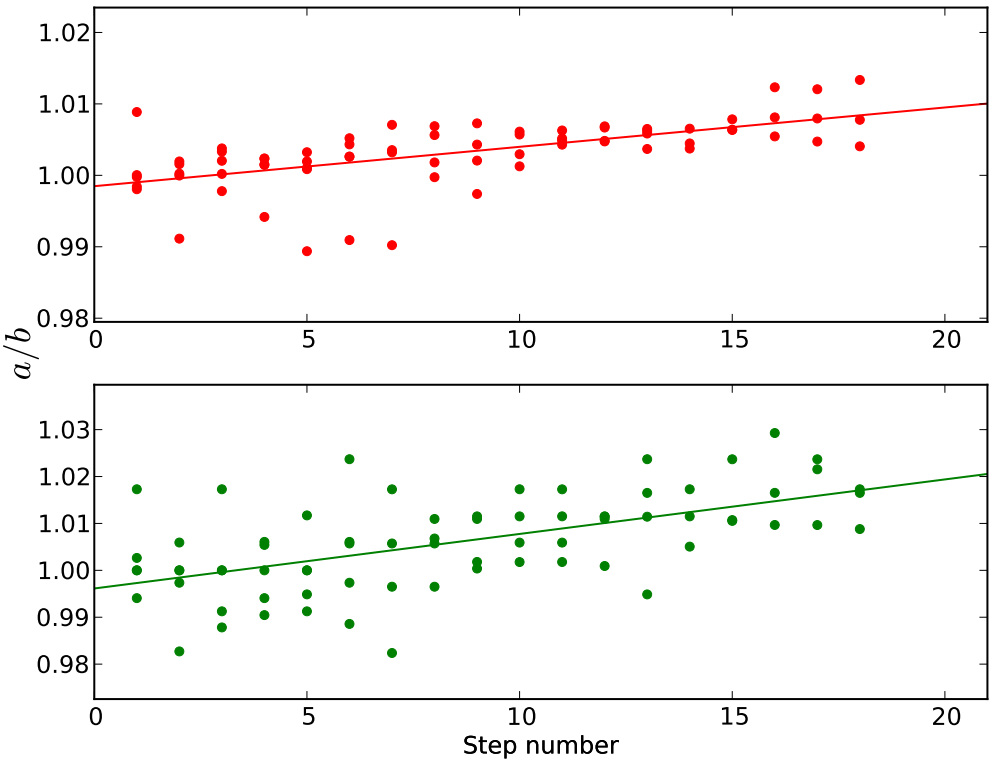

Figure 21: Oil: Marcol, Temperature: 21.5 °C.

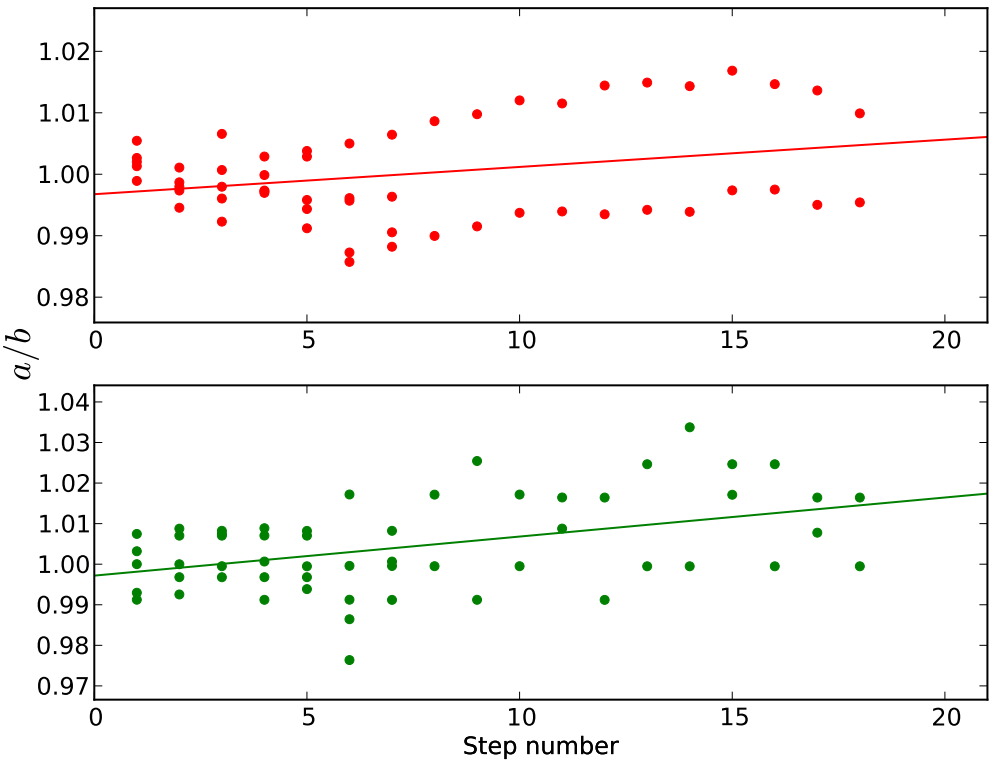

Figure 22: Oil: Marcol, Temperature: 50 °C.

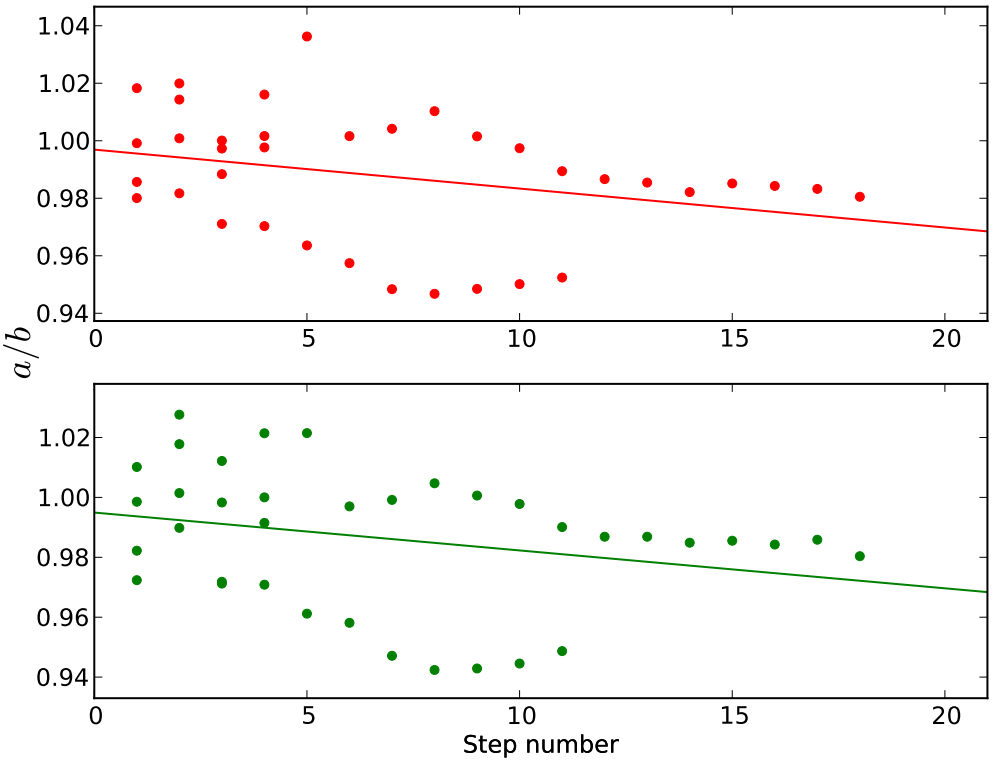

Figure 23: Oil: A, Temperature: 21.5 °C.

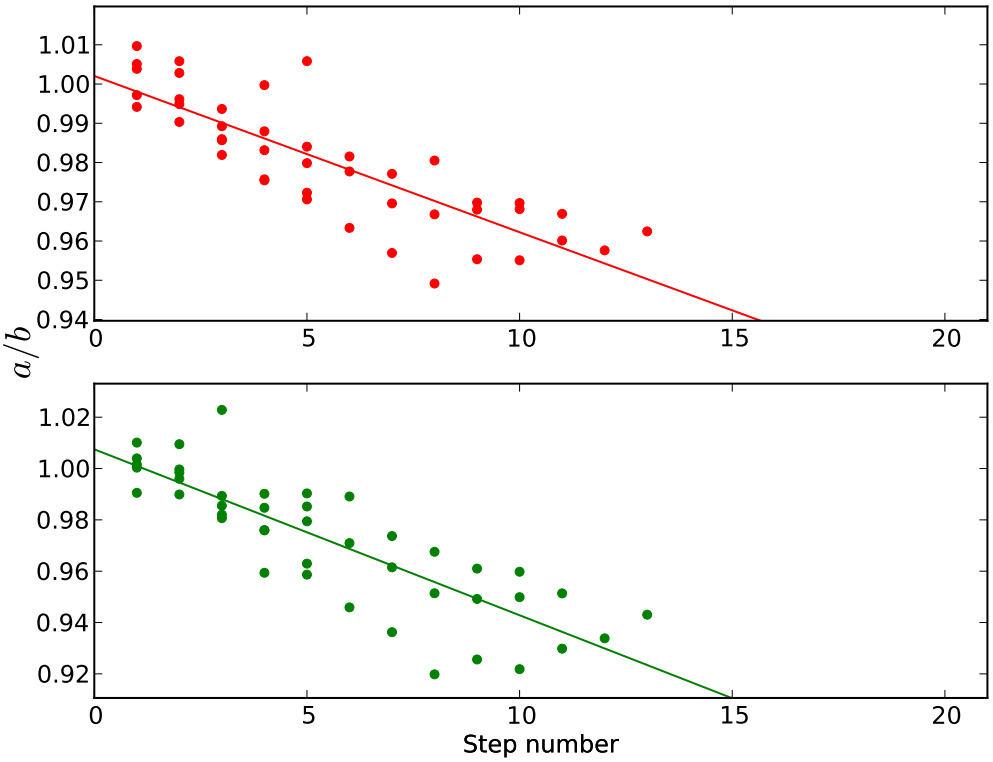

Figure 24: Oil: A, Temperature: 50 °C.

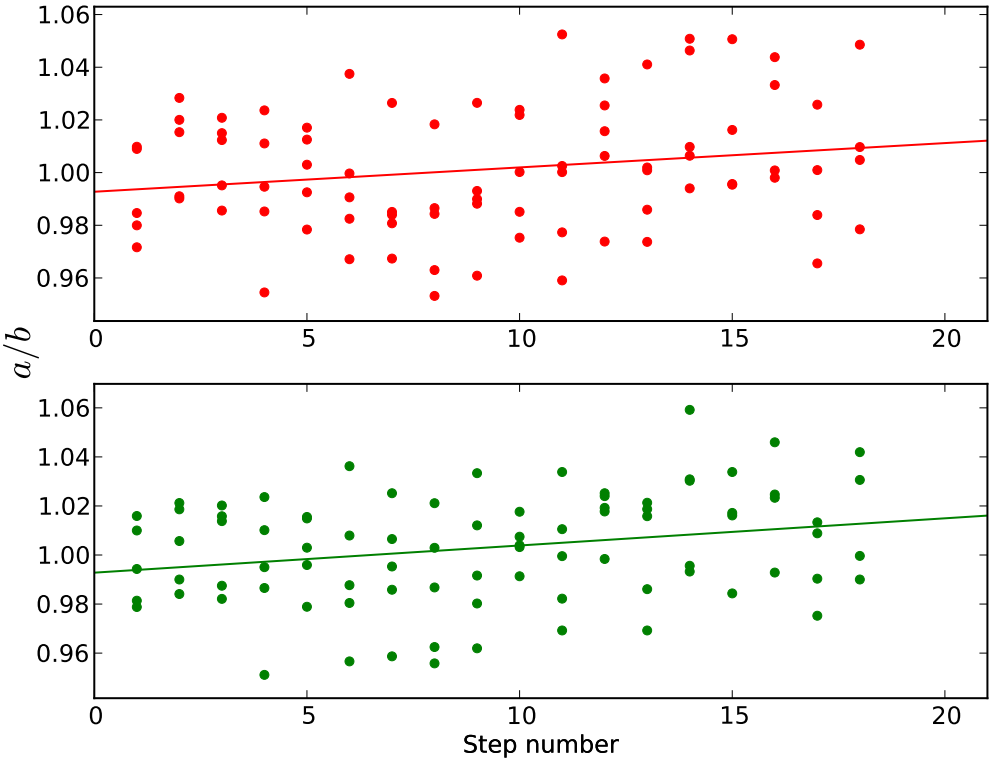

Figure 25: Oil: C, Temperature: 21.5 °C.

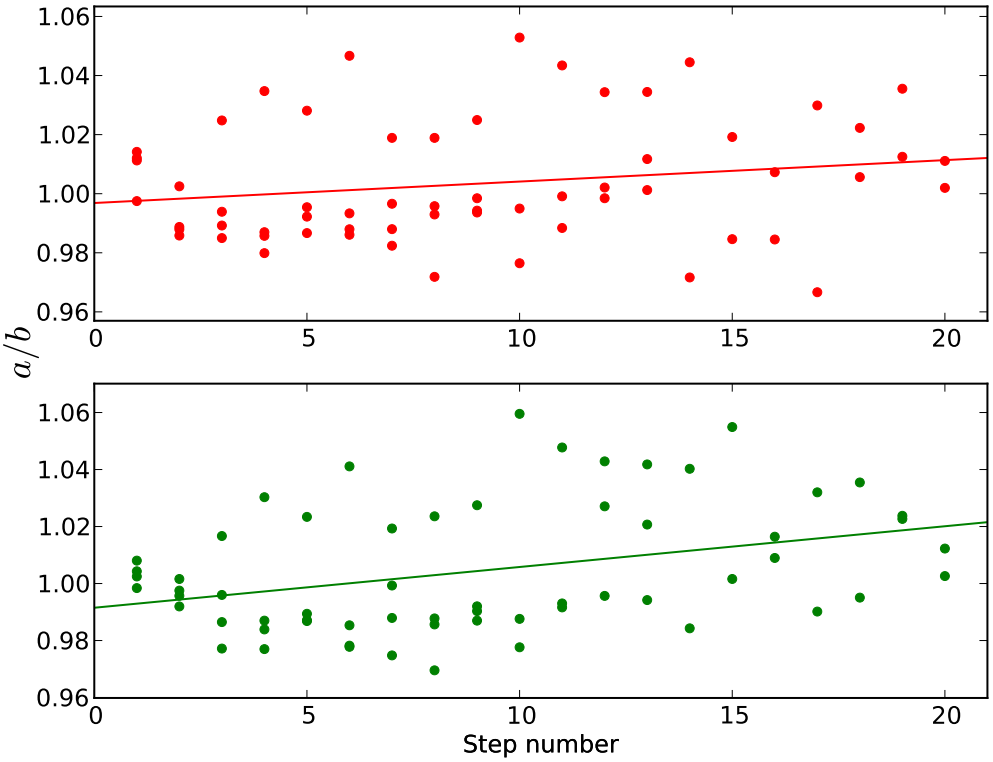

Figure 26: Oil: C, Temperature: 50 °C.

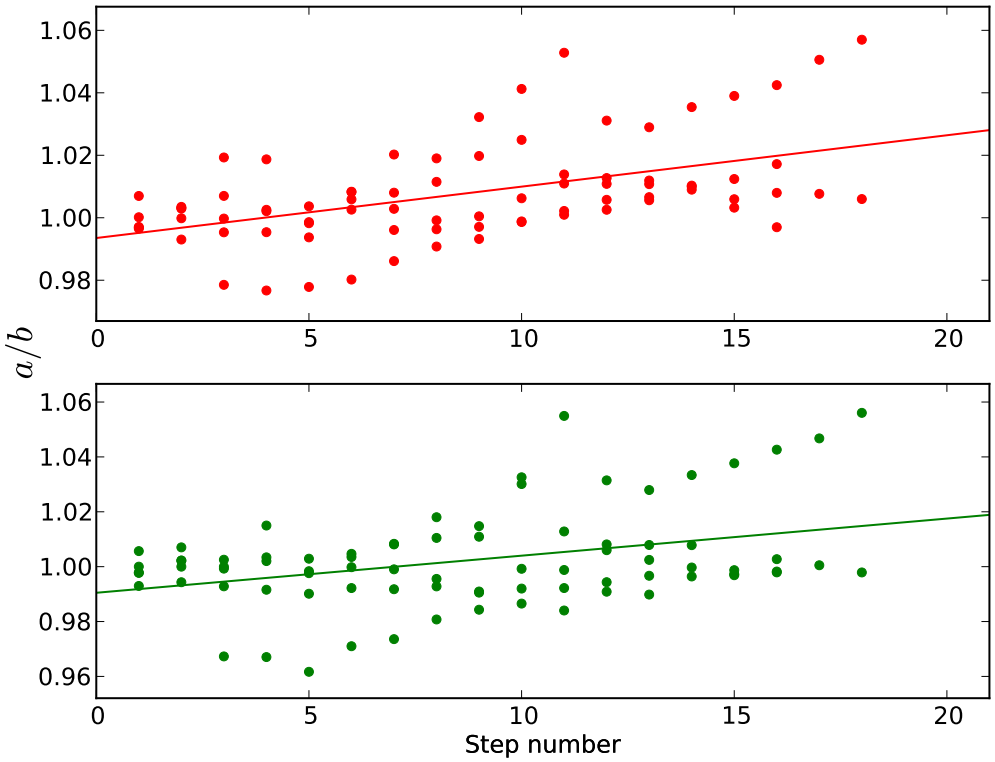

Figure 27: Oil: D, Temperature: 21.5 °C.

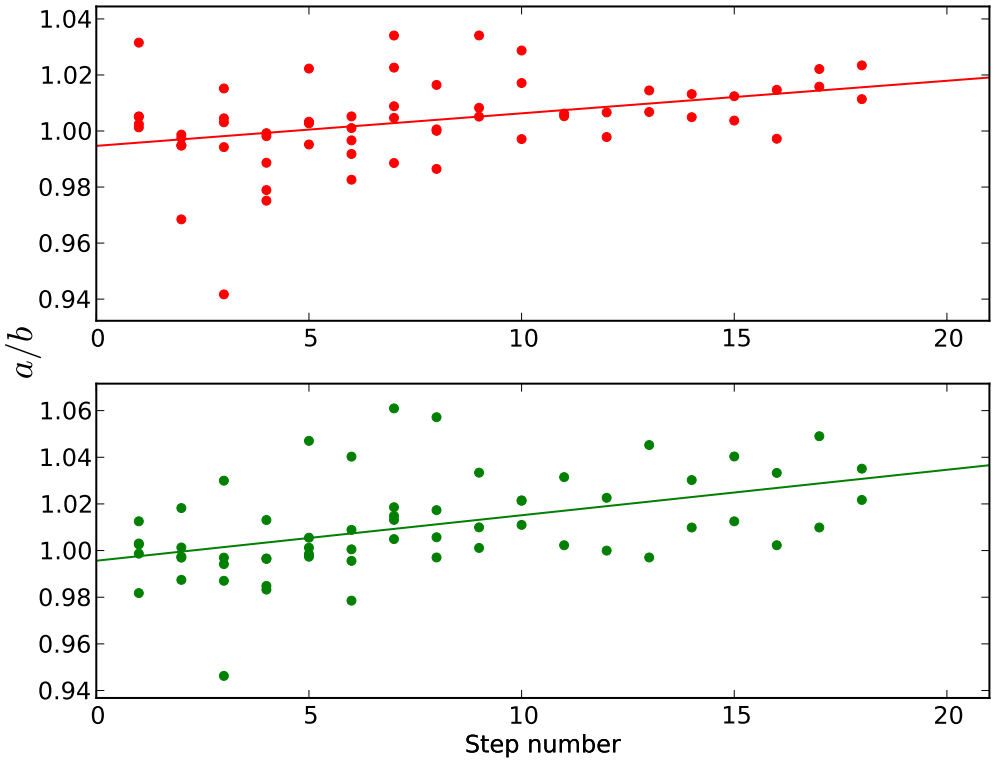

Figure 28: Oil: D, Temperature: 50 °C.

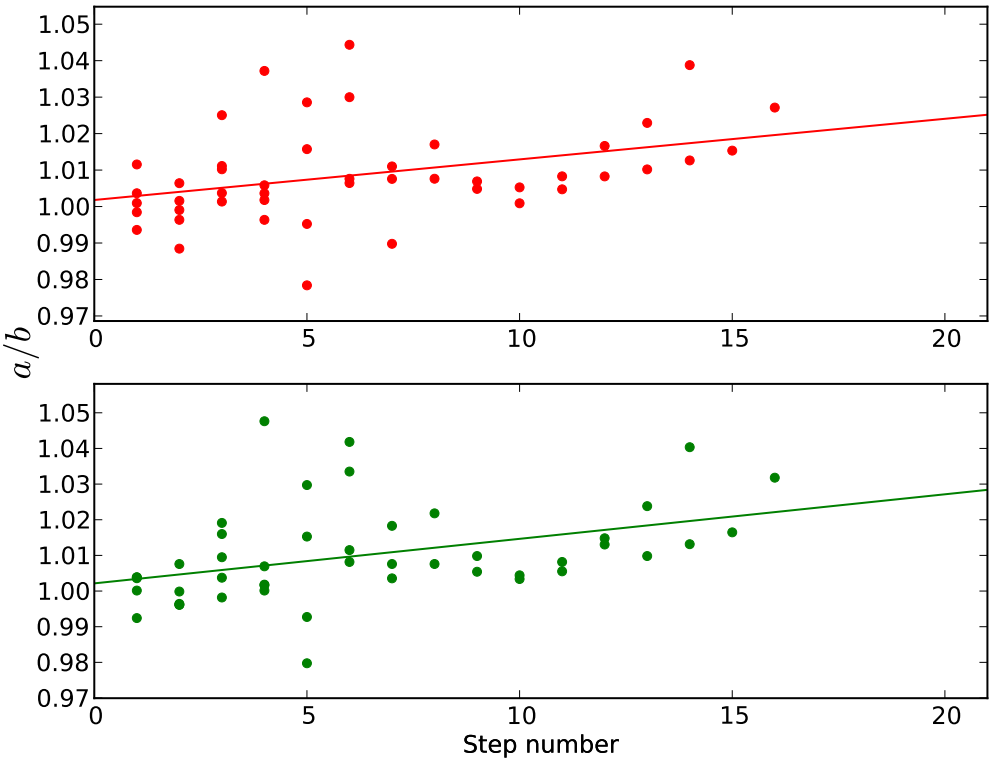

Figure 29: Oil: DE, Temperature: 21.5 °C.

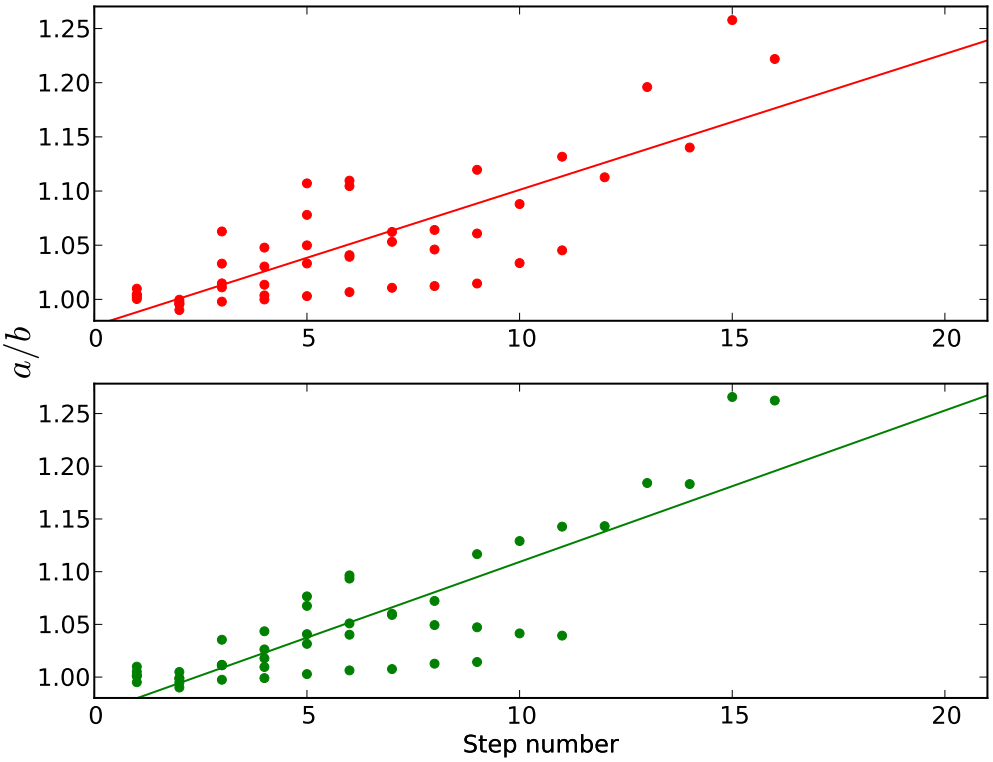

Figure 30: Oil: DE, Temperature: 50 °C. Note the change in scale.

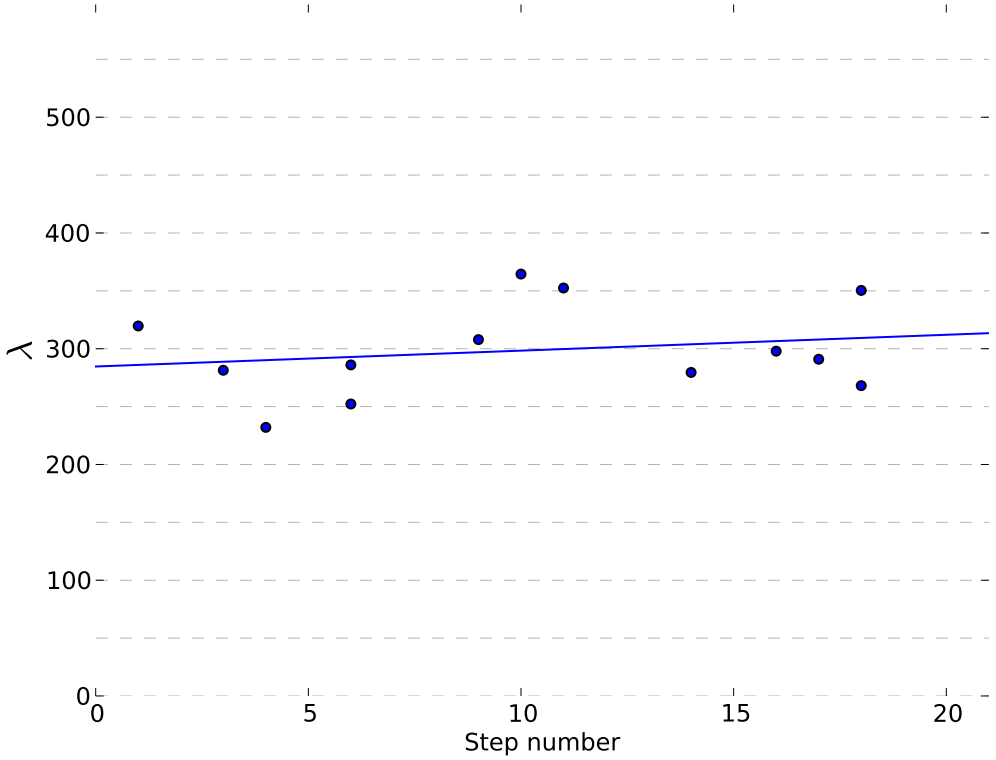

Figure 31: Oil: Marcol, Temperature: 21.5 °C.

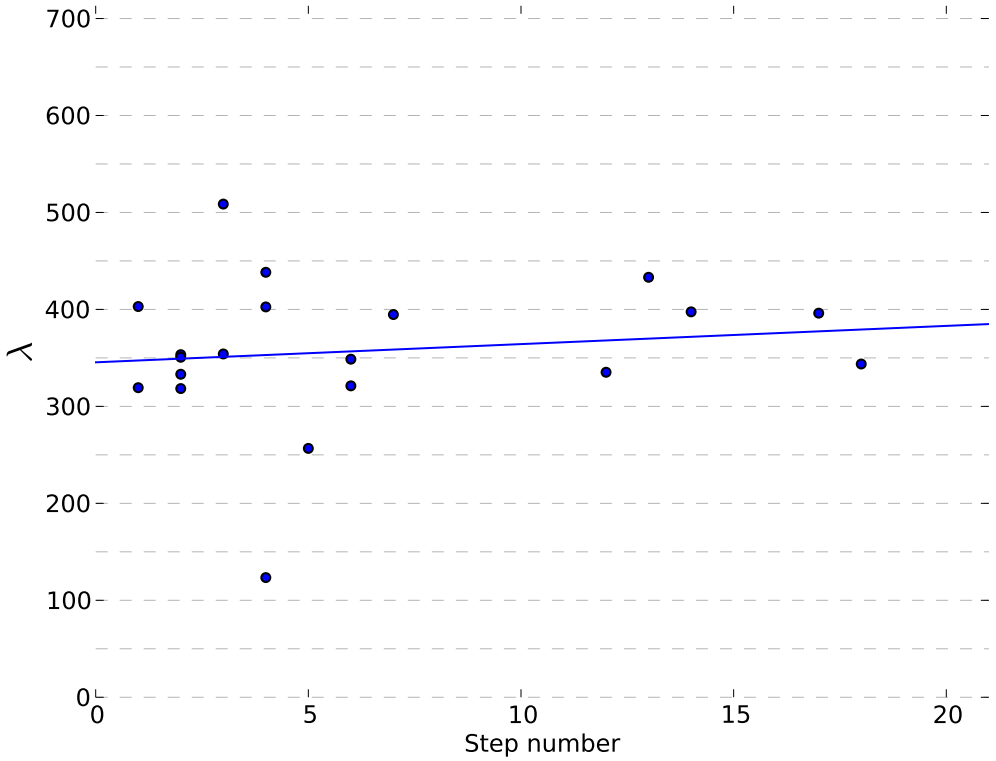

Figure 32: Oil: Marcol, Temperature: 50 °C.

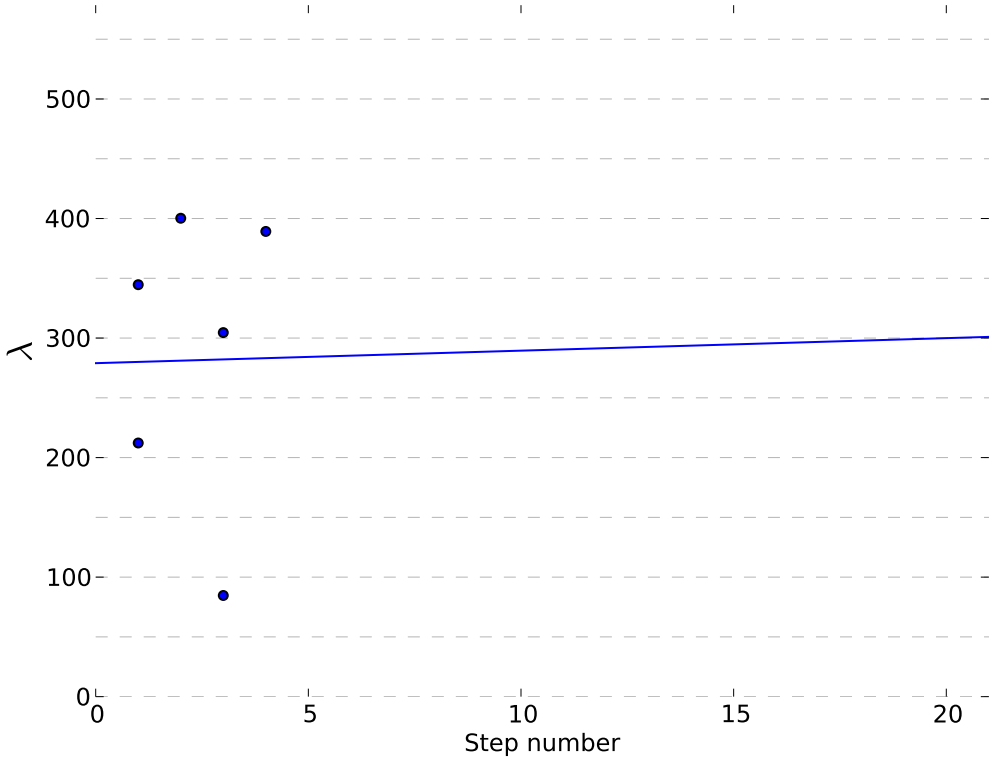

Figure 33: Oil: A, Temperature: 21.5 °C.

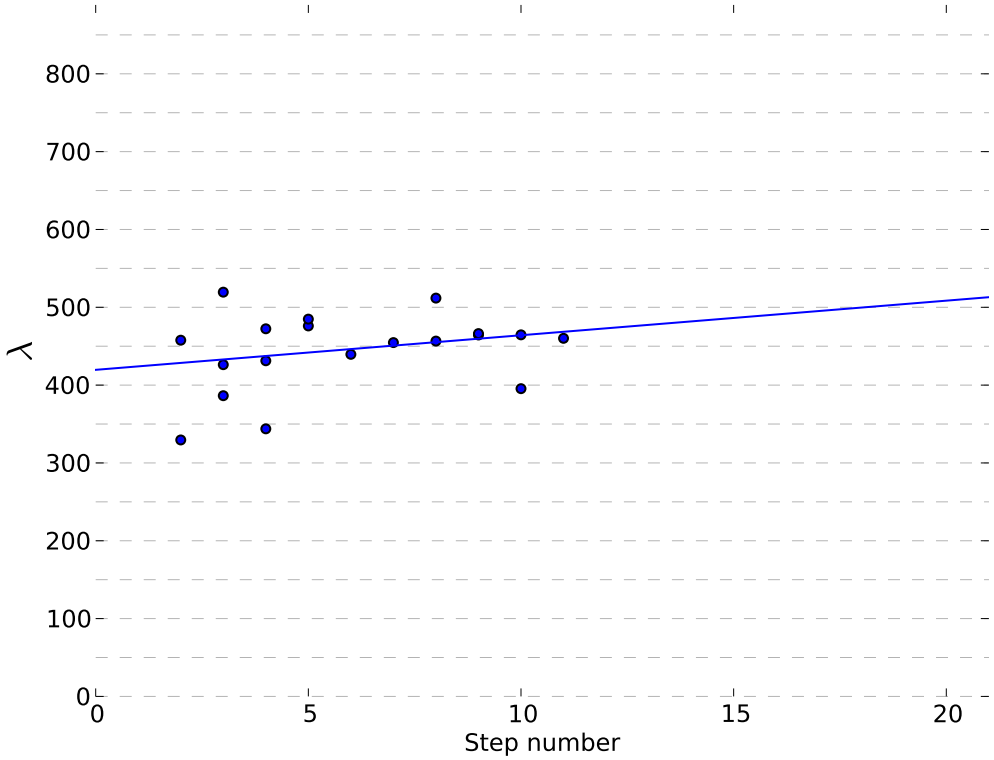

Figure 34: Oil: A, Temperature: 50 °C.

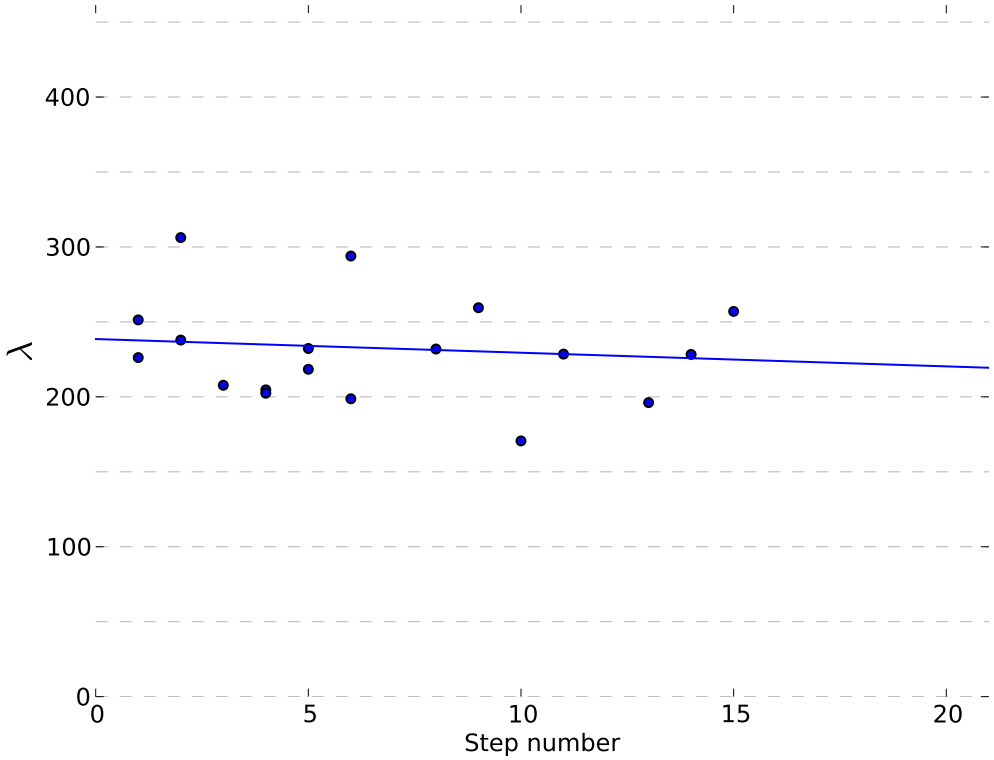

Figure 35: Oil: D, Temperature: 21.5 °C.

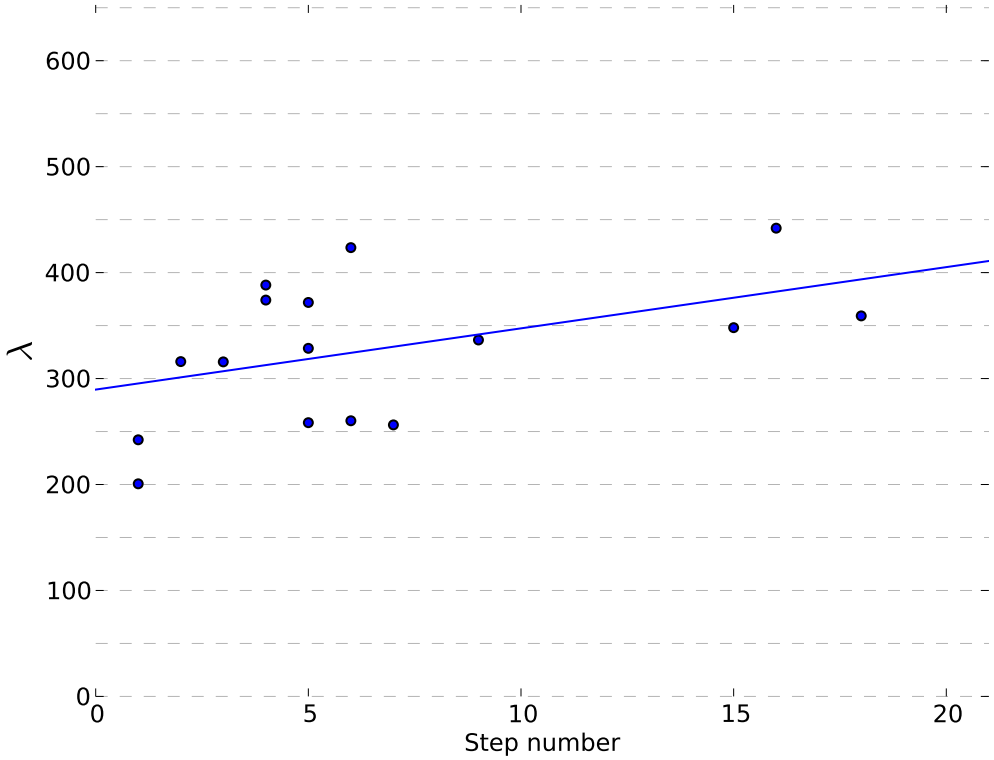

Figure 36: Oil: D, Temperature: 50 °C.

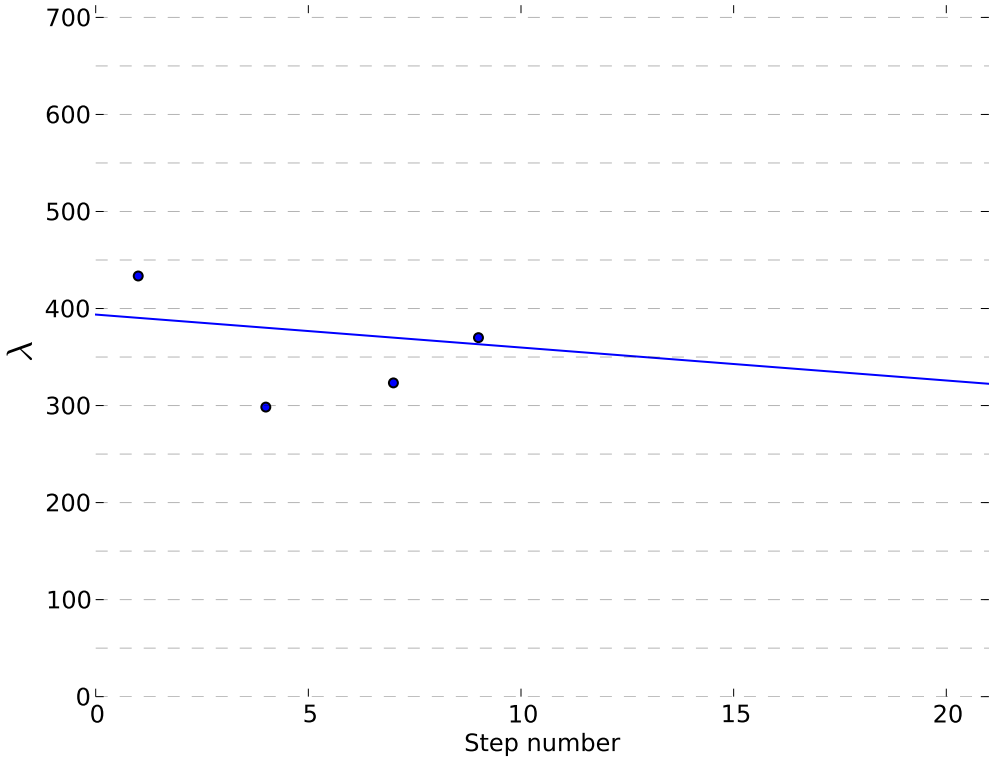

Figure 37: Oil: DE, Temperature: 50 °C.

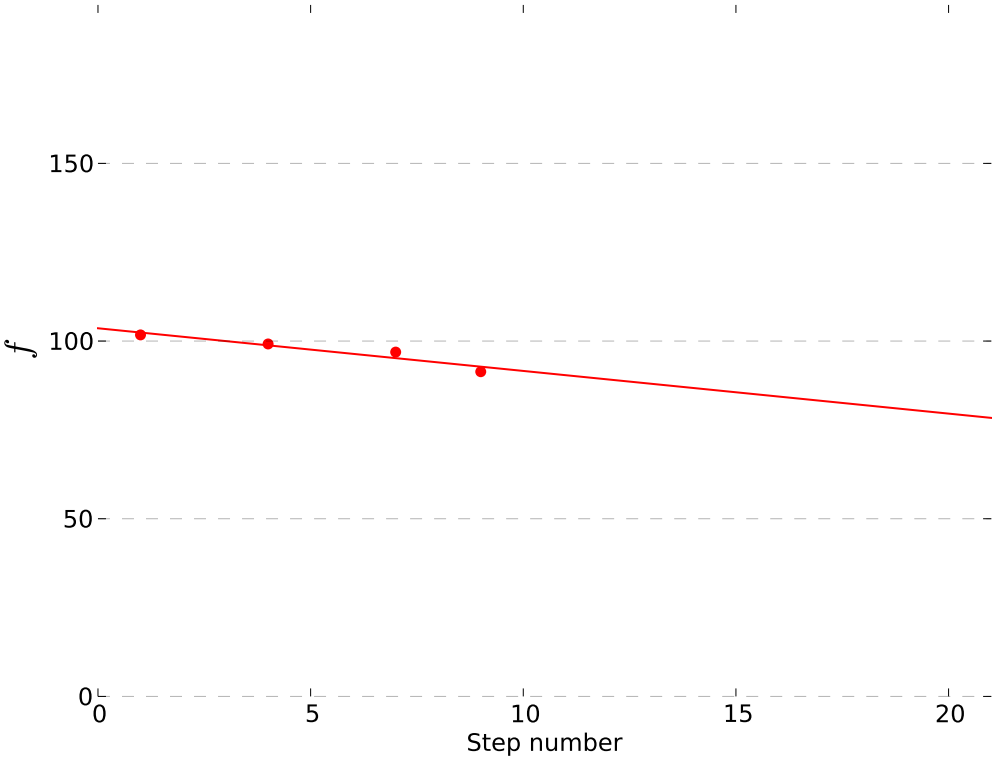

Figure 38: Oil: DE, Temperature: 50 °C.

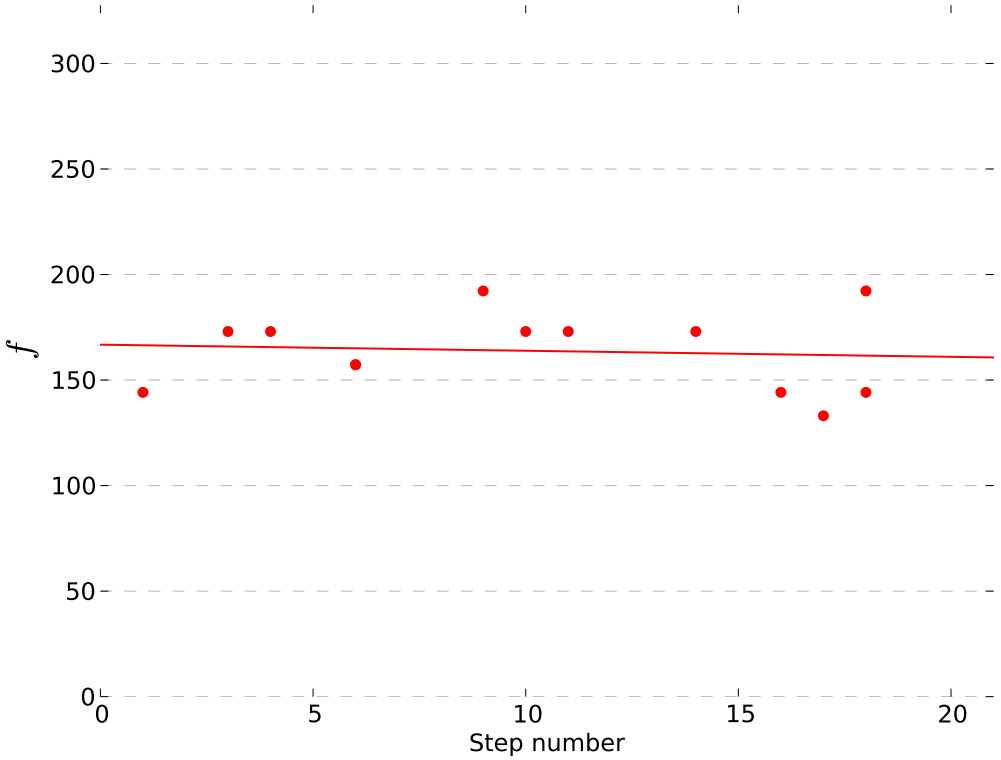

Figure 39: Oil: Marcol, Temperature: 21.5 °C.

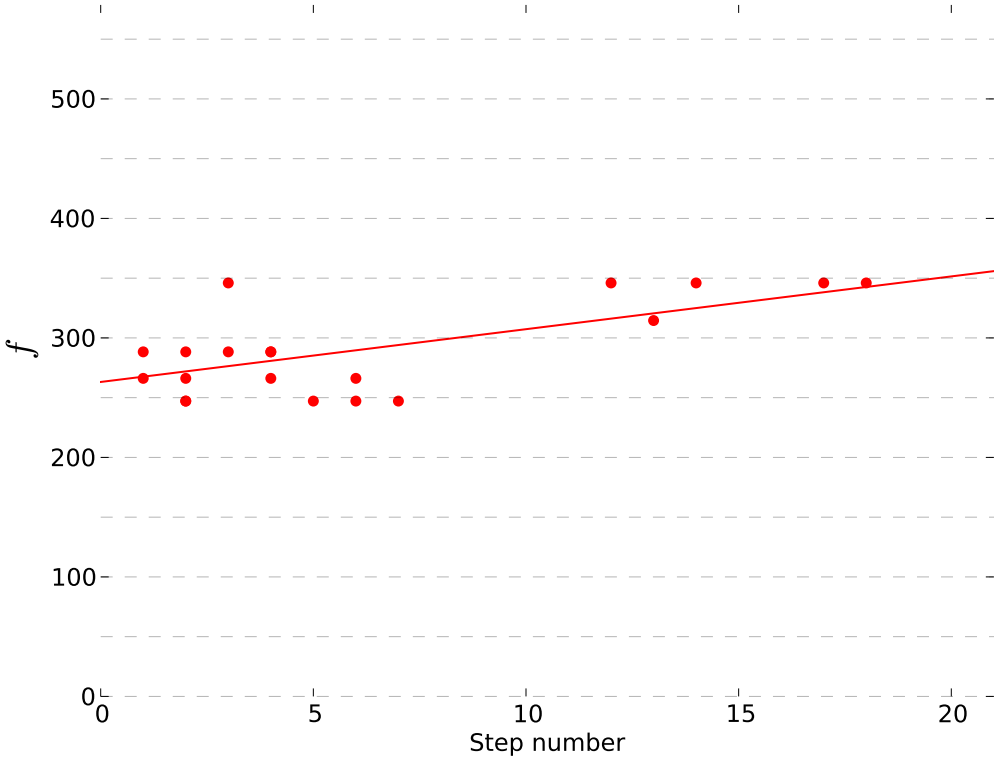

Figure 40: Oil: Marcol, Temperature: 50 °C.

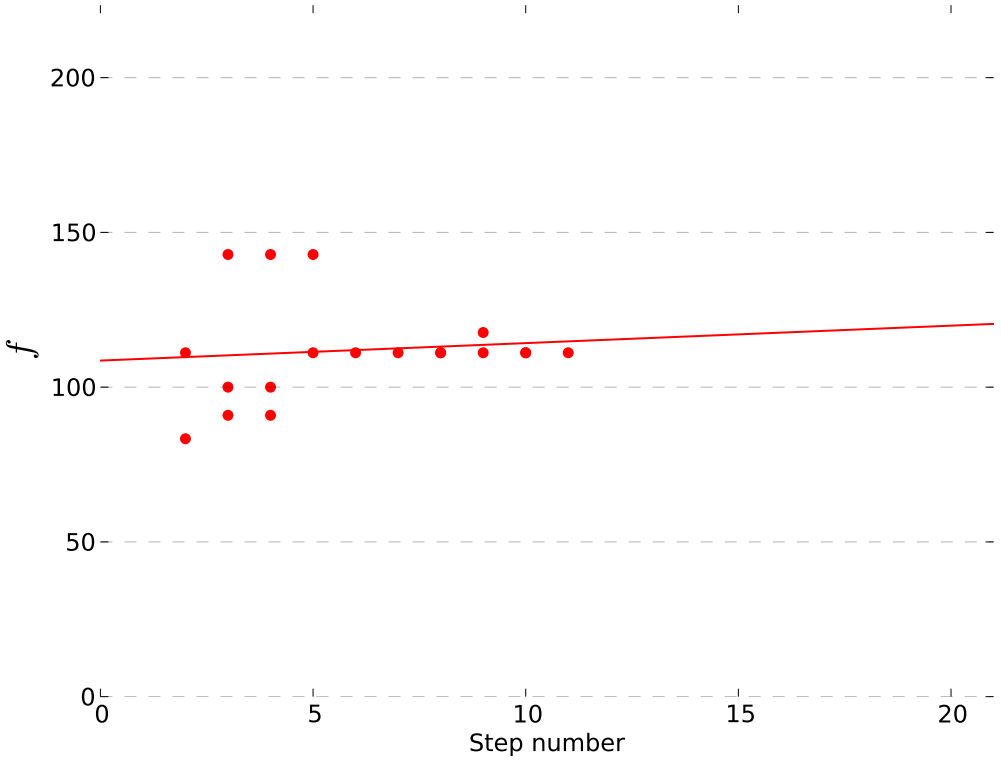

Figure 41: Oil: A, Temperature: 50 °C.

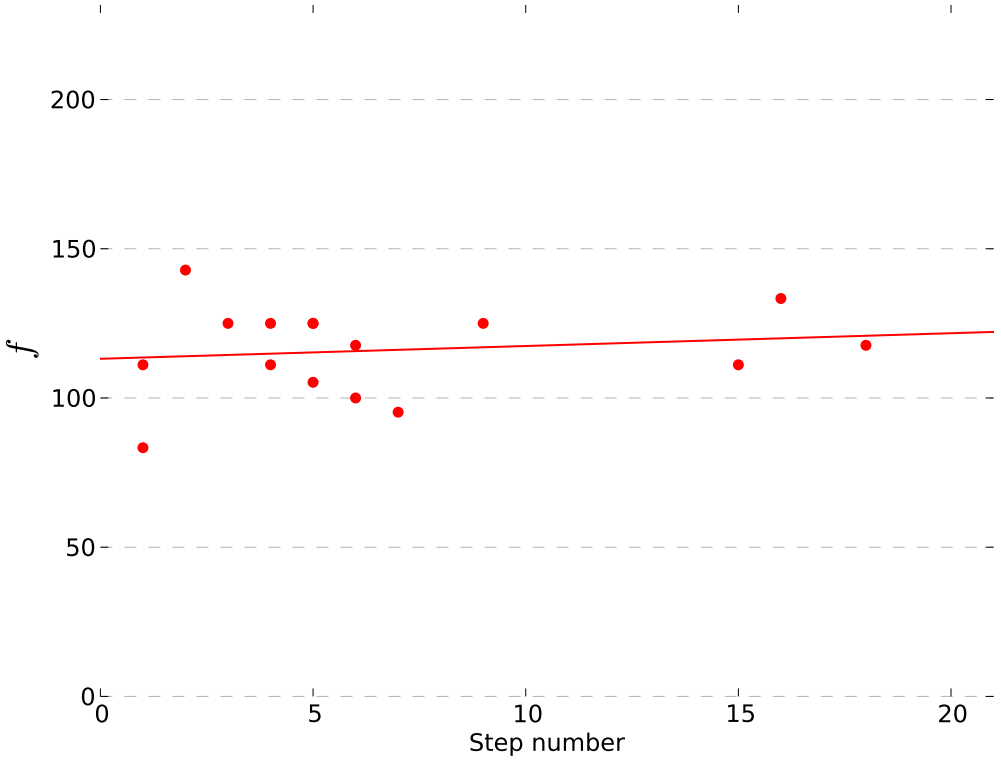

Figure 42: Oil: D, Temperature: 50 °C.

Marcol

Stable deformation

The stable deformations for a constant voltage do not show much change over time. Both stable and maximal deformations show a slight change over time, but this is so small that it looks more like an effect from the random spread of the results. The maximal deformation shows positive trends for both temperatures. What is most clear then from these experiments is that there are no serious changes in the deformations over time. This is however somewhat expected for such a pure oil as Marcol 52. The results can be seen in Figure 21 and Figure 22.

Damping coefficient

The development of damping coefficient might suggest a slight upward trend, but the measurements do not give good fits or show any clear trends. The results from 21.5 °C and 50 °C give average damping coefficients of respectively $299\,s^{-1}$ and $357\,s^{-1}$. The results can be seen in Figure 31 and Figure 32.

Oscillation frequency

The results for the frequency of the drop oscillations are greatly affected by the fact that the films frame rate is not much higher than the frequency itself. Therefore the period measured in the film is rounded off to the closest time step and only gives a few measurable values. Any change in frequency is therefore much harder to detect. Although the results from 50 °C show an upward trend, the results of these are considered arbitrary. What is worth noting is the difference in average frequency between the two temperatures. For 21.5 °C and 50 °C they are respectively 164 Hz and 289 Hz. The results can be seen in Figure 39 and Figure 40.

Oil A

Stable deformation

The deformations of the droplets in oil A do show a tendency for change over time. However, unlike all the other oils, oil A shows a decreasing trend. The change is clearer for higher temperatures than for the lower. This is the case both for rate of change, and for the fit of the data to a linear curve. The changing deformation of the droplets show a stiffening of the droplets. It is believed that substances in the oil will adsorb to the surface for the minute the droplet is aged before being dropped. Stretching the droplet gives the substances a greater area to adsorb to and accelerates the process. If this is the case, the droplet should exhibit signs of stiffening or softening, according to what substance is adsorbing to the surface. This depends on whether the substance e.g. acts as an emulsifier or a demulsifier. It is reasonable to assume that this adhesion speeds up with the random motion of these substances throughout the oil. This will increase with temperature, and can explain the increased stiffening for higher temperatures. The results can be seen in Figure 23 and Figure 24.

Damping coefficient
Neither 21.5 °C nor 50 °C show any real signs of increasing or decreasing over number of previous deformations. There is however a difference between average values between the two temperatures. They are $289\,s^{-1}$ and $444\,s^{-1}$ for 21.5 °C and 50 °C respectively. The results can be seen in Figure 33 and Figure 34.

Oscillation frequency
For the experiments at 21.5 °C there were not enough visible oscillations to extract a result, as the deformations seemed to exhibit critical, or near critical damping. For 50 °C the average is 112 Hz. The results can be seen in Figure 41.

Oil C

Stable deformation
The deformations of the droplets in oil C do show very small changes over time. Oil C shows the most spread and seemingly random results of the oils tested. 21.5 °C and 50 °C both show weak tendencies to increase. The results can be seen in Figure 25 and Figure 26.

Damping coefficient
Due to the viscosity and opacity of oil C, damping coefficients were not possible to detect. The viscosity of the oil produced overdamped oscillations, and the oil was so opaque that in order to get a clear image, the frame rate could not go over 200 frames per second. This resulted in deformations that seemed to jump to stable levels between shots, and stay there throughout the duration of the square wave of electric field.

Oscillation frequency
As there were no oscillations to be seen, no values for oscillation frequencies could be measured or calculated. The results of the sinusoidal voltages suggest the deformation of the water drops in oil C are overdamped. The fact that no oscillations were seen for square wave voltages fits well with this. Figure 15 and Figure 16 would also suggest that the droplets are overdamped.

Oil D

Stable deformation Oil D shows a slight upward trend for both 21.5 °C and 50 °C. In this sense it is the crude oil behaving most similarly to Marcol. Oil D is the only crude oil tested known to have no added substances. Considering this, it is not surprising that the two purest oils should behave in a similar manner. The results can be seen in Figure 27 and Figure 28.

Damping coefficient
As with oil A there are no real signs of changes in damping coefficients over time. The change between temperatures is quite similar. When going from 21.5 °C to 50 °C the damping coefficient increases from $231\,s^{-1}$ $326\,s^{-1}$. The results can be seen in Figure 35) and Figure 34.

Oscillation frequency

At 21.5 °C there were not enough visible oscillations to extract a result, as the deformations seemed to exhibit critical, or near critical damping. For 50 °C the average is 116 Hz. The results can be seen in Figure 42.

Oil D with demulsifier

Stable deformation

The deformation of oil D with demulsifier showed the most extreme effect of multiple deformations. The results can be seen in Figure 29 and Figure 30, and show an increase in both stable and maximal deformation. This does not give a complete picture of the drop behavior. For both temperatures, 3 of 5 droplets were ripped apart by the electric forces to one slightly smaller droplet and several tiny droplets. Since the electric field was held constant for each square pulse, the weakening of the droplets must be due to an effect over time. The demulsifier seems to have a profound effect on the stability of the droplets. Both temperatures had an equal amount of disintegrating droplets, but for 50 °C, the droplets disintegrated several times. When a droplet is ripped apart by an electric field like in these experiments, tiny droplets shoot of in both directions along the applied field. What remains then is a slightly smaller droplet. From the Taylor model it follows that a smaller droplet should be able to withstand a higher electric field strength. The fact that the smaller droplet left behind also disintegrated, and that this happened repeatedly, is a strong indication of an effect from multiple deformations! Droplets in this oil need to be substantially stronger to withstand e.g. its tenth deformation than to withstand its first.

Damping coefficient

Only a few deformations at 50 °C had results making it possible to extract a damping coefficients. Since there are so few, only the average value is of interest. The average value for 50 °C is $356\,\mathrm{s}^{-1}$. The results can be seen in Figure 37.

Oscillation frequency

The same deformations that gave damping coefficients gave frequencies for a few deformations. These values were very consistent and gave an average frequency of 97 Hz. The results can be seen in Figure 38.

6.3 Increasing square waves

Figures 43-52 show the AR for for transient oscillations with increasing voltage amplitude compared to the theoretical model Eq. (56). Red marks stable AR's, green marks maximum AR's, and black marks the best fit of stable AR's found by adjusting effective surface tension.

Figures 53-59 show the calculated damping coefficient for each square wave pulse with the closest linear fit.

Figures 60-64 show the observed oscillation frequency for each square wave pulse with the closest linear fit.

Table 12: Effective surface tensions in mN/m

Temp.\oil	Marcol	A	C	D	DE
21.5 °C	23.2	24.9	54.9	53.8	48.4
50 °C	28.7	34.4	77.9	35.7	23.1

Table 13: Damping coefficients for increasing voltages in s^{-1}

Temp.\oil	Marcol	A	C	D	DE
21.5 °C	310	412	-	163	-
50 °C	483	570	-	335	304

Table 14: Oscillation frequencies for increasing voltages in Hz

Temp.\oil	Marcol	A	C	D	DE
21.5 °C	155	-	-	-	-
50 °C	332	151	-	120	92

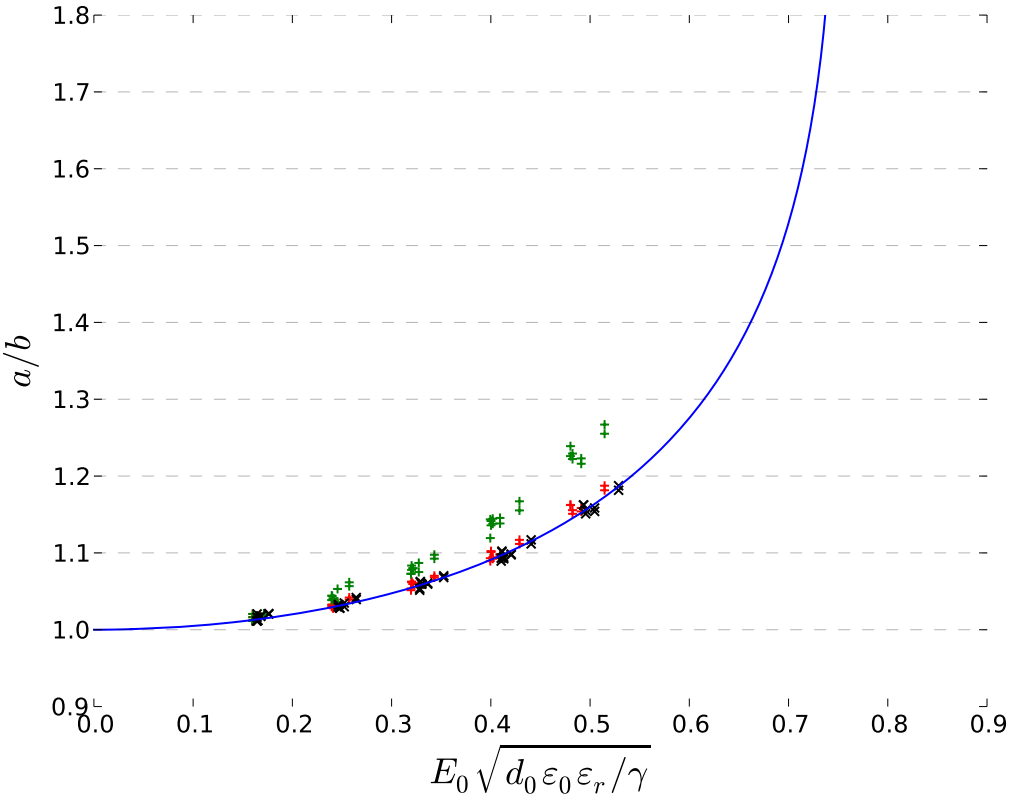

Figure 43: Oil: Marcol, Temperature: 21.5 °C.

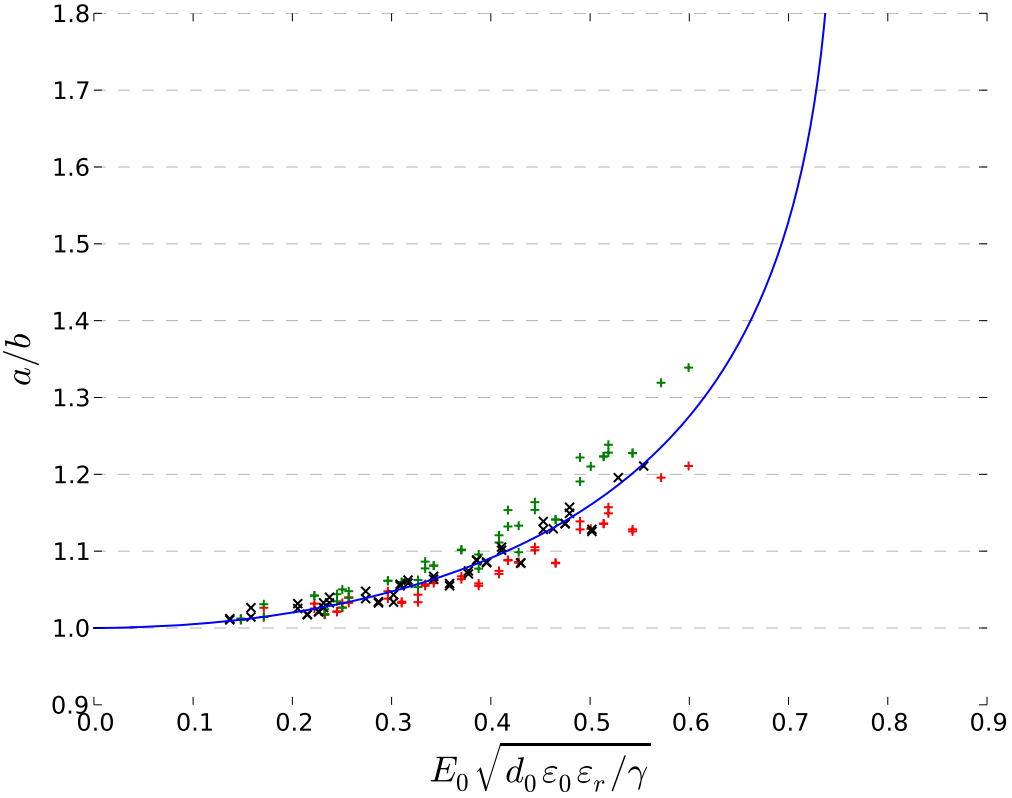

Figure 44: Oil: Marcol, Temperature: 50 °C.

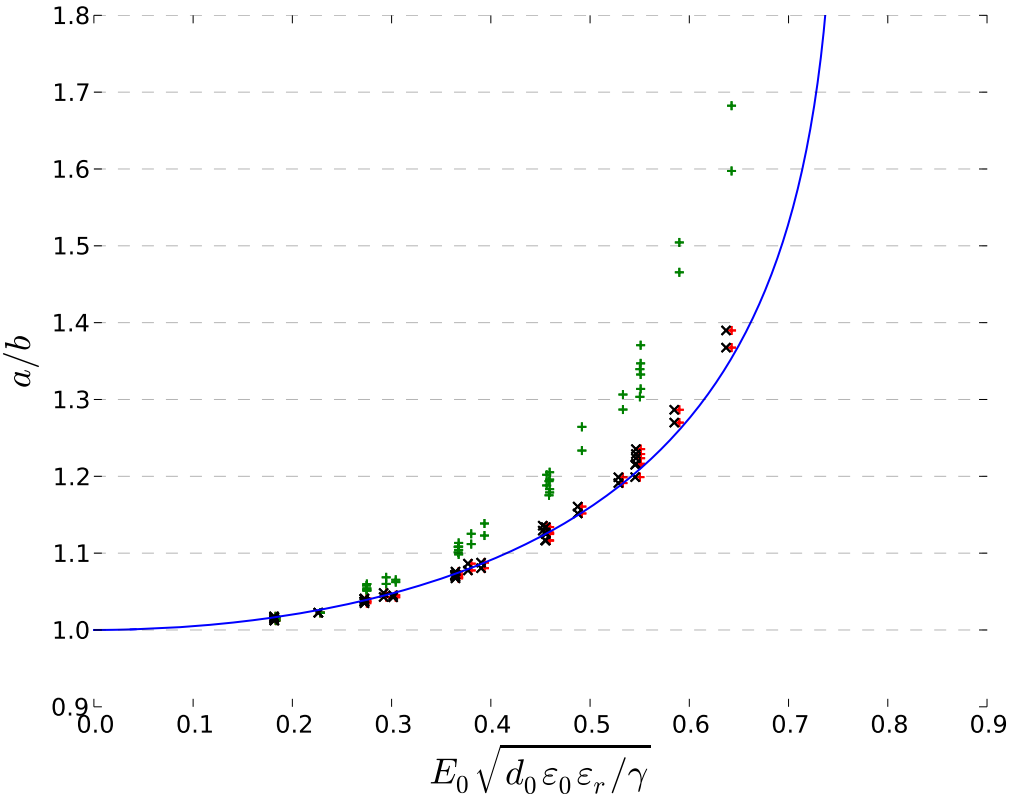

Figure 45: Oil: A, Temperature: 21.5 °C.

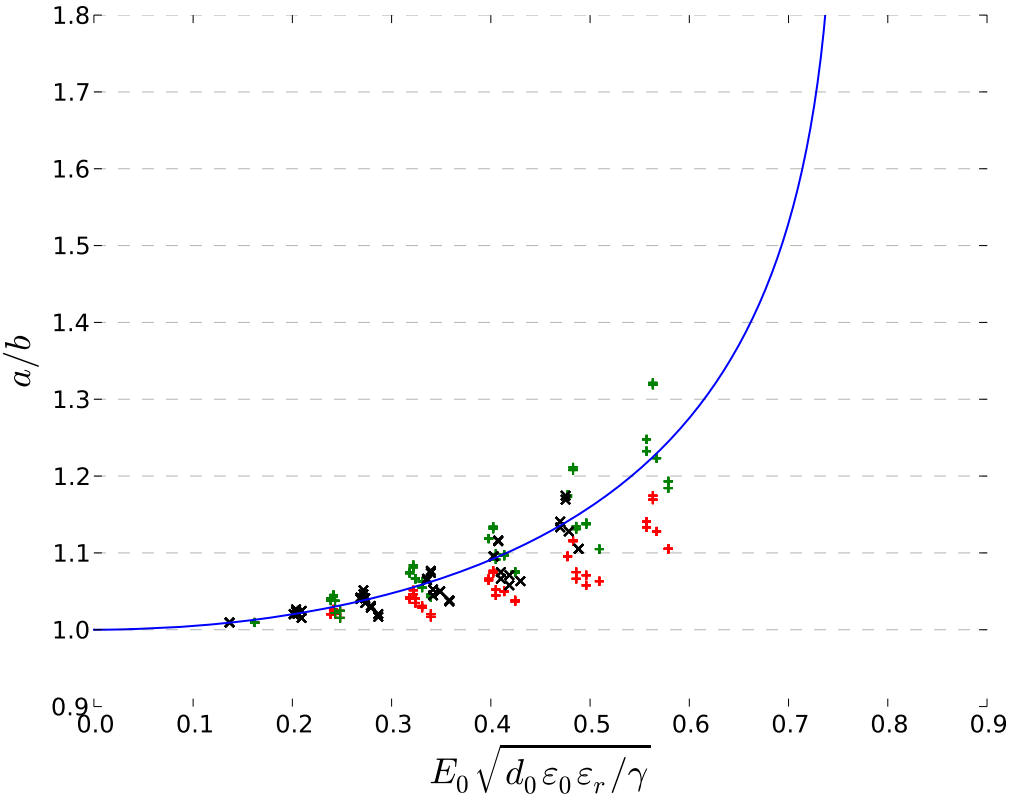

Figure 46: Oil: A, Temperature: 50 °C.

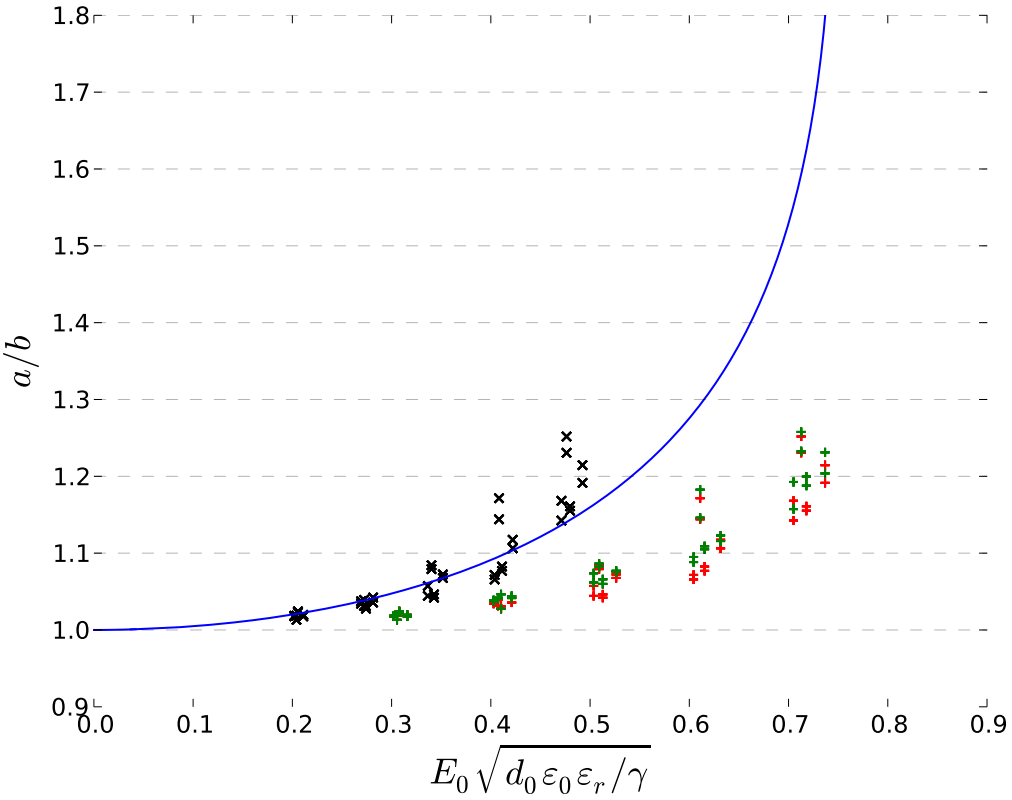

Figure 47: Oil: C, Temperature: 21.5 °C.

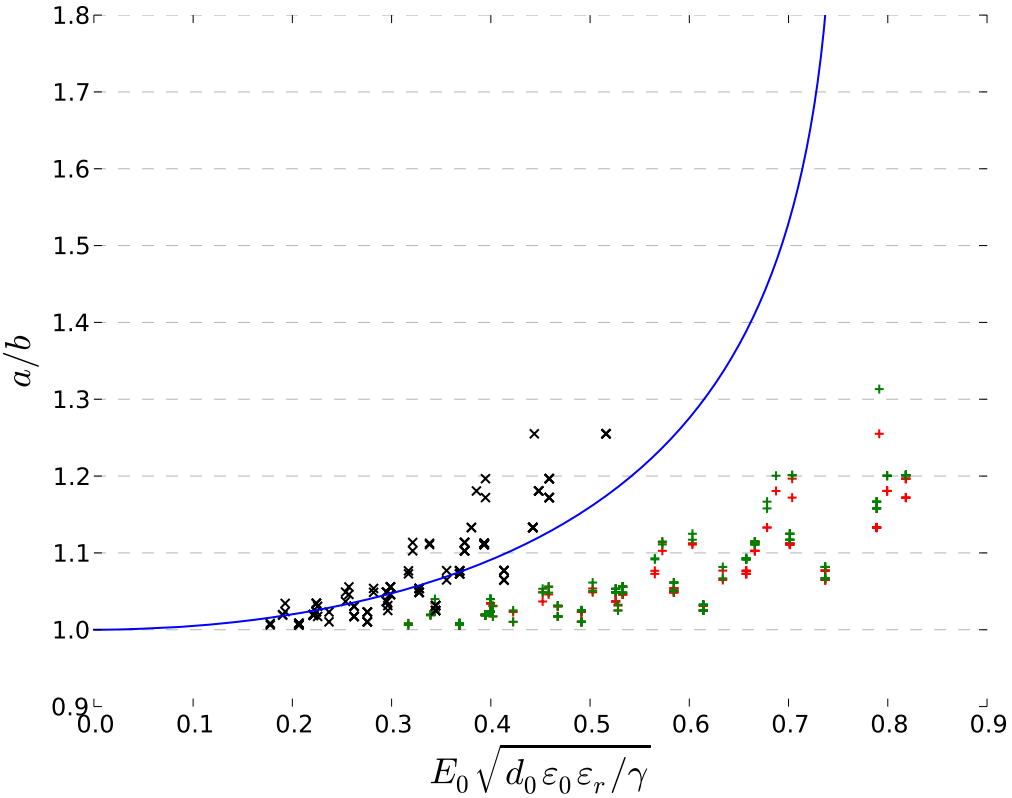

Figure 48: Oil: C, Temperature: 50 °C.

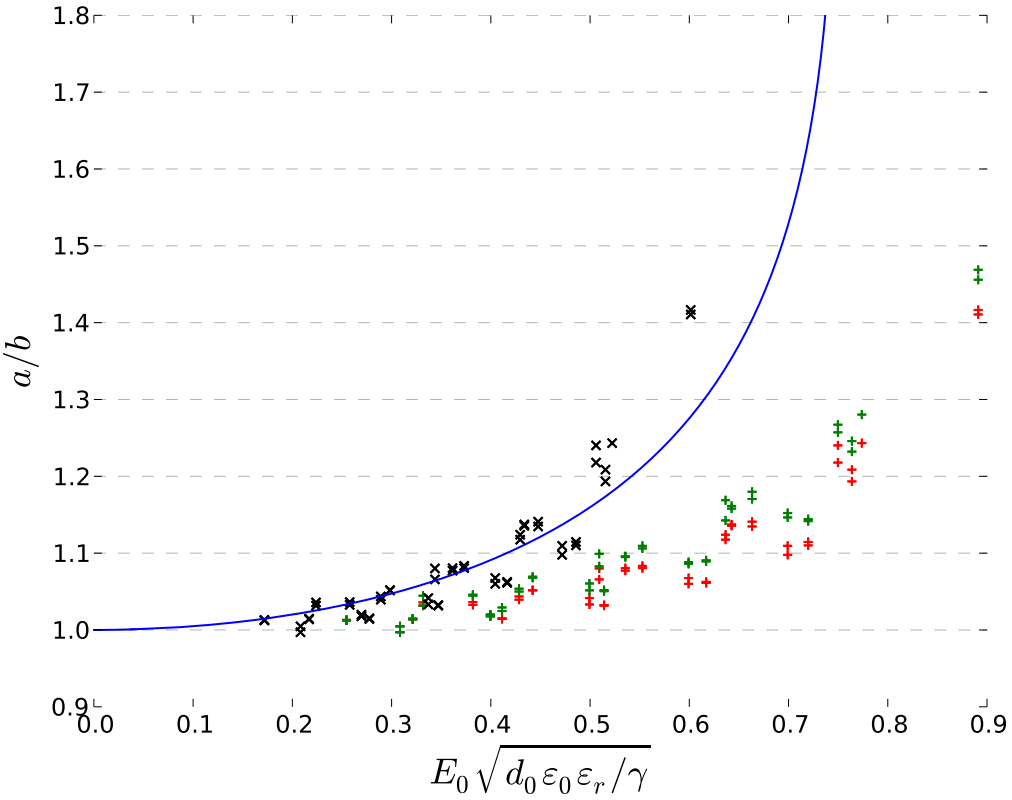

Figure 49: Oil: D, Temperature: 21.5 °C.

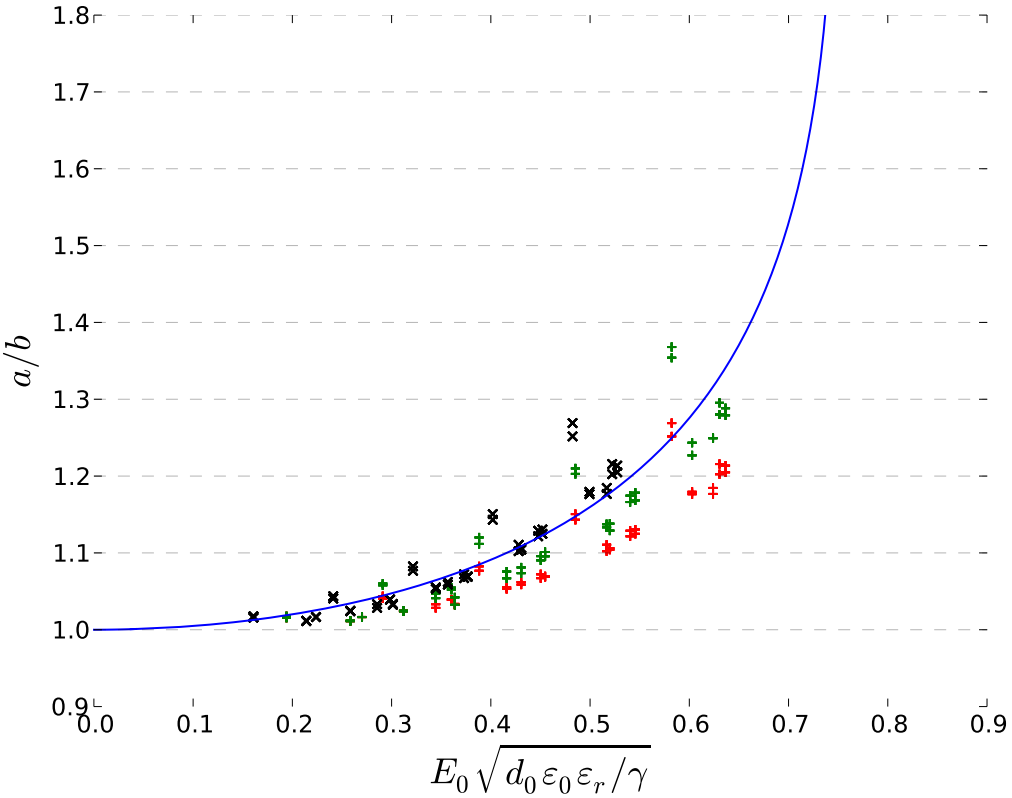

Figure 50: Oil: D, Temperature: 50 °C.

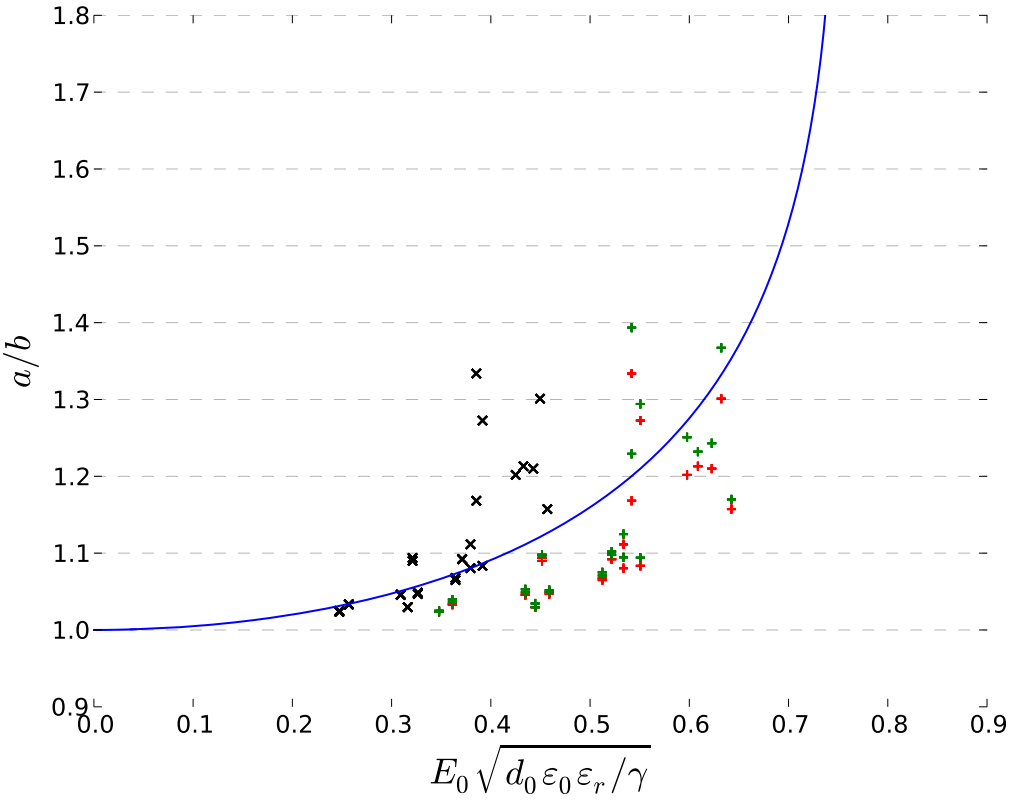

Figure 51: Oil: DE, Temperature: 21.5 °C.

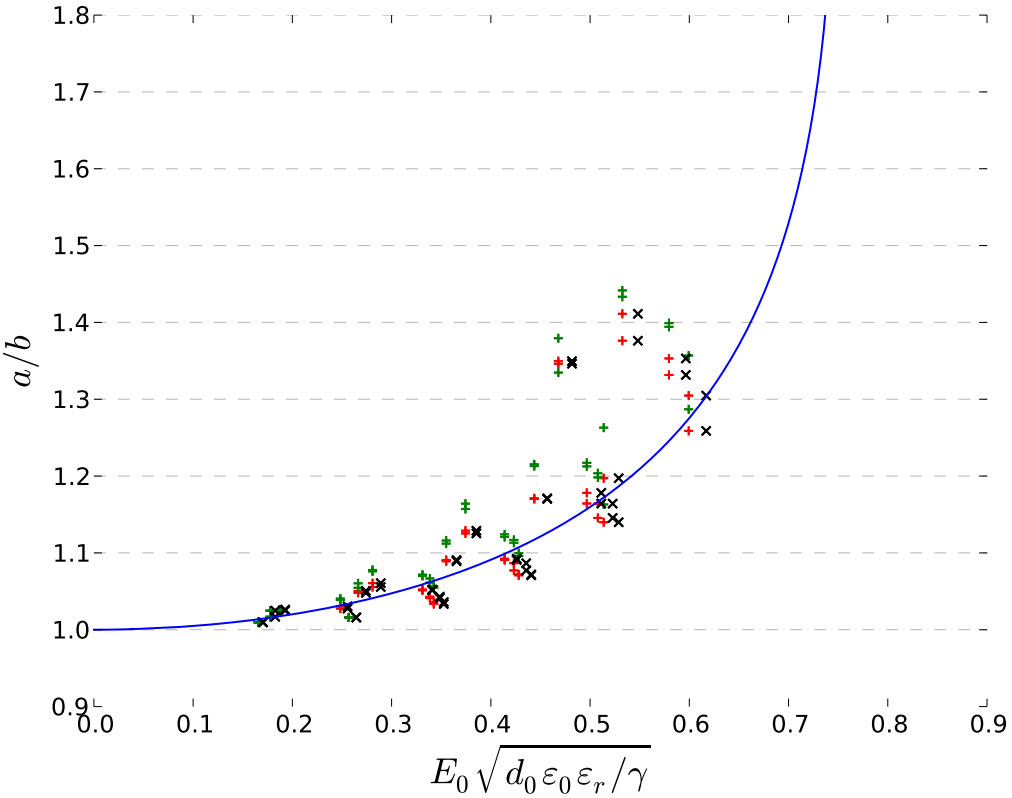

Figure 52: Oil: DE, Temperature: 50 °C.

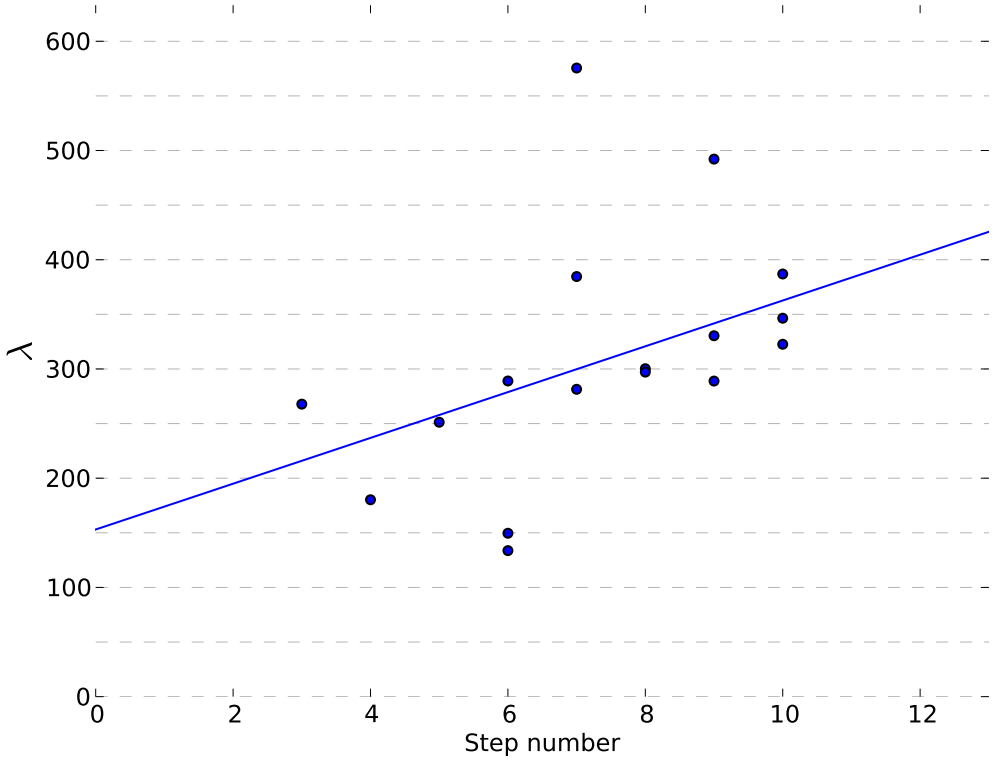

Figure 53: Oil: Marcol, Temperature: 21.5 °C.

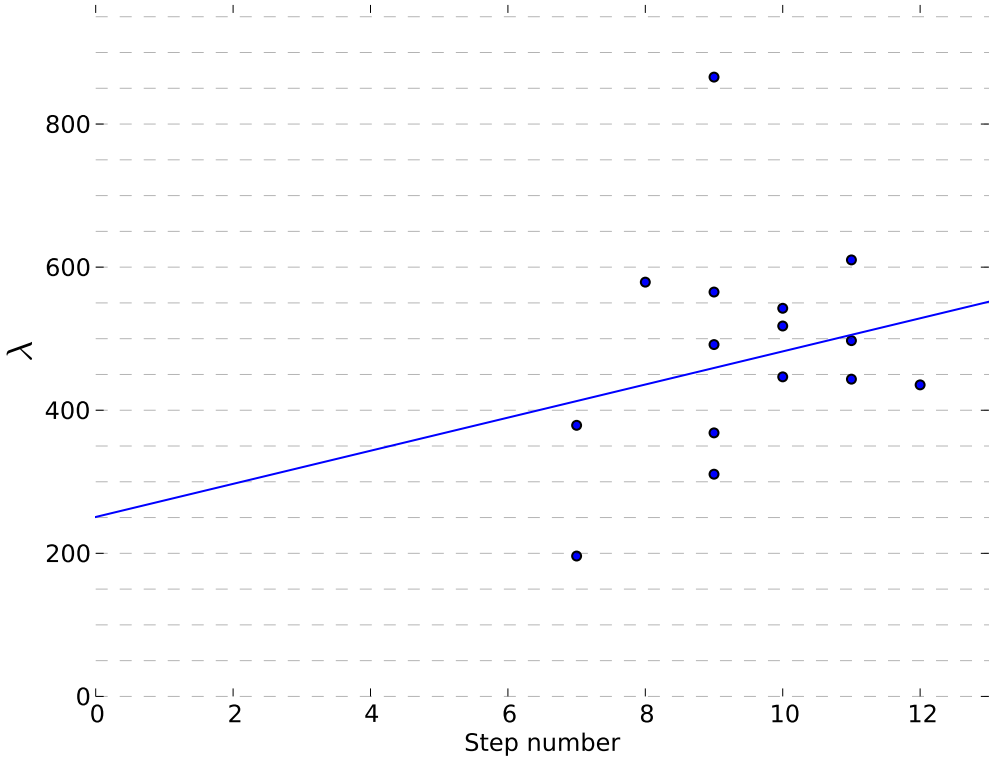

Figure 54: Oil: Marcol, Temperature: 50 °C.

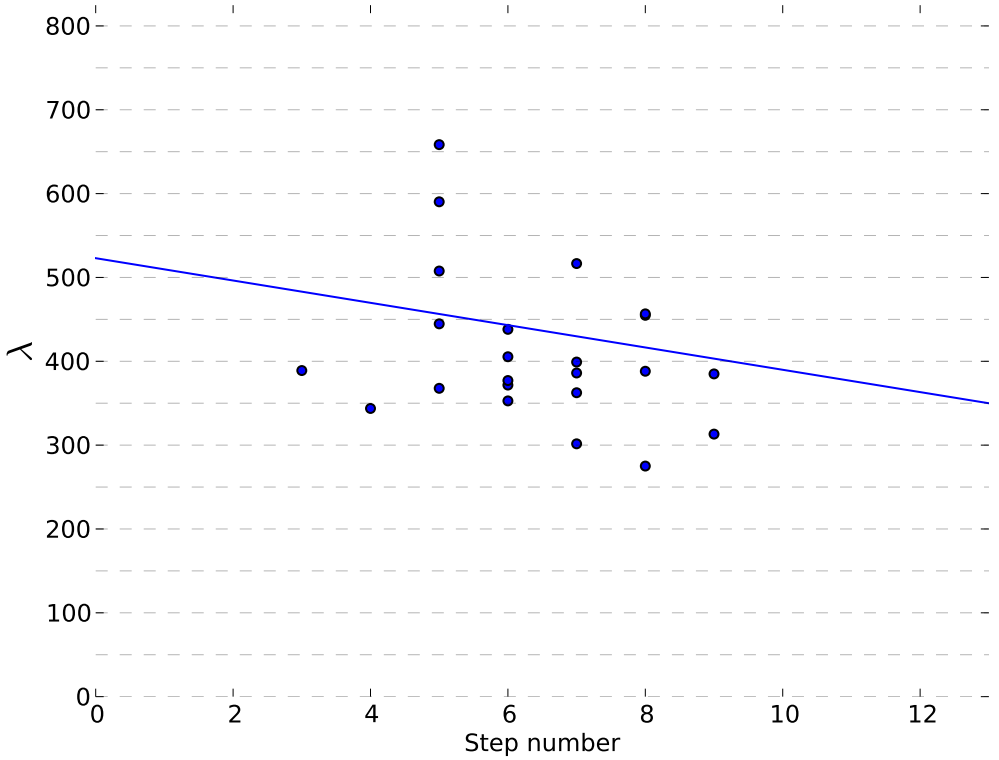

Figure 55: Oil: A, Temperature: 21.5 °C.

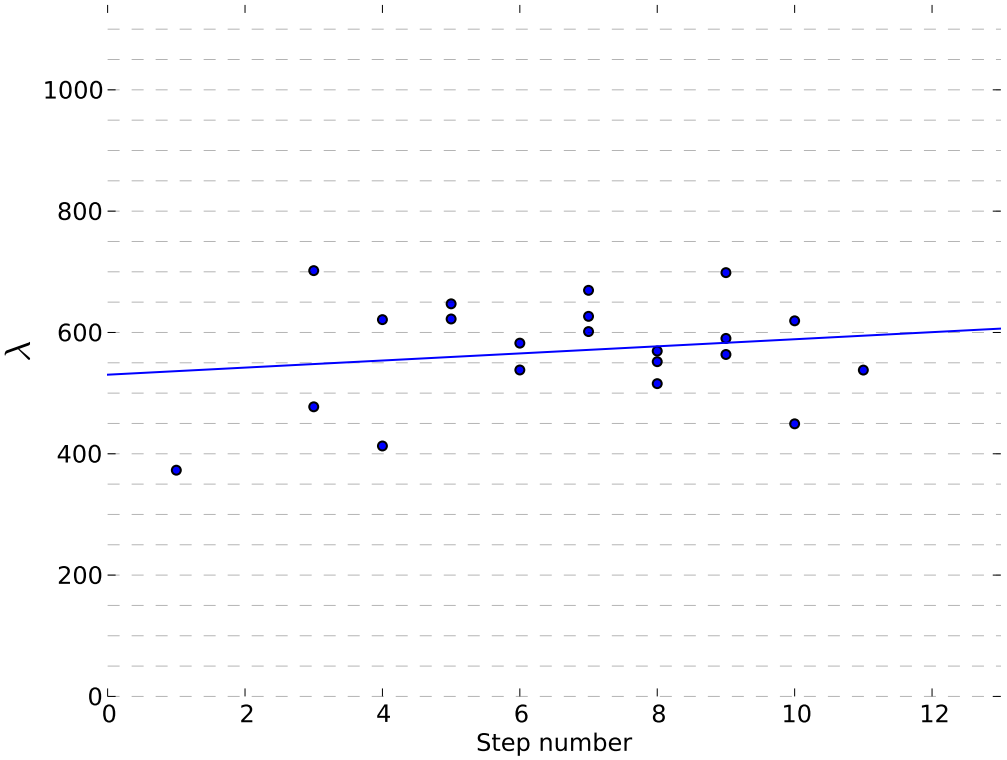

Figure 56: Oil: A, Temperature: 50 °C.

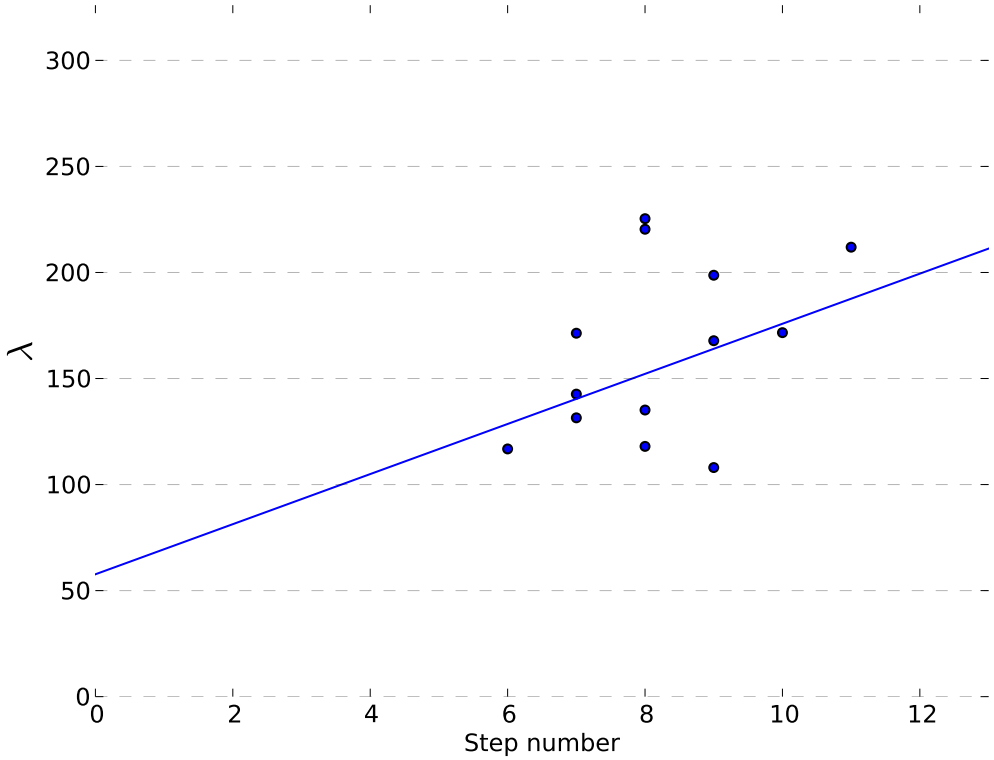

Figure 57: Oil: D, Temperature: 21.5 °C.

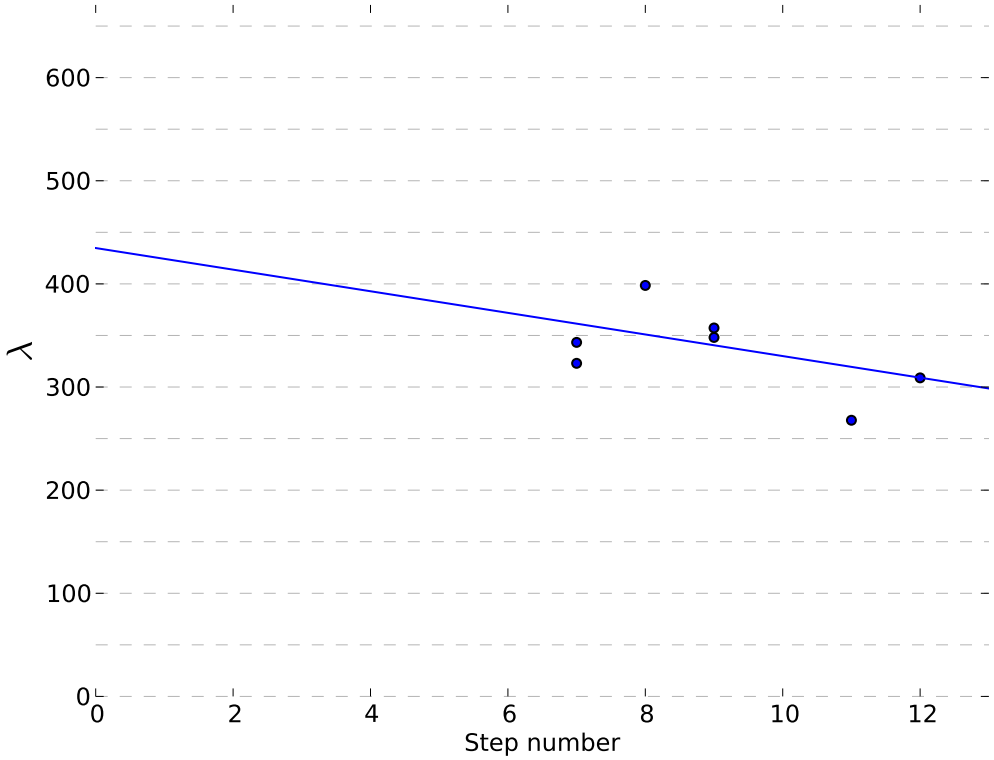

Figure 58: Oil: D, Temperature: 50 °C.

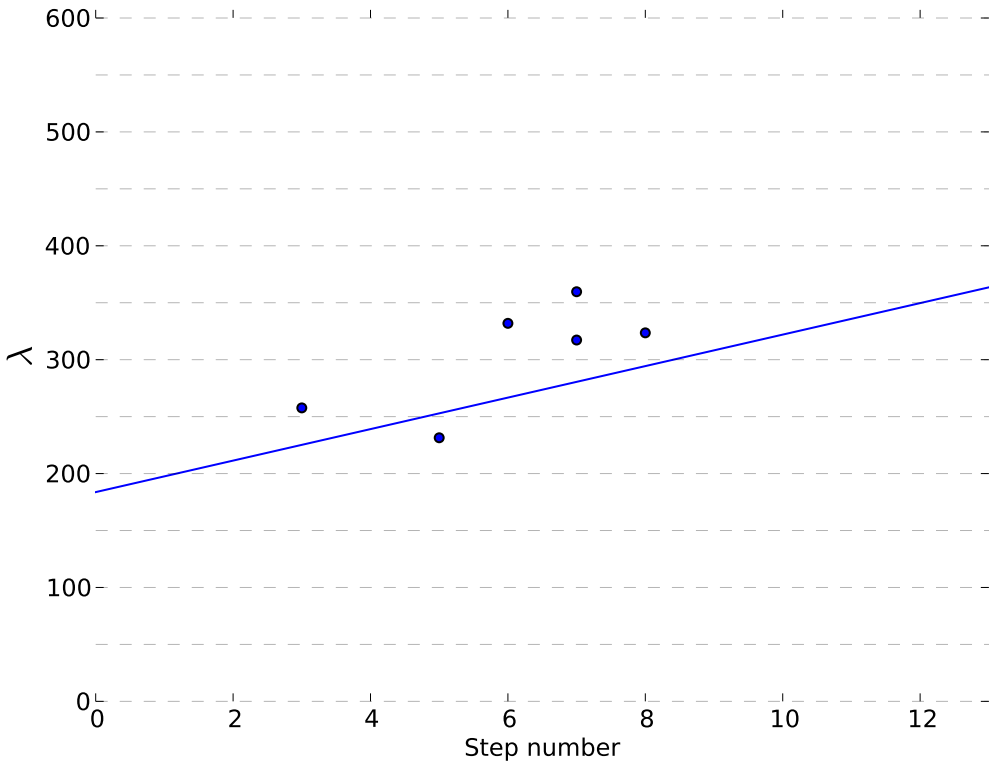

Figure 59: Oil: DE, Temperature: 50 °C.

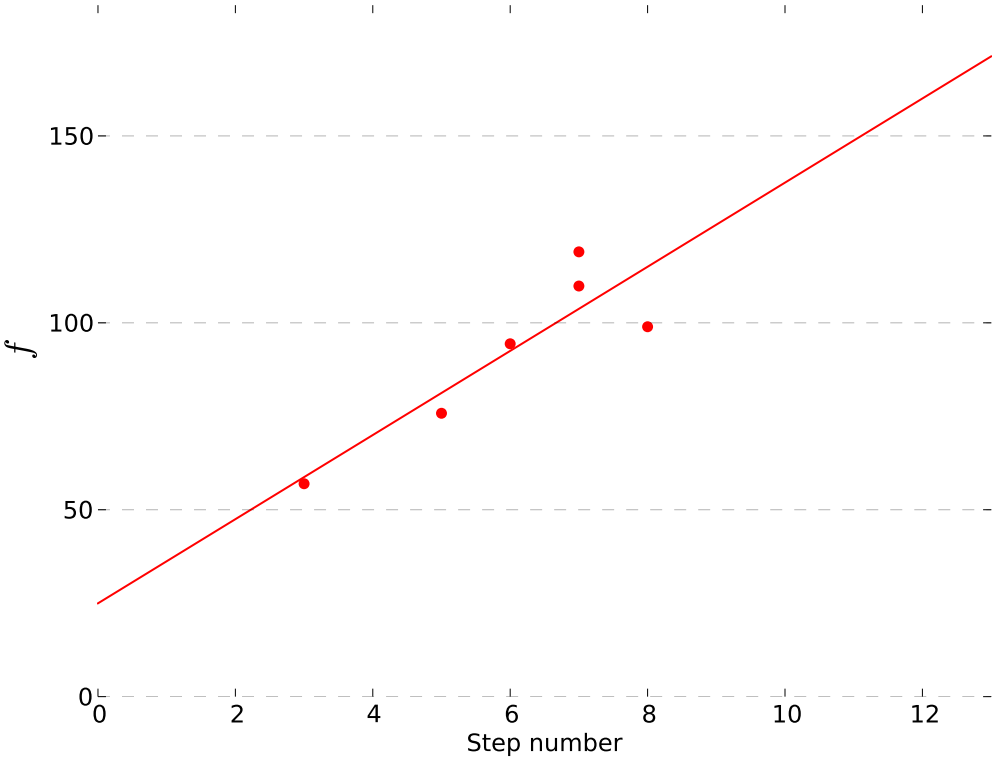

Figure 60: Oil: DE, Temperature: 50 °C.

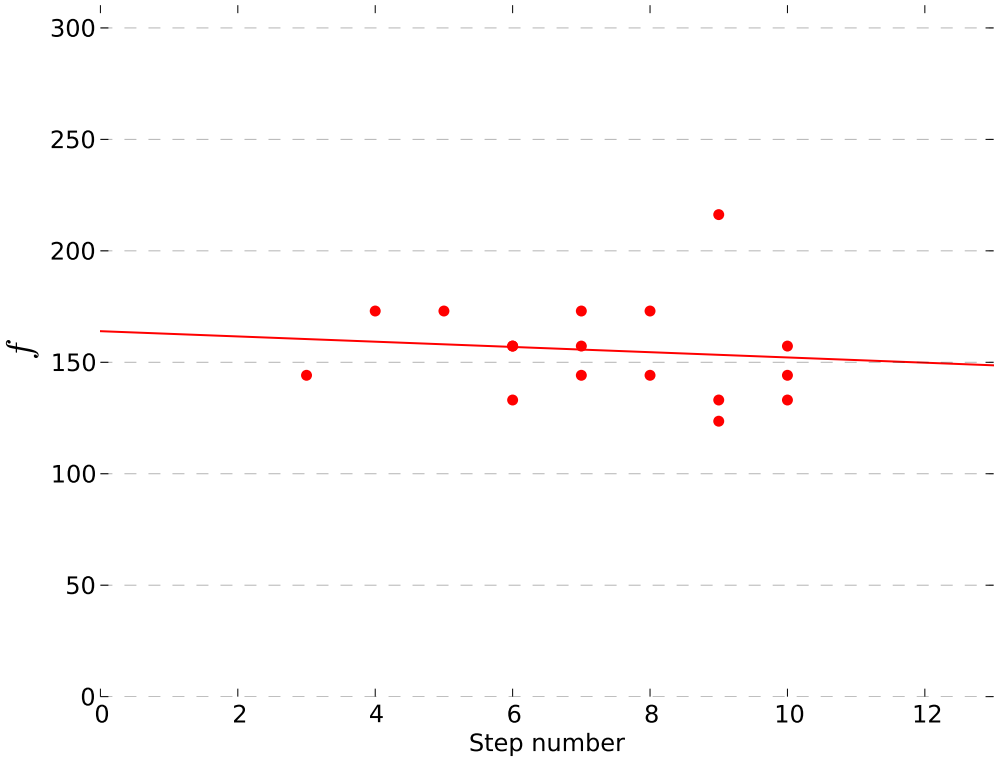

Figure 61: Oil: Marcol, Temperature: 21.5 °C.

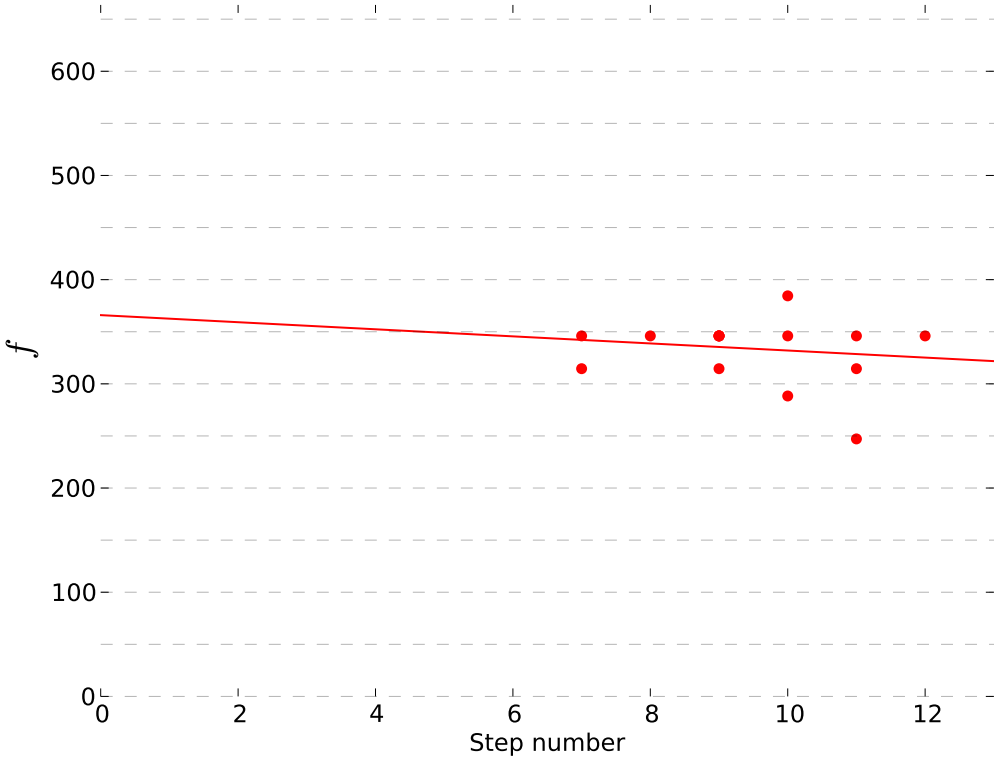

Figure 62: Oil: Marcol, Temperature: 50 °C.

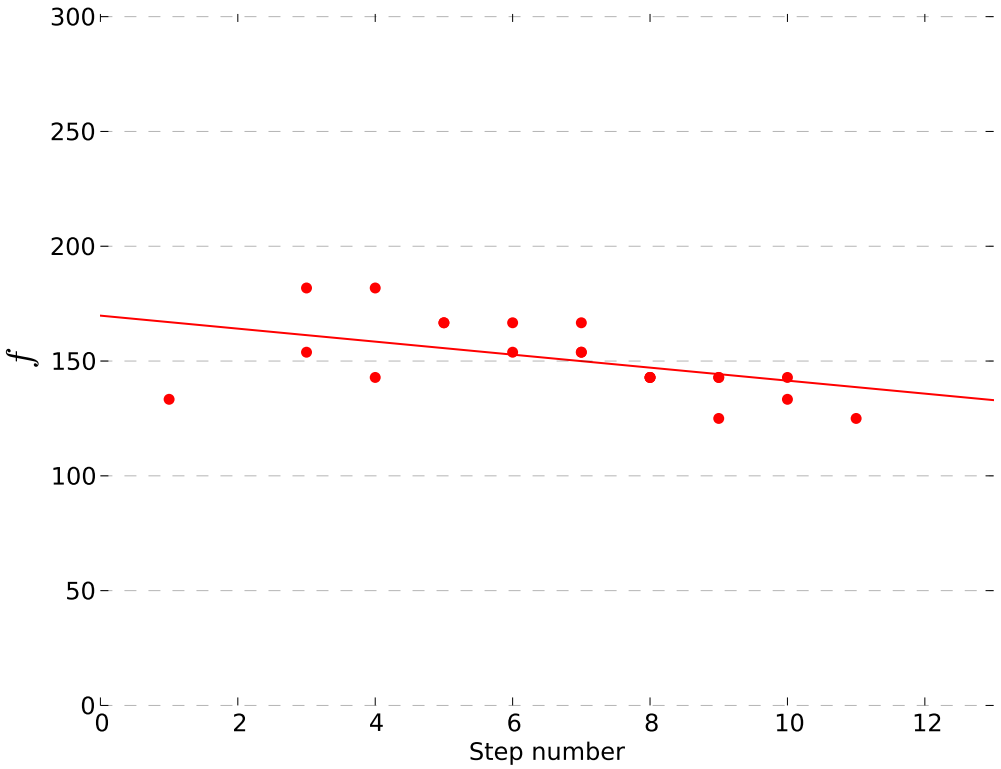

Figure 63: Oil: A, Temperature: 50 °C.

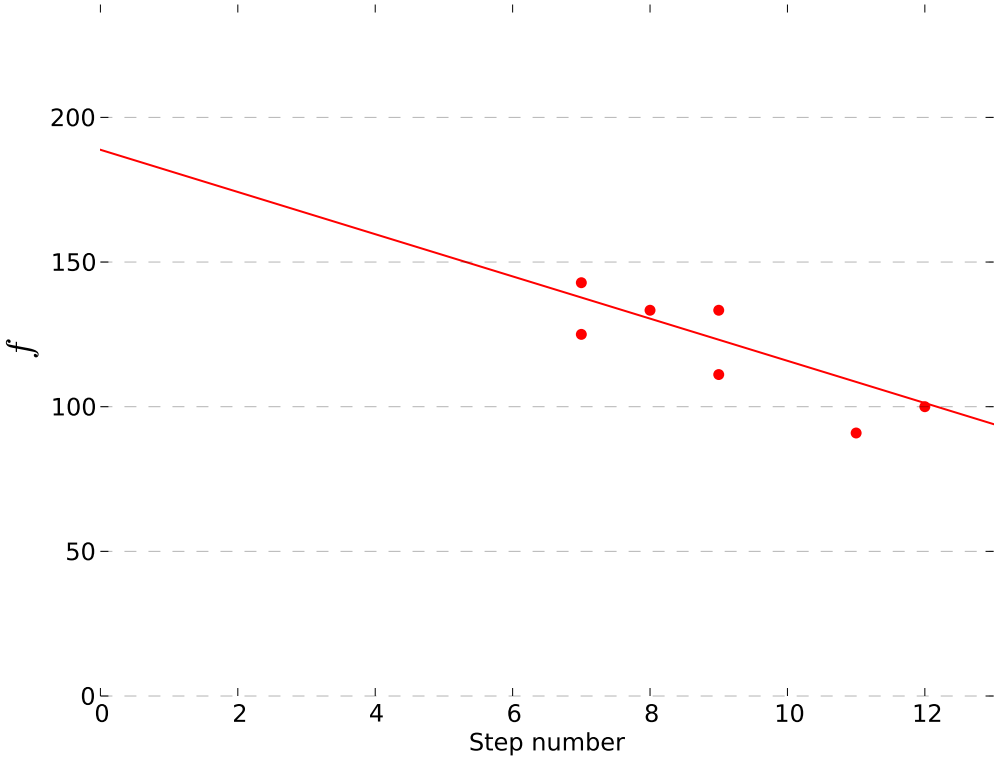

Figure 64: Oil: D, Temperature: 50 °C.

Marcol

Stable deformation

The behavior of the stable deformations was very close to theoretical values. For lower values of field strength, and thus smaller deformations the maximal and stable deformations become indistinguishable and tend to fit very well with the theory. For higher field strengths the fit is worse. The results are similar for 21.5 °C and 50 °C, although the results seem to fit better with the theory for lower temperatures The electric field strength could be the explanation, or the surface tension of the drops could be dependent on temperature. The effective surface tensions were 23.2 mN/m and 28.7 mN/m for respectively 21.5 °C and 50 °C. The results can be seen in Figure 43 and Figure 44.

Damping coefficient

The damping coefficient of the deformation oscillations show a tendency of growing with each time step. It is important to note that as time increases so does the field strength and deformation. This might be a bigger contribution than just the number of previous pulses. The average values for 21.5 °C and 50 °C are respectively $310\,s^{-1}$ and $483\,s^{-1}$. The results can be seen in Figure 53 and Figure 54.

Oscillation frequency

The frame rate of the films is not very much higher than the frequency of drop oscillations. This makes it impossible to measure the oscillation's period precisely, and is the reason why the frequencies found are comprised of only a few different values, most visibly at 50 °C. Because of this, small changes in frequency will not be detectable. No change can be said to be found in the frequency of the oscillations. As for constant voltage, there is a difference in average frequency between the two temperatures. For 21.5 °C and 50 °C they are respectively 155 Hz and 332 Hz. The results can be seen in Figure 61 and Figure 62.

Oil A

Stable deformation

The behavior of the stable deformations was close to the theoretical values. The results do however show a difference between 21.5 °C and 50 °C. While deformations at lower temperatures are very close to the theoretical values, the results for higher temperatures show more spread aspect ratios slightly below the theory. This suggests that heating the oil stiffens the droplets. These results are in concurrence with those of the constant voltage experiments. The effective surface tensions were 24.9 mN/m and 34.4 mN/m for respectively 21.5 °C and 50 °C. The results can be seen in Figure 45 and Figure 46.

Damping coefficient

Oil A shows similar results for increasing voltages as for constant. Coefficients

for both temperatures seem fairly constant, but with a wide variations of values, especially for 21.5 °C. The damping coefficient is higher at the highest of the temperatures, as before. Average coefficients are $412\,s^{-1}$ and $570\,s^{-1}$ for 21.5 °C and 50 °C respectively. The results can be seen in Figure 55 and Figure 56.

Oscillation frequency

As for constant voltages, at 21.5 °C there were not enough plainly visible oscillations to extract a result, as the deformations seemed to exhibit critical, or near critical damping. The average is 151 Hz for 50 °C. The results can be seen in Figure 63.

Oil C

Stable deformation

The behavior of the stable deformations stayed well below the theoretical values for both temperatures tested. The results do show a slight difference between 21.5 °C and 50 °C. While both are below the theoretical values, the results from the higher temperature show the smallest deformations. This suggests that heating the oil stiffens the droplets. These results are opposite to those from constant voltages. The results from the experiments with increasing voltages were not very good, and showed a wide spread of results and many unusable results. This was a problem for all experiments with oil C. The effective surface tensions were 54.9 mN/m and 77.9 mN/m for respectively 21.5 °C and 50 °C. The results can be seen in Figure 47 and Figure 48.

Damping coefficient

Due to the viscosity and opacity of oil C, damping coefficients were not possible to detect for increasing voltages. This was similar as for constant voltage

Oscillation frequency

As no oscillations were detected, no values for oscillation frequencies could be measured or calculated. These results fit well with those of the sinusoidal voltages. Figure 15 and Figure 16 would also suggest that the droplets are overdamped.

Oil D

Stable deformation

The results of stable deformations of oil D suggest that the higher temperature leads to softer droplets, allowing it to stretch further with the same electric field. These results agree with those from constant voltage. The effective surface tensions were 53.8 mN/m and 35.7 mN/m for respectively 21.5 °C and 50 °C. The results can be seen in Figure 49 and Figure 50.

Damping coefficient

Oil D also shows increased damping coefficients for higher temperatures.

Nothing can really be said about changes because of previous deformations. Average coefficients are $163\,s^{-1}$ and $335\,s^{-1}$ for 21.5 °C and 50 °C respectively. The results can be seen in Figure 57 and Figure 58.

Oscillation frequency

At 21.5 °C there were not enough plainly visible oscillations to extract a result. For 50 °C the average was 120 Hz. The results show a strong decrease in frequency over time, but as only 7 deformations showed clear enough oscillations, these result are not very convincing. The results can be seen in Figure 64.

Oil D with demulsifier

Stable deformation

The stable deformations for oil D with demulsifier and increasing voltages stayed around theoretical values for 21.5 °C and 50 °C. This is somewhat misleading as all 5 droplets at 21.5 °C initially showed lower than expected deformations, but eventually disintegrated. For the droplets at 50 °C this happened in 2 of 5 experiments. The effective surface tensions were 48.4 mN/m and 23.1 mN/m for respectively 21.5 °C and 50 °C. The results can be seen in Figure 51 and Figure 52.

Damping coefficient

There were not enough visible exponential decays in the data gathered from the experiments of oil D with demulsifier for increasing voltages. For 50 °C some damping coefficients could be found. These were still not enough to give a confident conclusion. The average coefficient for 50 °C is $304\,s^{-1}$. The results can be seen in Figure 59.

Oscillation frequency

As with the damping coefficients, no oscillations could be detected for 21.5 °C. The few oscillations found at 50 °C give an average oscillation frequency of 92 Hz. The results can be seen in Figure 60.

6.4 Decreasing square waves

Figures 65-74 show the AR for for transient oscillations with decreasing voltage amplitude compared to the theoretical model Eq. (56). Red marks stable AR's, green marks maximum AR's, and black marks the best fit for stable AR's found by adjusting effective surface tension.

Figures 75-81 show the calculated damping coefficient for each square wave pulse with the closest linear fit.

Figures 82-86 show the observed oscillation frequency for each square wave pulse with the closest linear fit.

Table 15: Effective surface tensions in mN/m

Temp.\oil	Marcol	A	C	D	DE
21.5 °C	22.8	28.0	28.4	66.7	39.1
50 °C	32.2	32.7	22.6	38.1	20.5

Table 16: Damping coefficients for decreasing voltages in s^{-1}

Temp.\oil	Marcol	A	C	D	DE
21.5 °C	314	325	-	174	-
50 °C	414	526	-	279	247

Table 17: Oscillation frequencies for decreasing voltages in Hz

Temp.\oil	Marcol	A	C	D	DE
21.5 °C	147	-	-	-	-
50 °C	283	134	-	119	90

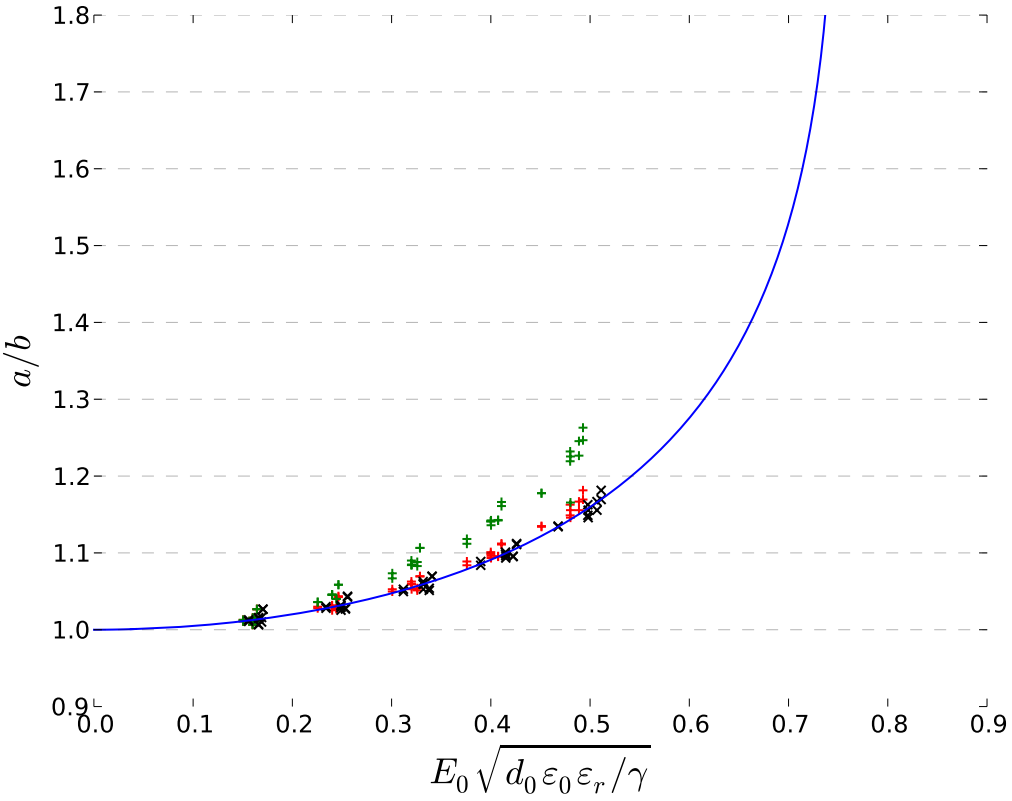

Figure 65: Oil: Marcol, Temperature: 21.5 °C.

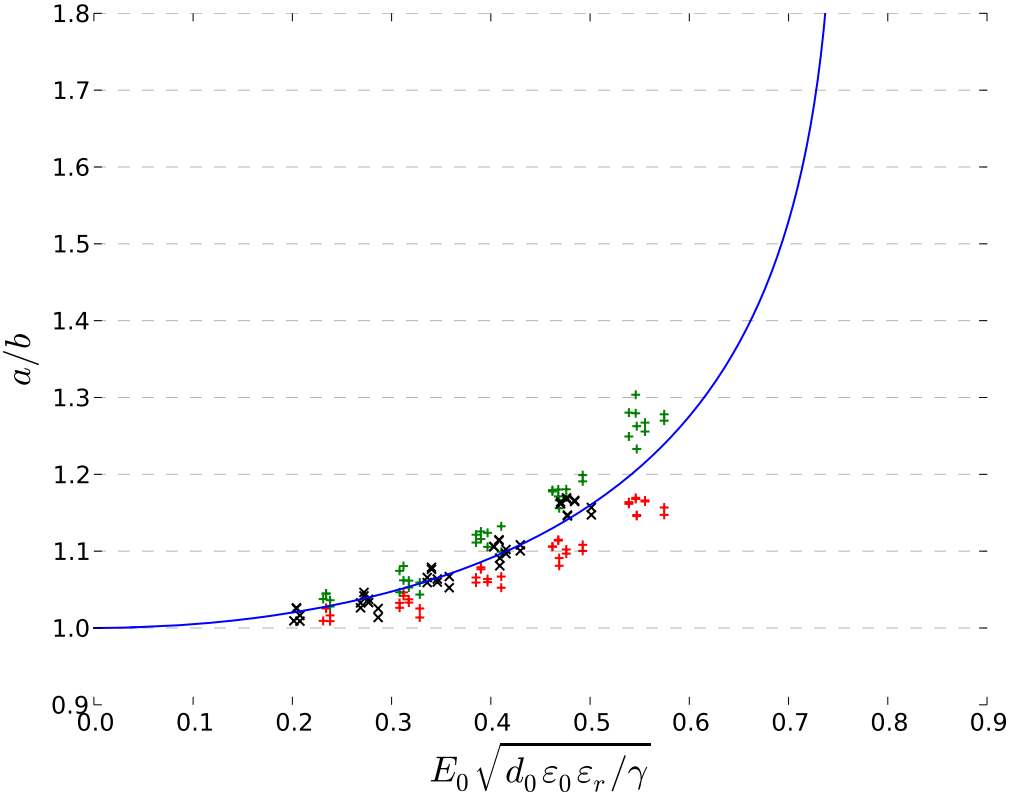

Figure 66: Oil: Marcol, Temperature: 50 °C.

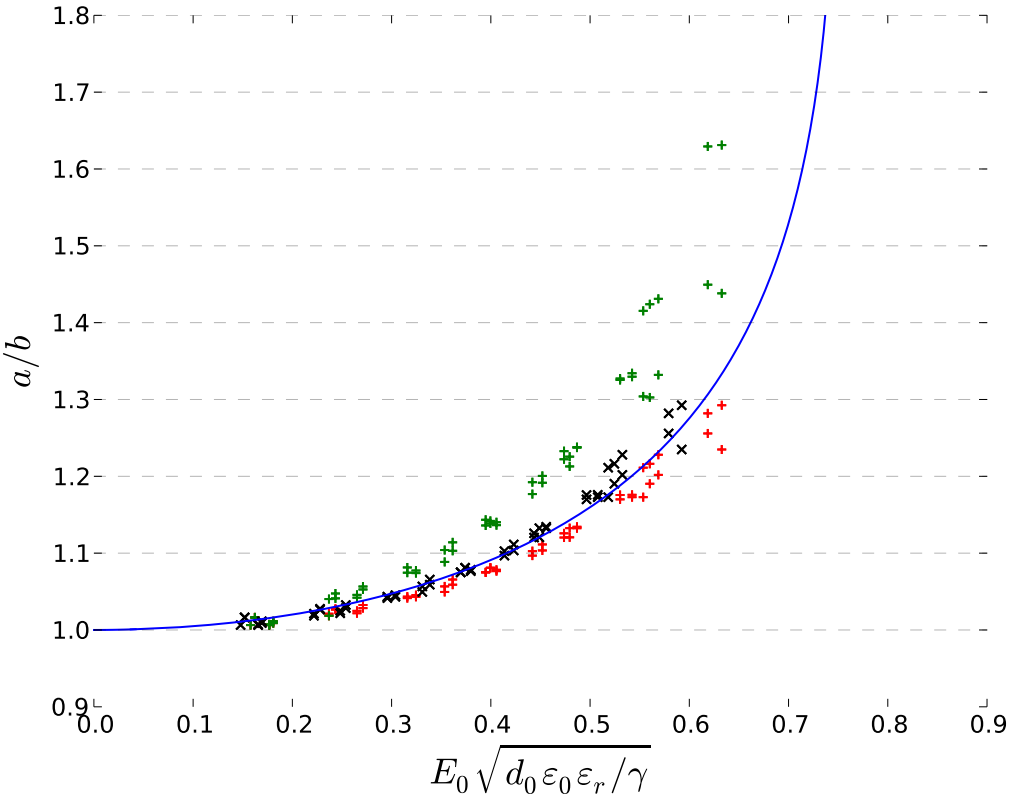

Figure 67: Oil: A, Temperature: 21.5 °C.

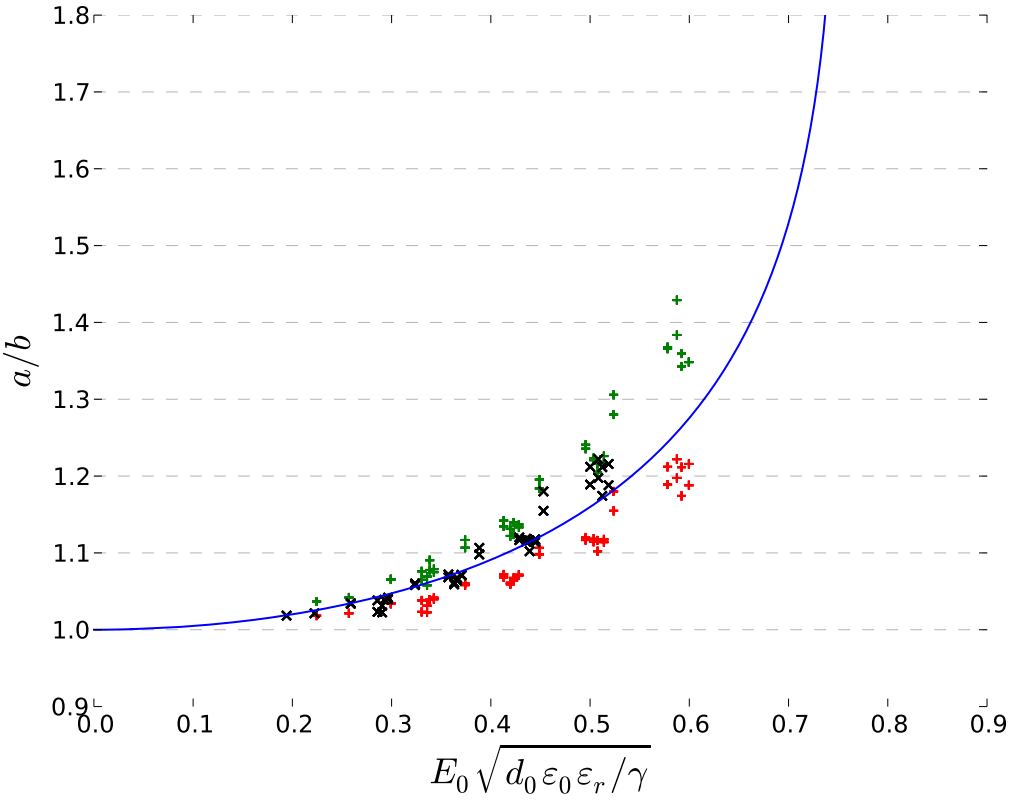

Figure 68: Oil: A, Temperature: 50 °C.

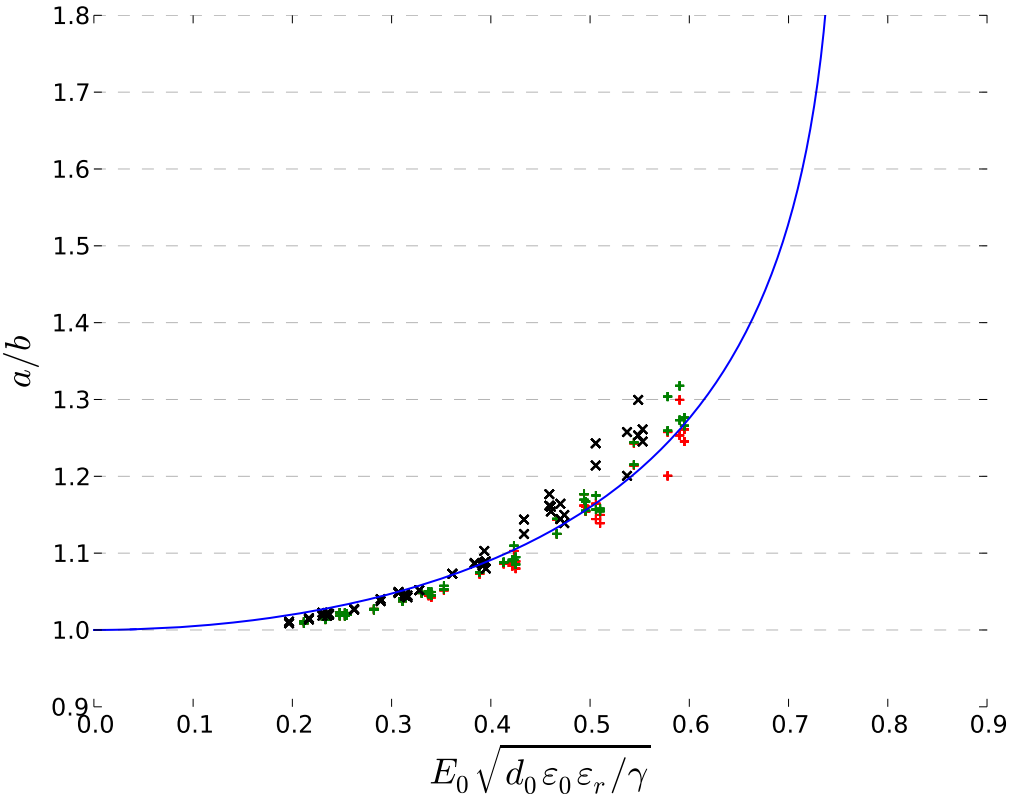

Figure 69: Oil: C, Temperature: 21.5 °C.

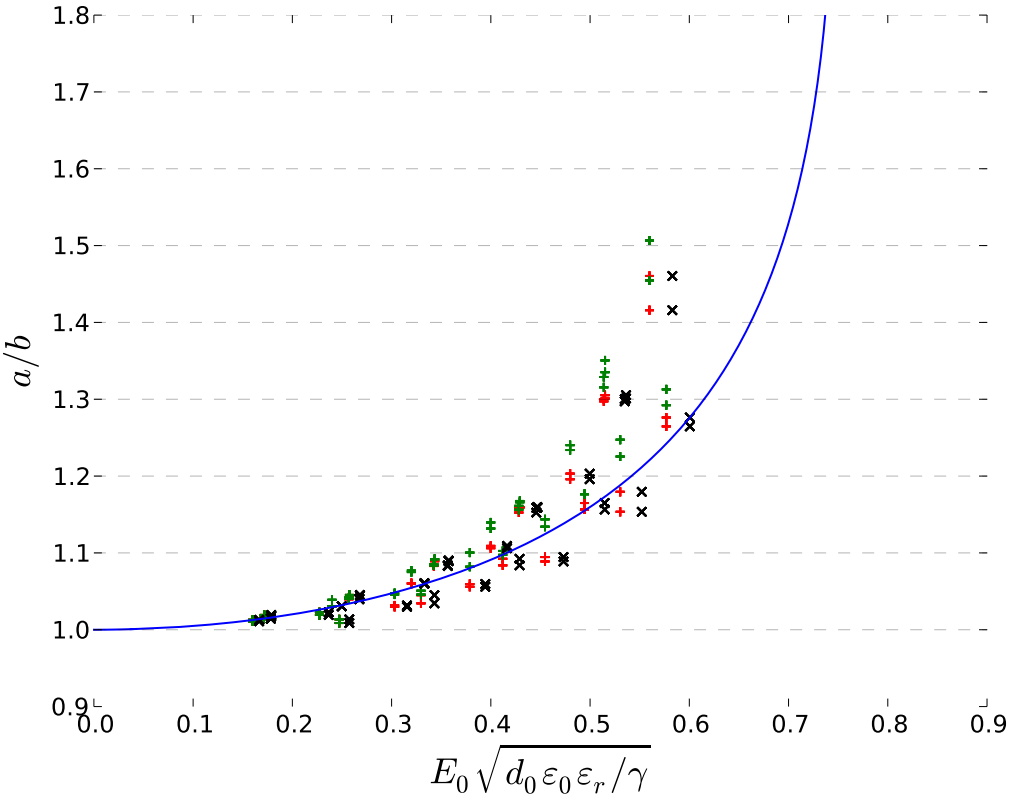

Figure 70: Oil: C, Temperature: 50 °C.

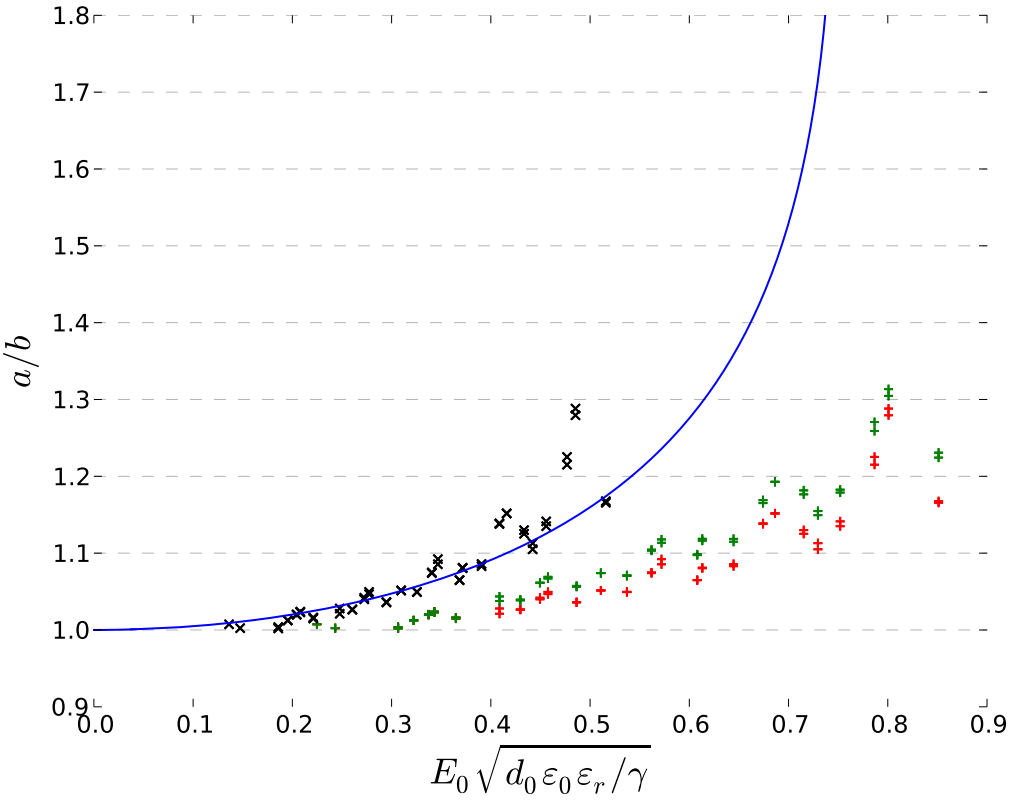

Figure 71: Oil: D, Temperature: 21.5 °C.

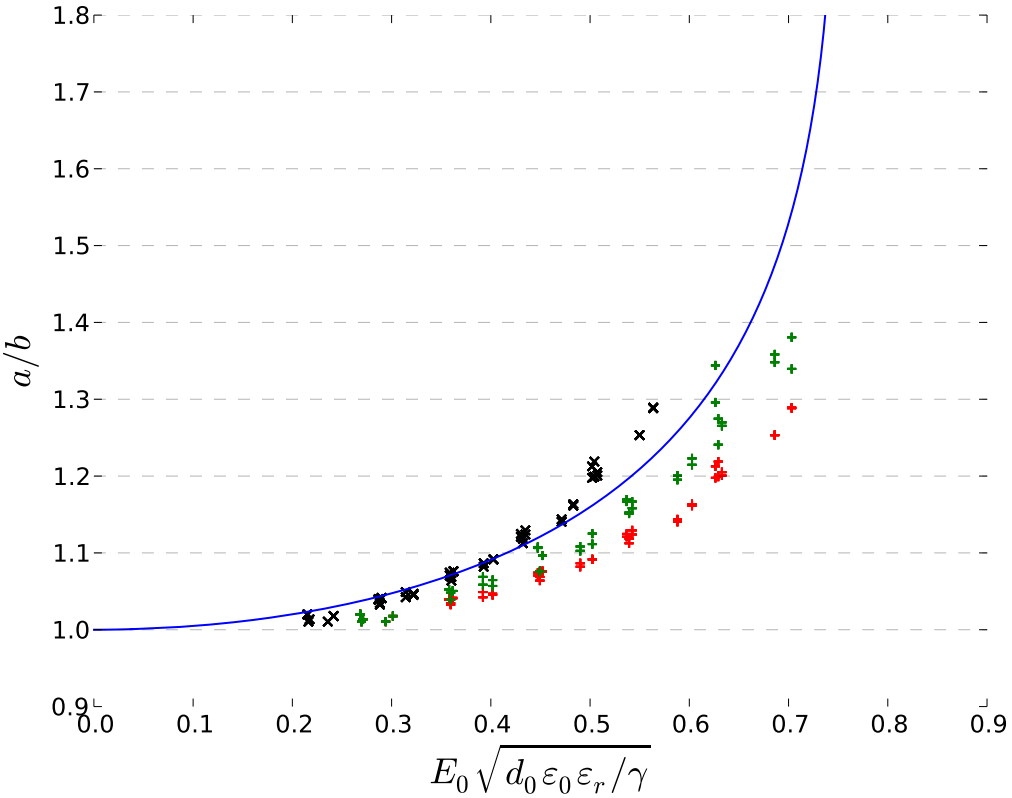

Figure 72: Oil: D, Temperature: 50 °C.

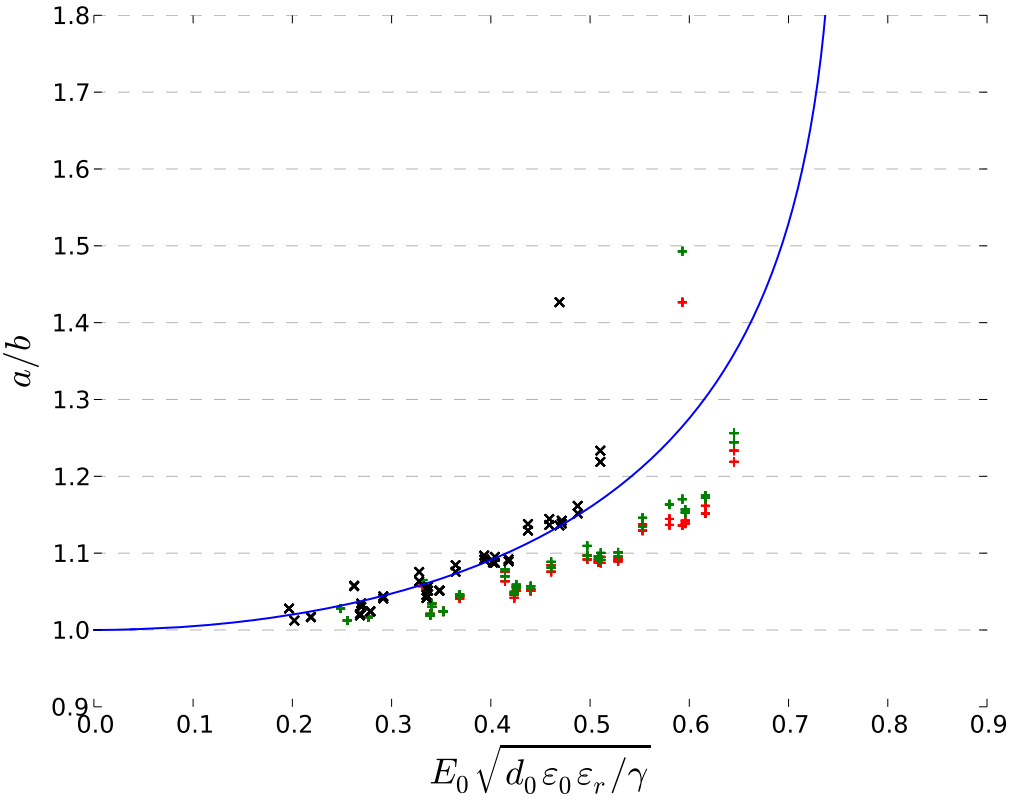

Figure 73: Oil: DE, Temperature: 21.5 °C.

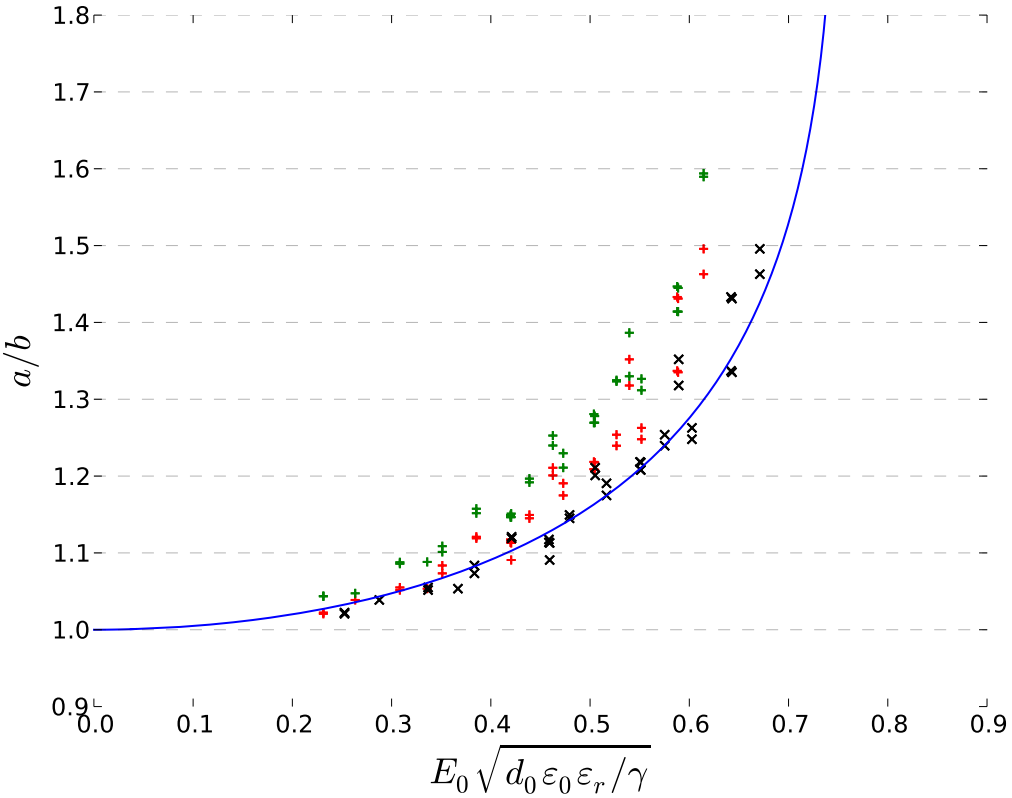

Figure 74: Oil: DE, Temperature: 21.5 °C.

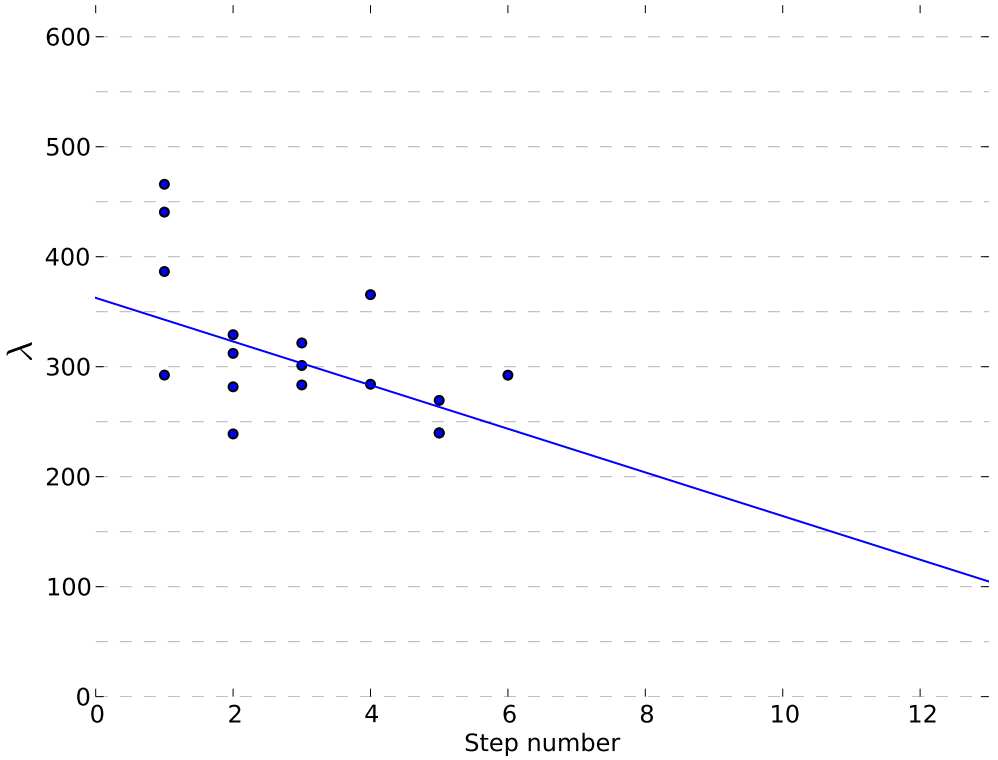

Figure 75: Oil: Marcol, Temperature: 21.5 °C.

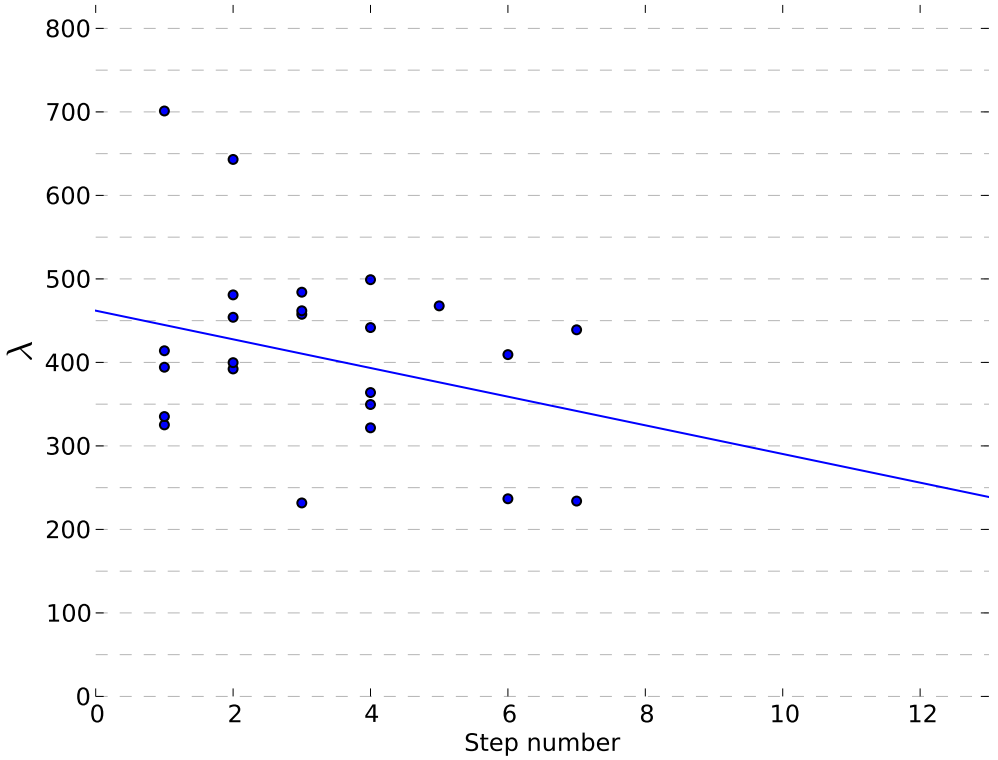

Figure 76: Oil: Marcol, Temperature: 50 °C.

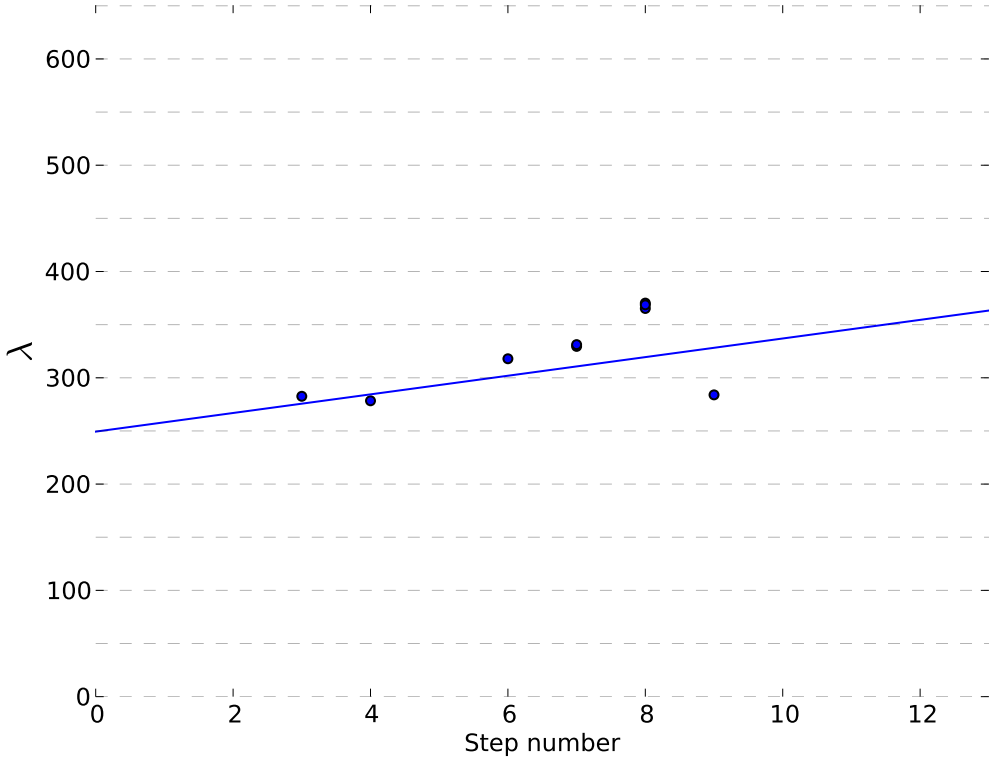

Figure 77: Oil: A, Temperature: 21.5 °C.

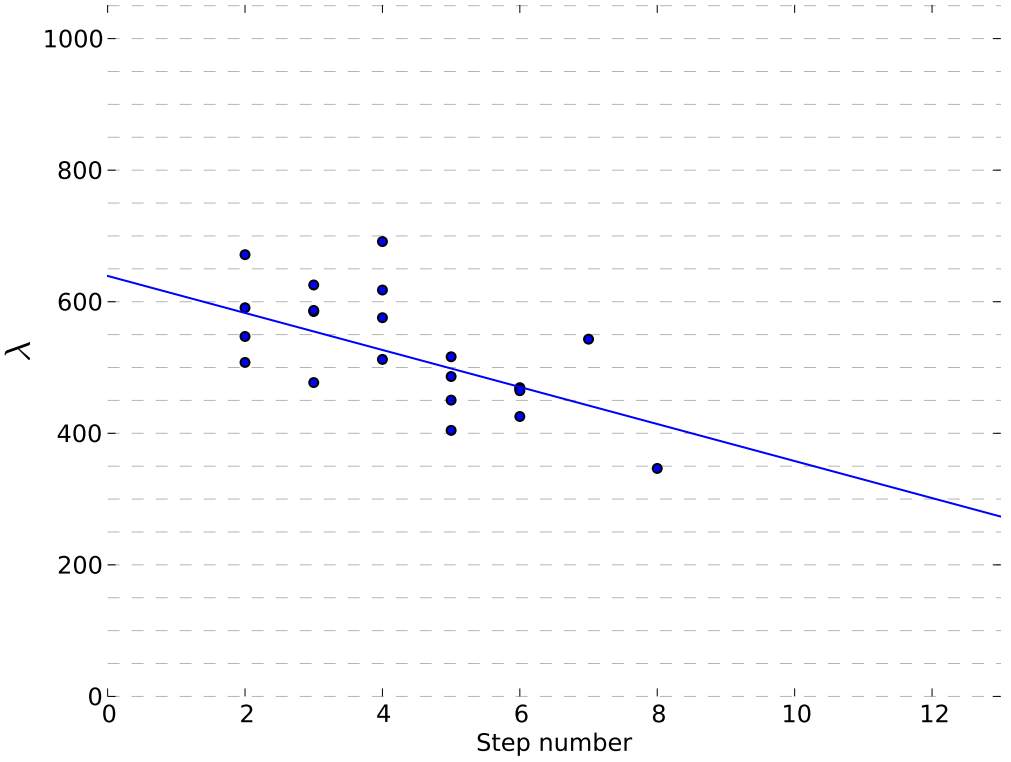

Figure 78: Oil: A, Temperature: 50 °C.

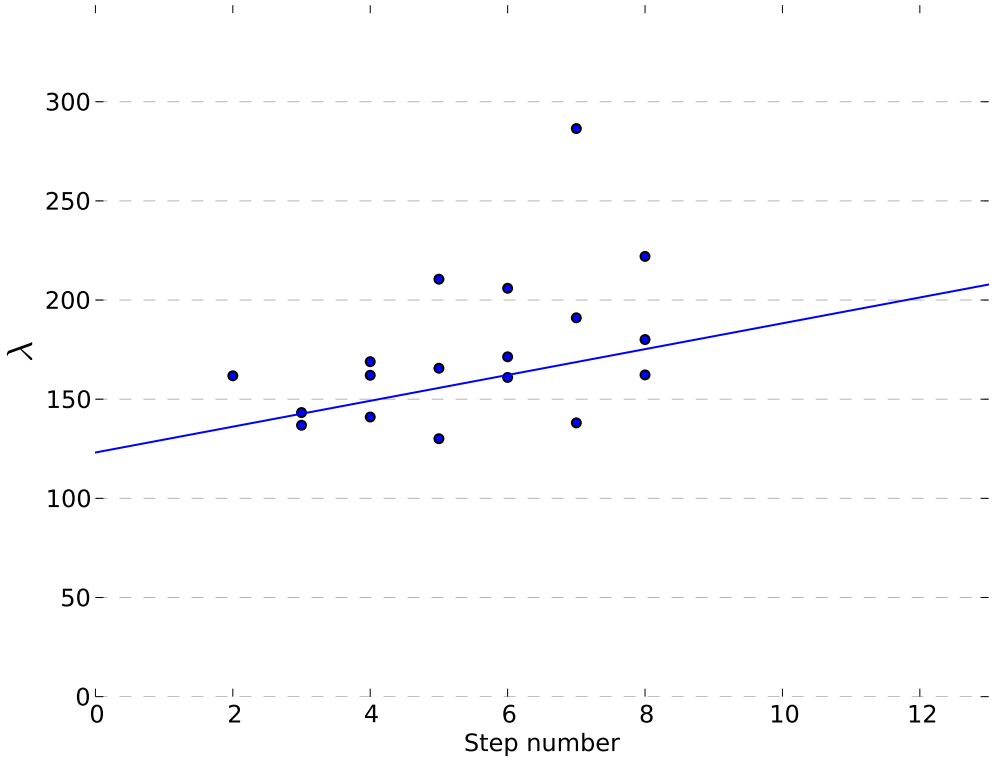

Figure 79: Oil: D, Temperature: 21.5 °C.

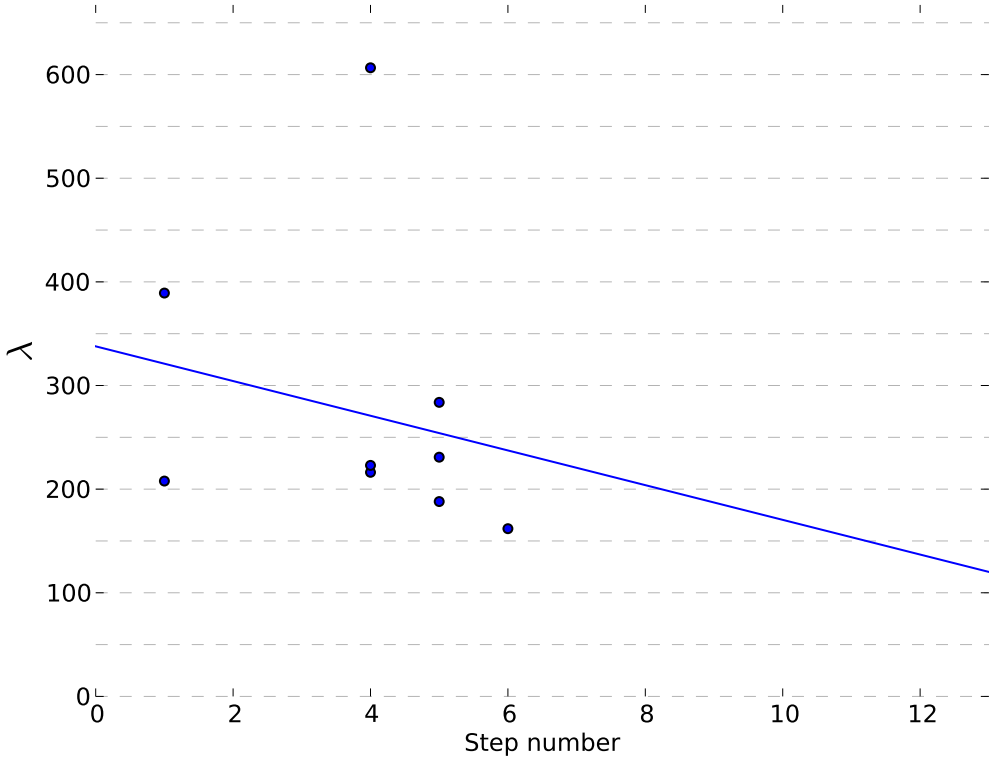

Figure 80: Oil: D, Temperature: 50 °C.

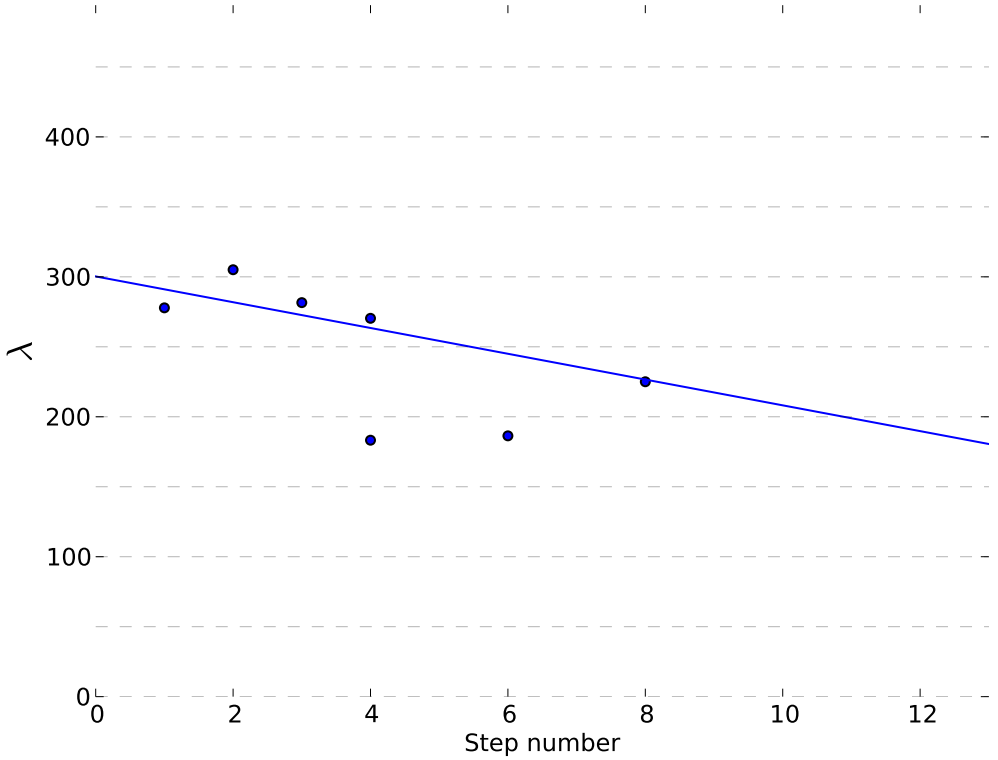

Figure 81: Oil: DE, Temperature: 50 °C.

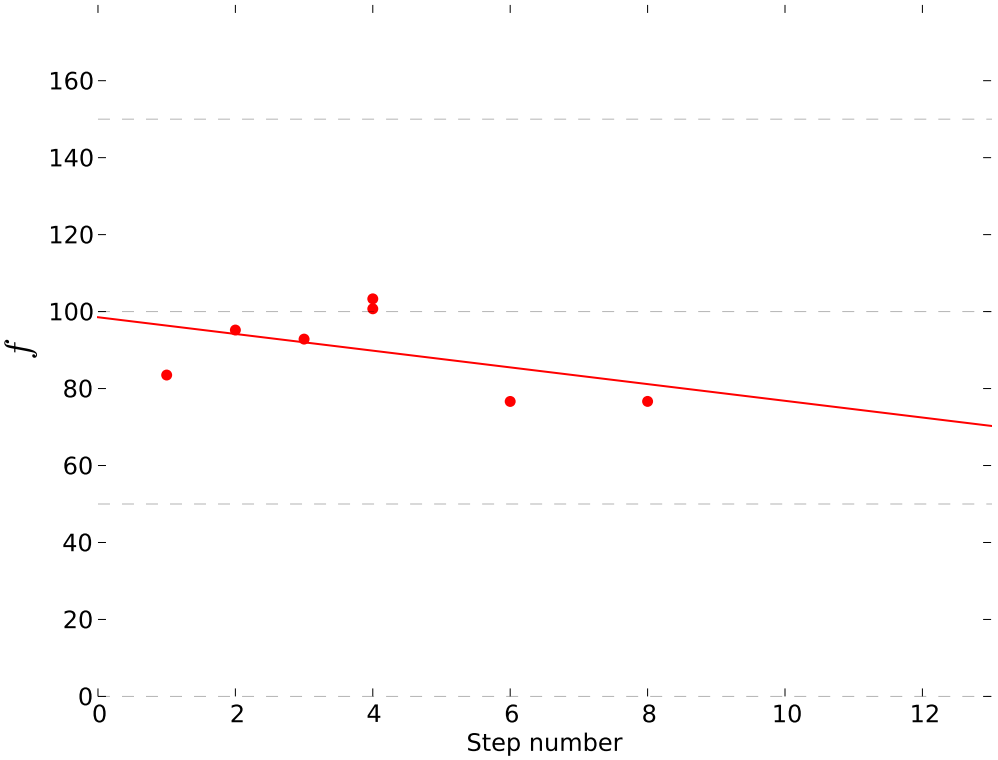

Figure 82: Oil: DE, Temperature: 50 °C.

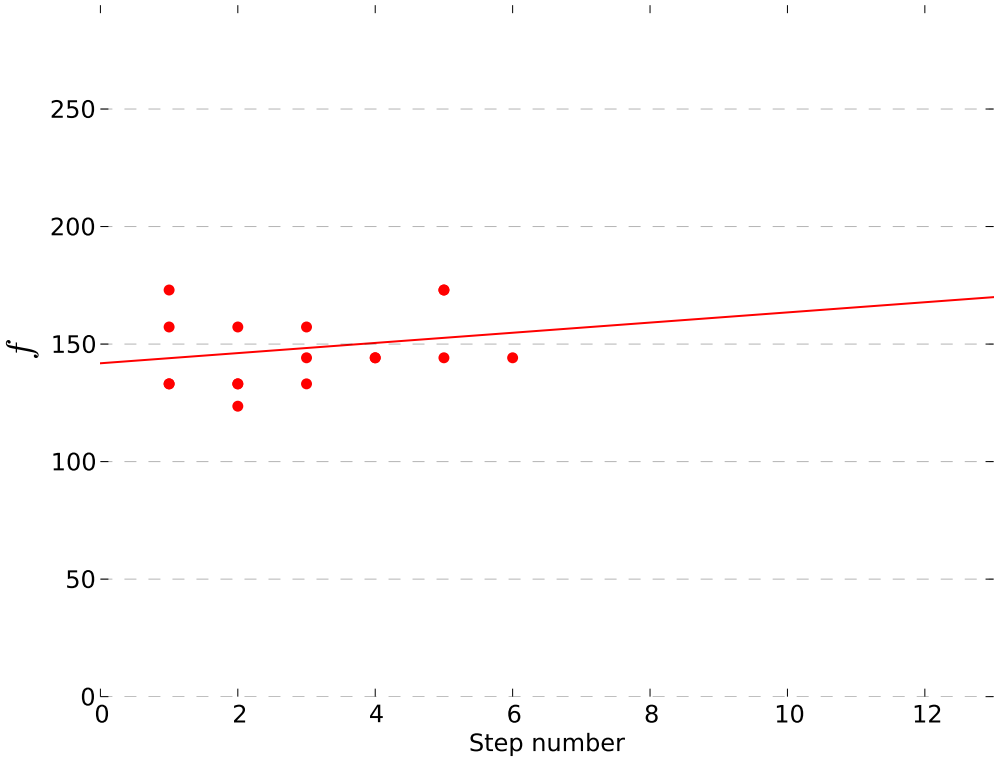

Figure 83: Oil: Marcol, Temperature: 21.5 °C.

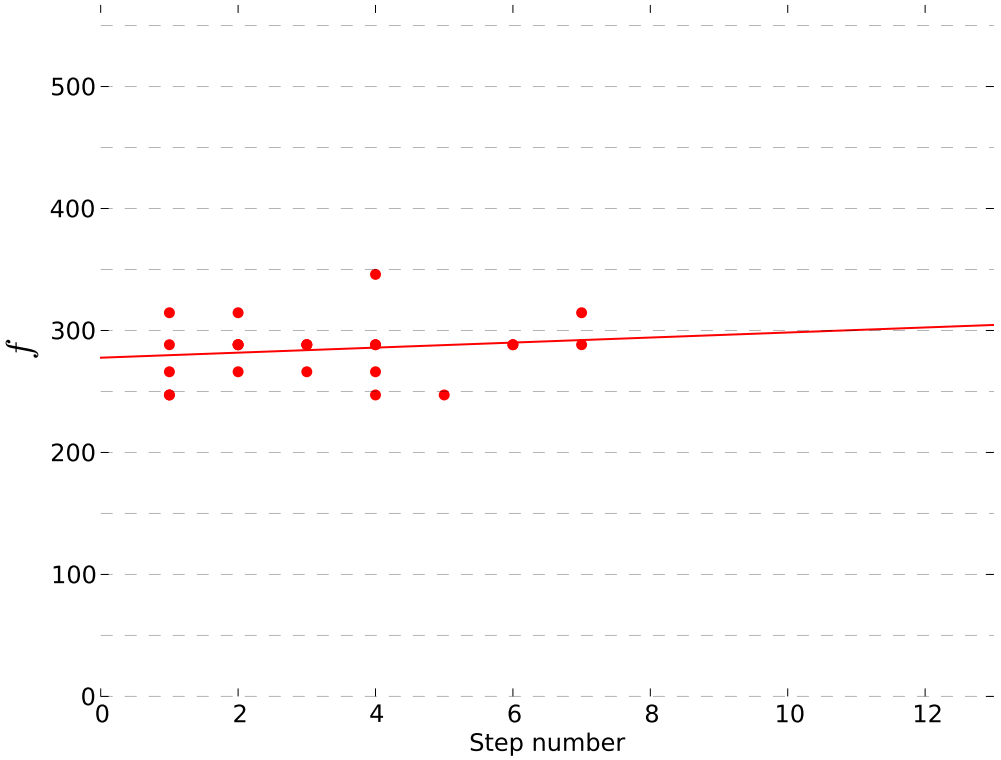

Figure 84: Oil: Marcol, Temperature: 50 °C.

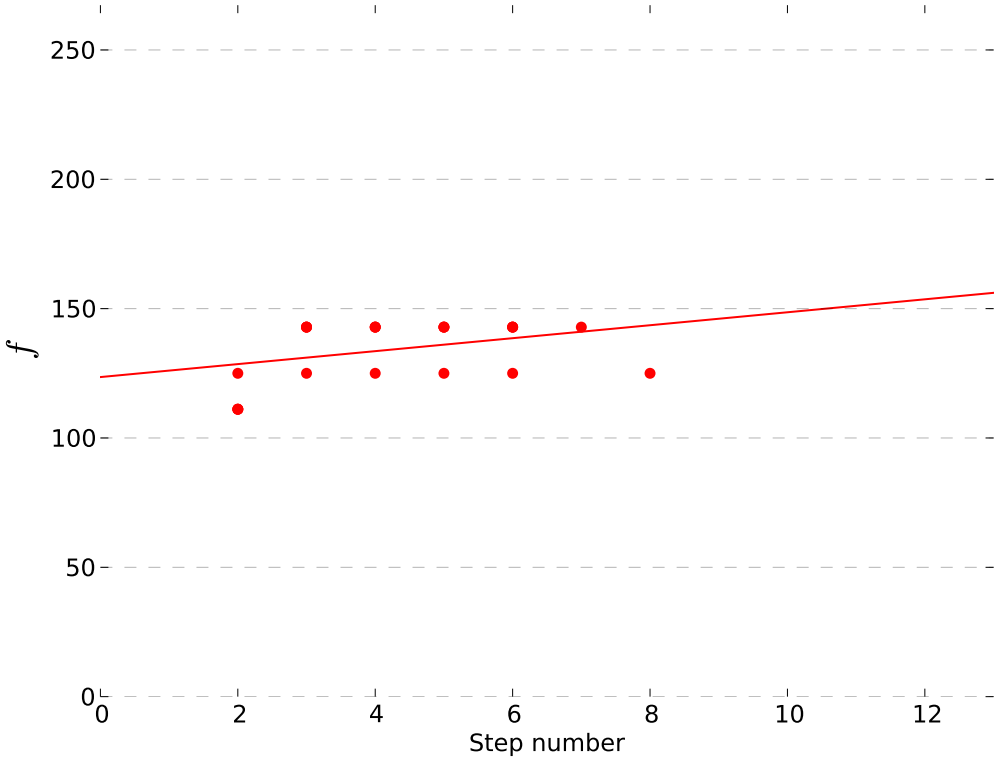

Figure 85: Oil: A, Temperature: 50 °C.

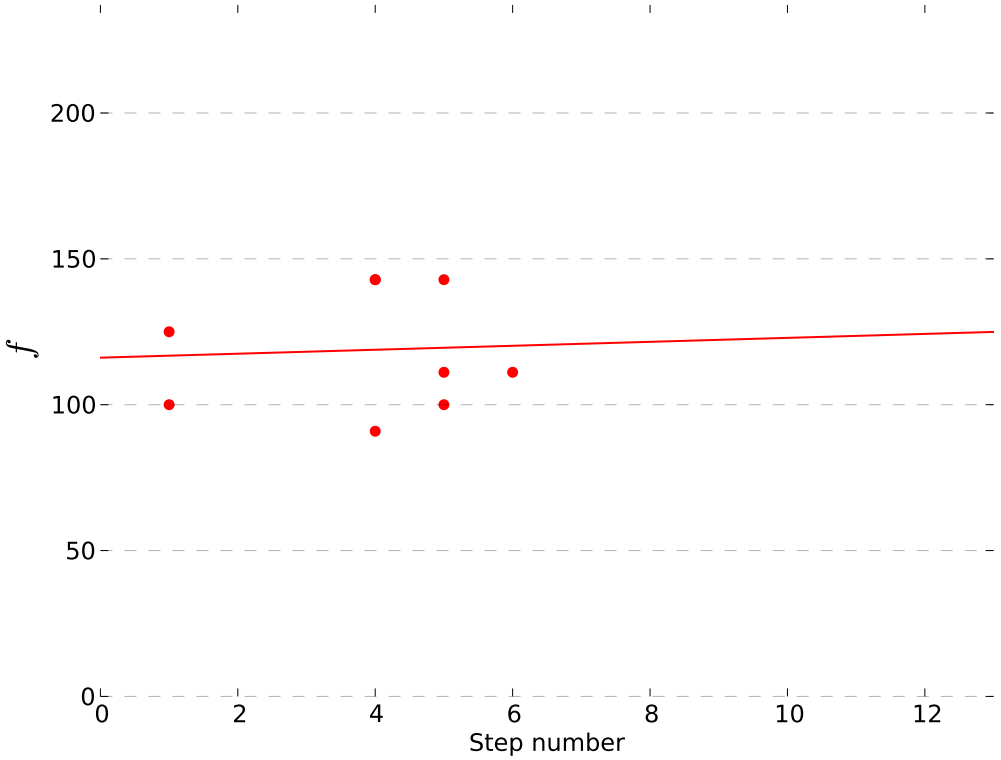

Figure 86: Oil: D, Temperature: 50 °C.

Marcol

Stable deformation

The behavior of the stable deformations was similar to that of the increasing voltage experiments, and close to theoretical values. As for increasing voltage, the results are similar for 21.5 °C and 50 °C, but seem to fit better with the theory for lower temperatures. The effective surface tensions were 22.8 mN/m and 32.2 mN/m for respectively 21.5 °C and 50 °C. The results can be seen in Figure 65 and Figure 66.

Damping coefficient

As for increasing voltage, the damping coefficient changes over time. In this case however it decreases. The rate of decrease is almost the same as for increasing voltages, only negative. This is true for both temperatures studied. This is another indication that the field strength and deformation are factors that affect the damping coefficient. The average values found for 21.5 °C and 50 °C are respectively $314\,s^{-1}$ and $414\,s^{-1}$. The results can be seen in Figure 75 and Figure 76.

Oscillation frequency

The same issues as with increasing voltage appear with decreasing voltage. The rate of change is in the opposite direction from the increasing voltage's frequency, but this looks rather coincidental and does not seem to indicate a real effect. As for the other two square pulse experiments, there is a difference in average frequency between the two temperatures. For 21.5 °C and 50 °C they are respectively 147 Hz and 283 Hz. The results can be seen in Figure 83 and Figure 84.

Oil A

Stable deformation

The behavior of the stable deformations was close to the theoretical values. The results do show a difference between 21.5 °C and 50 °C. The droplets at 50 °C are deformed slightly less. They seem to have stiffened due to the higher temperature as for increasing temperature and constant voltage experiments. This effect is not as pronounced as for increasing voltages. If the stretching of the droplets increase adsorption and this affects the stiffness of the droplets, this effect will be most visible in the later deformations. For the experiments with decreasing voltage, the largest deformations are made with the first deformations. The effects are therefore expected to be smaller than those of increasing voltages, where more of oil substances have had time to adsorb to the surface. The stiffening observed in oil A does seem to be more clear for increasing voltages. These results are in concurrence with those of the constant voltage experiments. The effective surface tensions were 28.0 mN/m and 32.7 mN/m for respectively 21.5 °C and 50 °C. The results can be seen in Figure 67 and Figure 68.

Damping coefficient

Not many damping coefficients could be found for 21.5 °C, as for 50 °C. Both

experiment series gave averages similar to those seen before for increasing voltages. The damping coefficient is yet again higher for higher temperatures. The average values are 325 Hz and 526 Hz for 21.5 °C and 50 °C respectively. The results can be seen in Figure 77 and Figure 78.

Oscillation frequency
No oscillations were found for oil A at 21.5 °C. The average is 134 Hz for 50 °C. The results can be seen in Figure 85.

Oil C

Stable deformation
The stable deformations of droplet in oil C with decreasing voltages stay close to the theoretical values for both temperatures. It is however worth noting that oil C often acted unpredictably, and that the experiments on decreasing voltage square waves on oil C had to be repeated due to unexplainable and irreproducible results. Any conclusions from decreasing voltage on oil C is therefore not very strong. The effective surface tensions were 28.4 mN/m and 22.6 mN/m for respectively 21.5 °C and 50 °C. The results can be seen in Figure 69 and Figure 70.

Damping coefficient
No damping coefficients could be measured or calculated from the results of decreasing voltage experiments on oil C.

Oscillation frequency
No frequencies could be measured or calculated from the results of decreasing voltage experiments on oil C.

Oil D

Stable deformation
The results for decreasing voltage for oil D do show a difference for the different temperatures as expected. The droplets at 50 °C are deformed more than for 21.5 °C. These results are very similar to those for increasing voltages. There does not seem to be as big a difference between increasing and decreasing voltages as was observed for oil A. Oil D seems to have had a lesser effect from previous deformations, but a greater effect from the temperature difference. These results are in concurrence with those of the constant voltage experiments. The effective surface tensions were 66.7 mN/m and 38.1 mN/m for respectively 21.5 °C and 50 °C. The results can be seen in Figure 71 and Figure 72.

Damping coefficient
Damping coefficients for decreasing voltages give similar results to those of increasing voltages. The results from 50 °C are however quite spread. The average damping coefficients are $174\,s^{-1}$ and $279\,s^{-1}$ for 21.5 °C and 50 °C respectively. The results can be seen in Figure 79 and Figure 80.

Oscillation frequency

The average is 119 Hz for 50 °C. The results can be seen in Figure 86.

Oil D with demulsifier

Stable deformation

The voltages used in these experiments were deliberately kept low enough to avoid disintegration of the droplets. One droplet at 21.5 °C did however experience high deformation on its second square wave, showing an effect already after only one previous deformation. All other deformations seem to agree with the theory that adsorption of the demulsifiers soften the droplet, as there is a greater deformation for all droplets at 50 °C than at 21.5 °C. The effective surface tensions were 39.1 mN/m and 20.5 mN/m for respectively 21.5 °C and 50 °C. The results can be seen in Figure 73 and Figure 74.

Damping coefficient

Results for damping coefficients were only found for 50 °C. The average damping coefficient is 247 Hz which is lower than for increasing voltages. The results can be seen in Figure 81

Oscillation frequency

The average oscillation frequency found for decreasing voltages is 90 Hz, which is very close to that of increasing voltages. No real change is observed from the number of previous deformations. The results can be seen in Figure 82.

6.5 Phase shift

For all experiments conducted, the phase shifts were in the same order of magnitude as the time between each frame. Due to this fact, and the flatness of a sinusoidal peak, accurately detecting the time of a peak of deformation was difficult. A small time difference in the peak's true position could make the difference needed to shift it one frame forwards or backwards. This is believed to be the reason some drops were measured to have a negative time shift. No droplets exhibited a negative phase shift big enough for this not to be a satisfactory explanation. Although they represent an error in precision, these droplets were included, as it is believed they will contribute to a more accurate average.

Figures 87 - 96 show the phase shift in milliseconds of the drop oscillations compared to the sinusoidal voltage applied. This is plotted against the number of deformations. Also included is a line showing the value of the average phase shift. Standard deviation of the measurements giving the averages are also shown.

Table 18: Phase shifts found in ms

Temp.\oil	Marcol	A	C	D	DE
21.5 °C	0.35	-0.02	3.30	1.90	1.96
50 °C	0.56	0.17	2.47	1.07	0.56

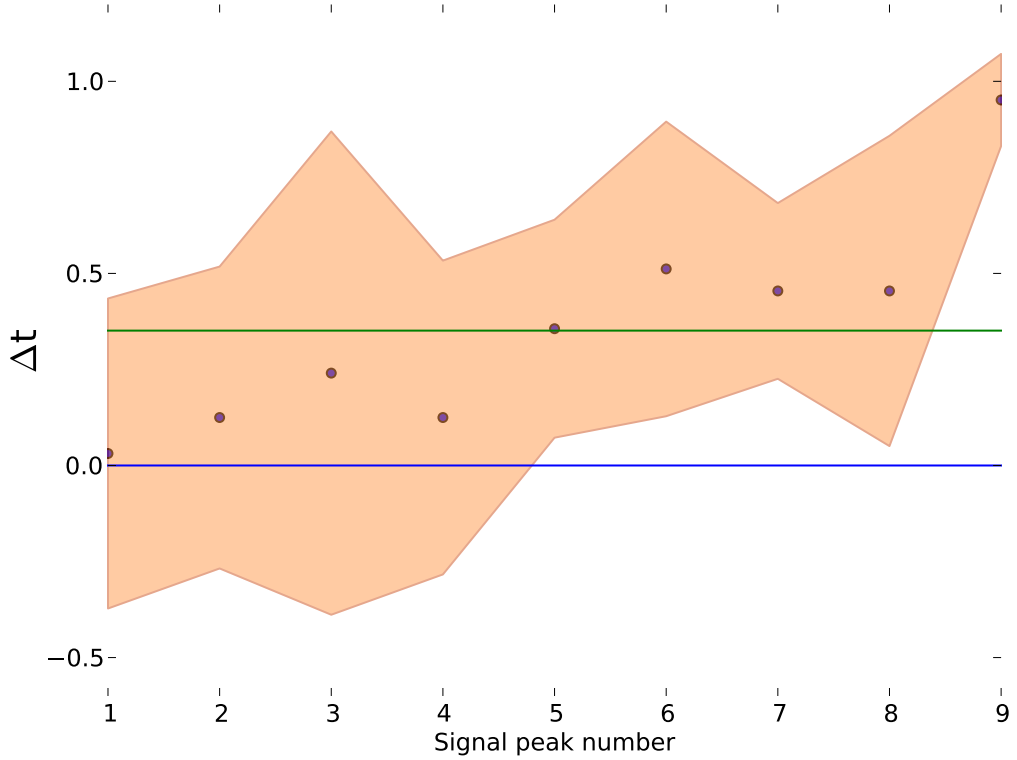

Figure 87: Oil: Marcol, Temperature: 21.5 °C.

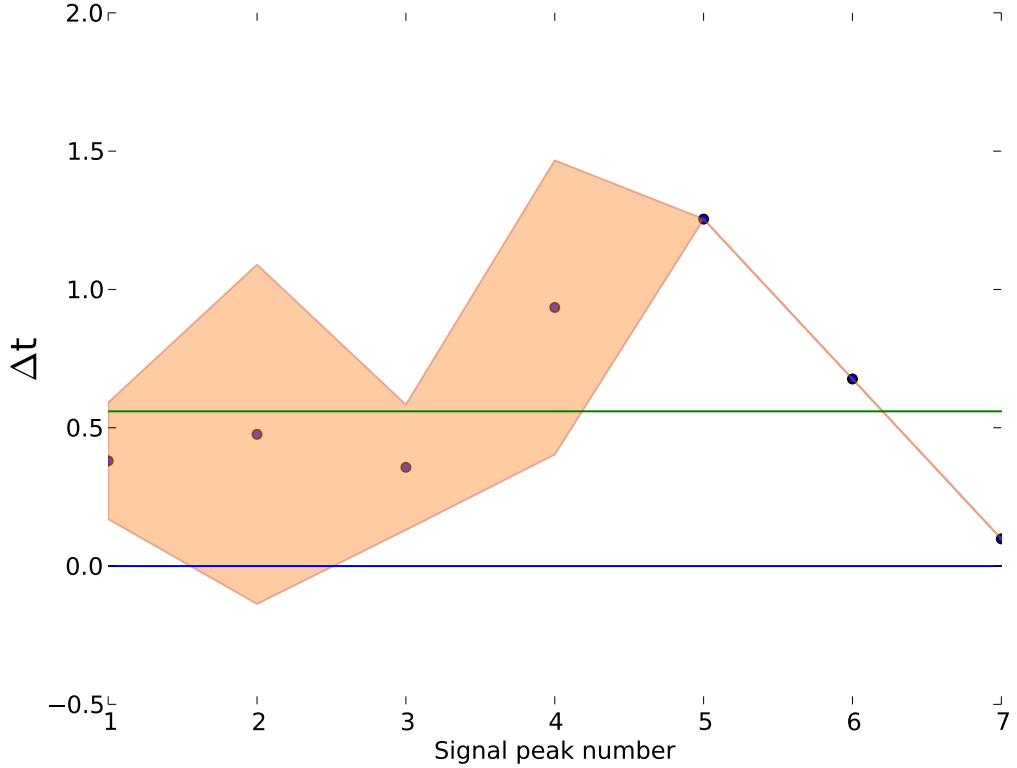

Figure 88: Oil: Marcol, Temperature: 50 °C.

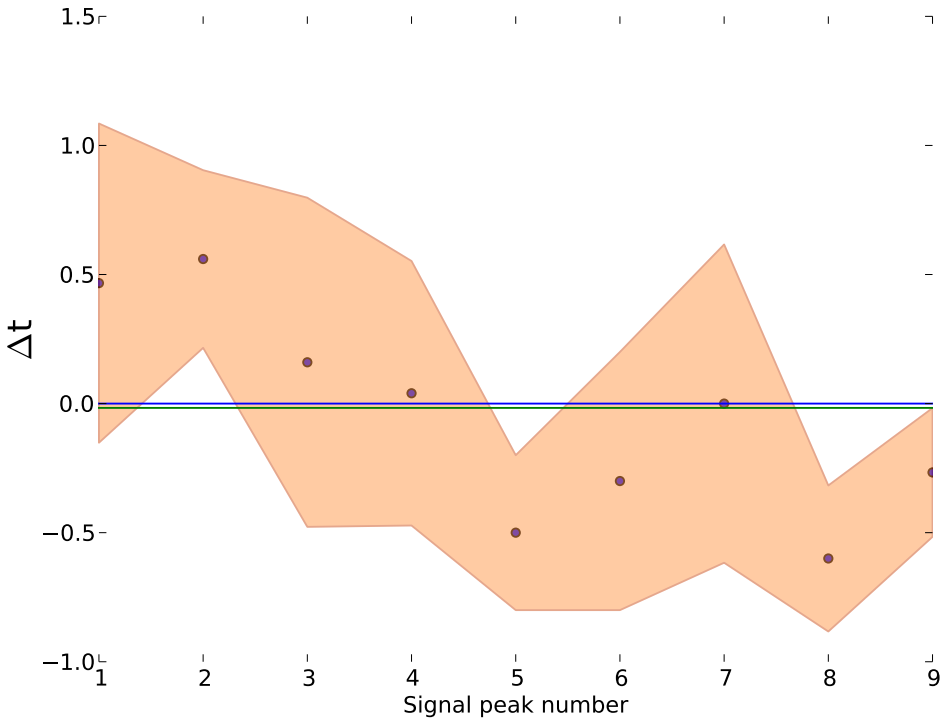

Figure 89: Oil: A, Temperature: 21.5 °C.

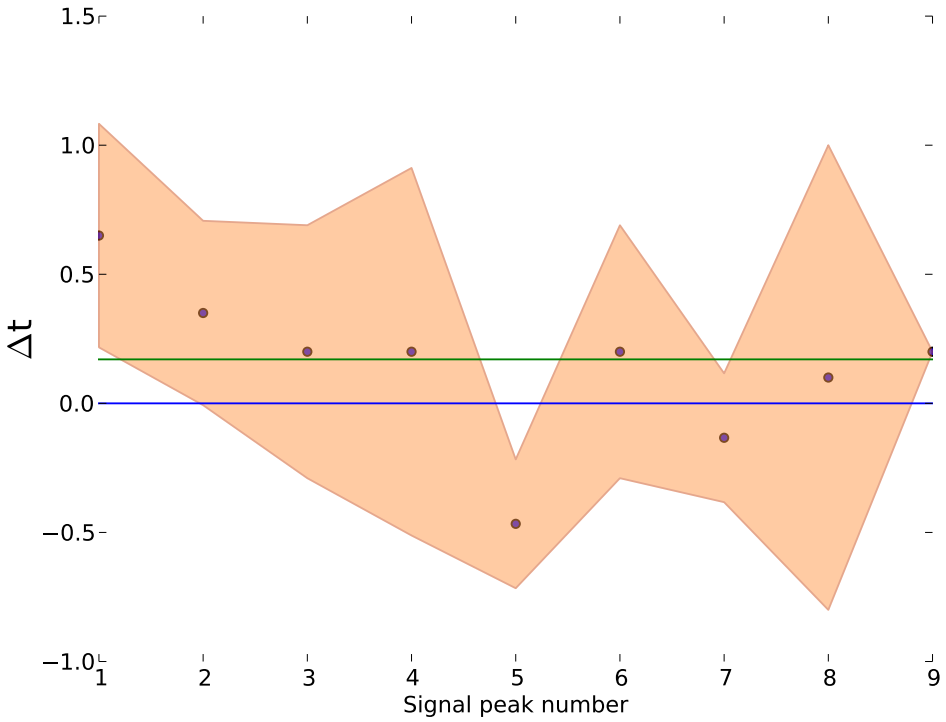

Figure 90: Oil: A, Temperature: 50 °C.

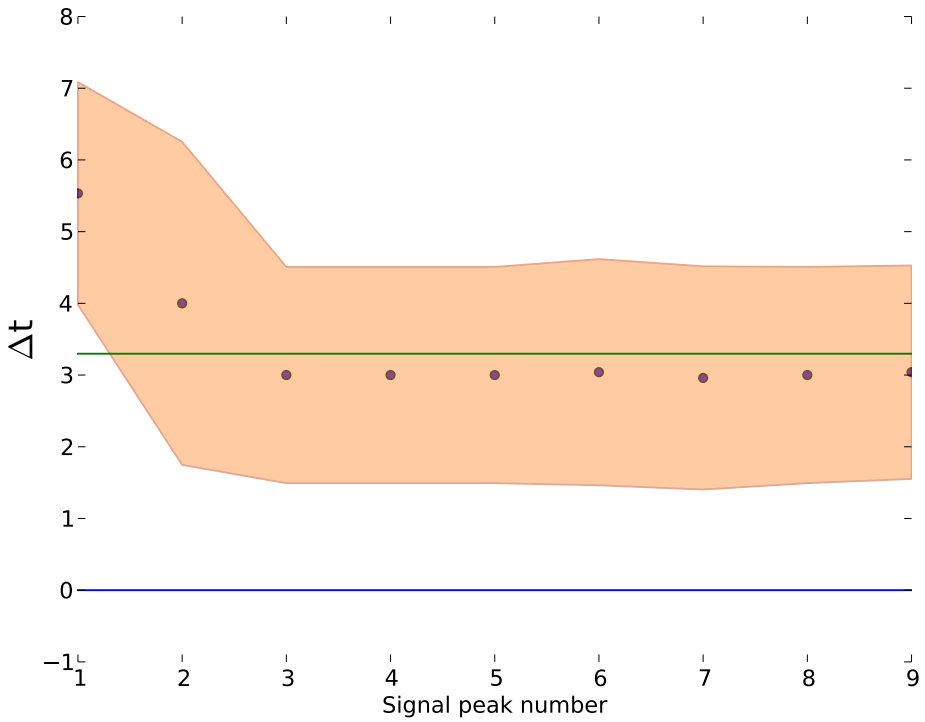

Figure 91: Oil: C, Temperature: 21.5 °C.

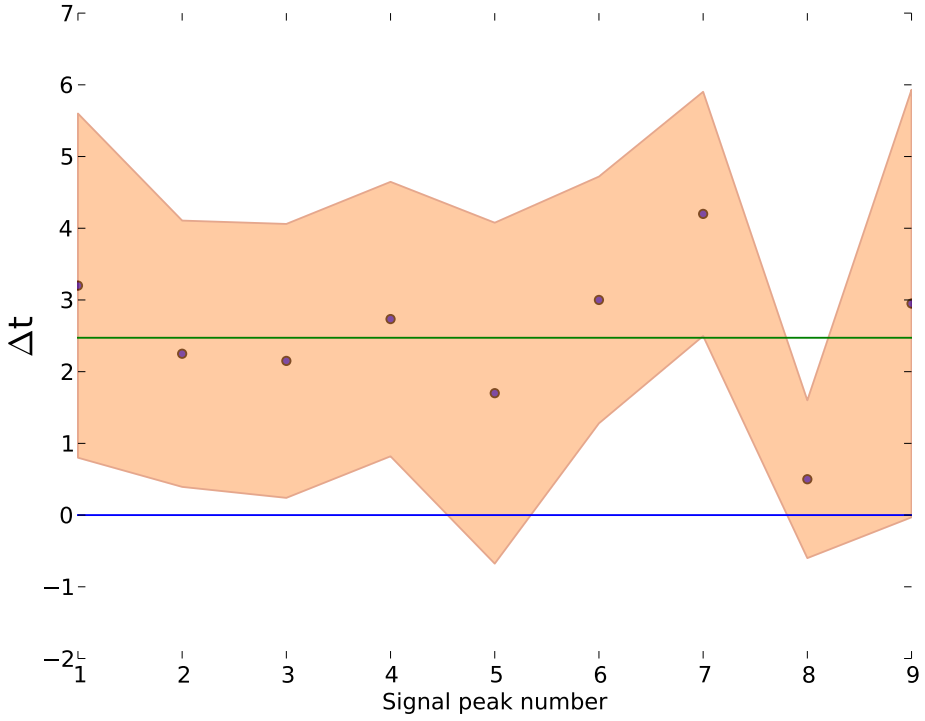

Figure 92: Oil: C, Temperature: 50 °C.

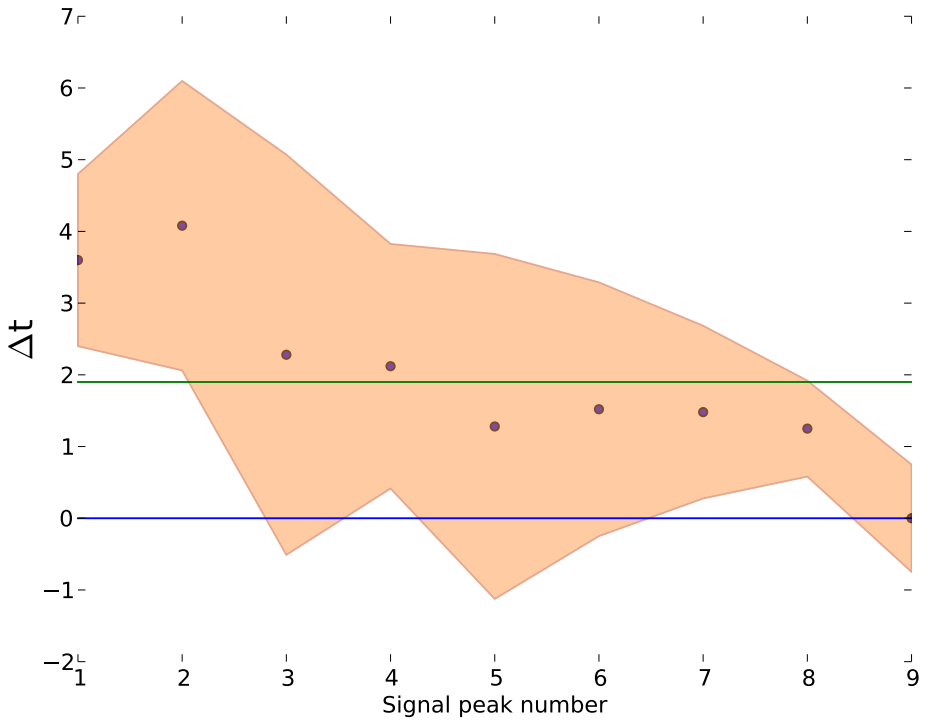

Figure 93: Oil: D, Temperature: 21.5 °C.

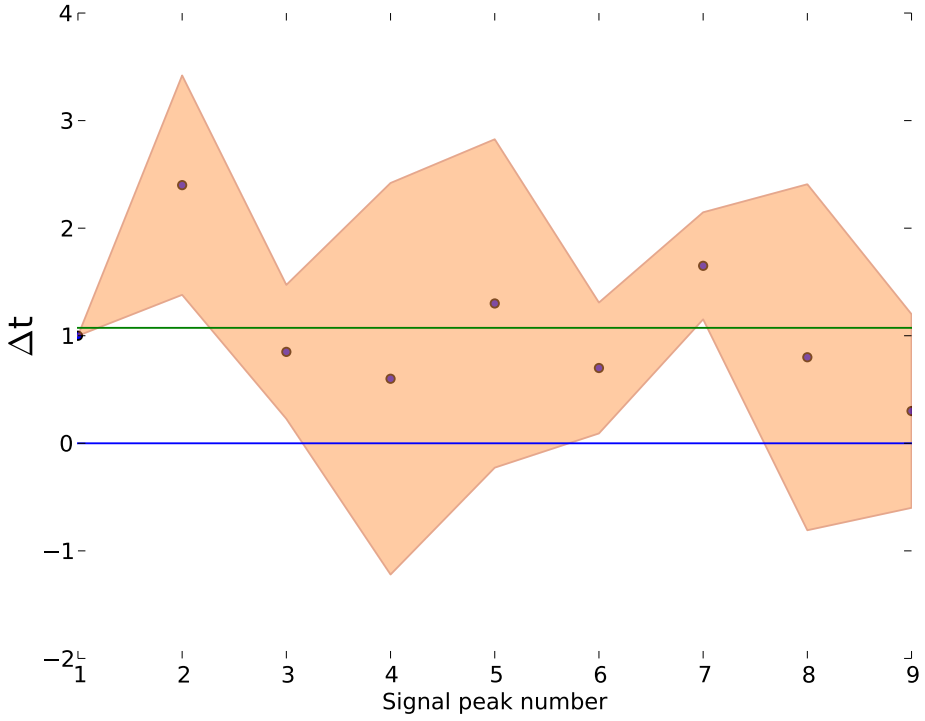

Figure 94: Oil: D, Temperature: 50 °C.

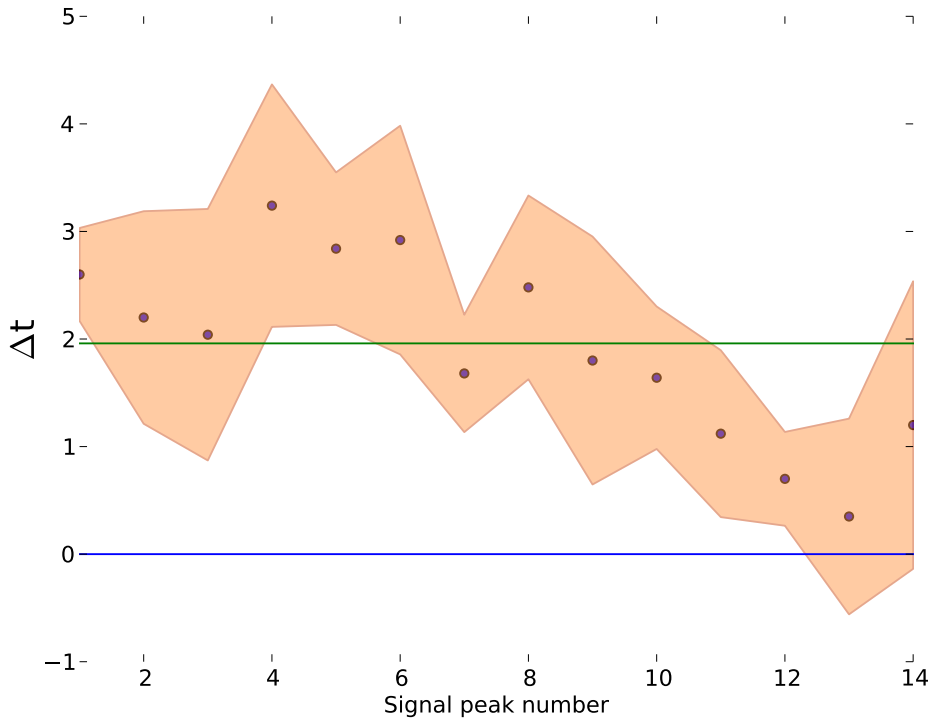

Figure 95: Oil: DE, Temperature: 21.5 °C.

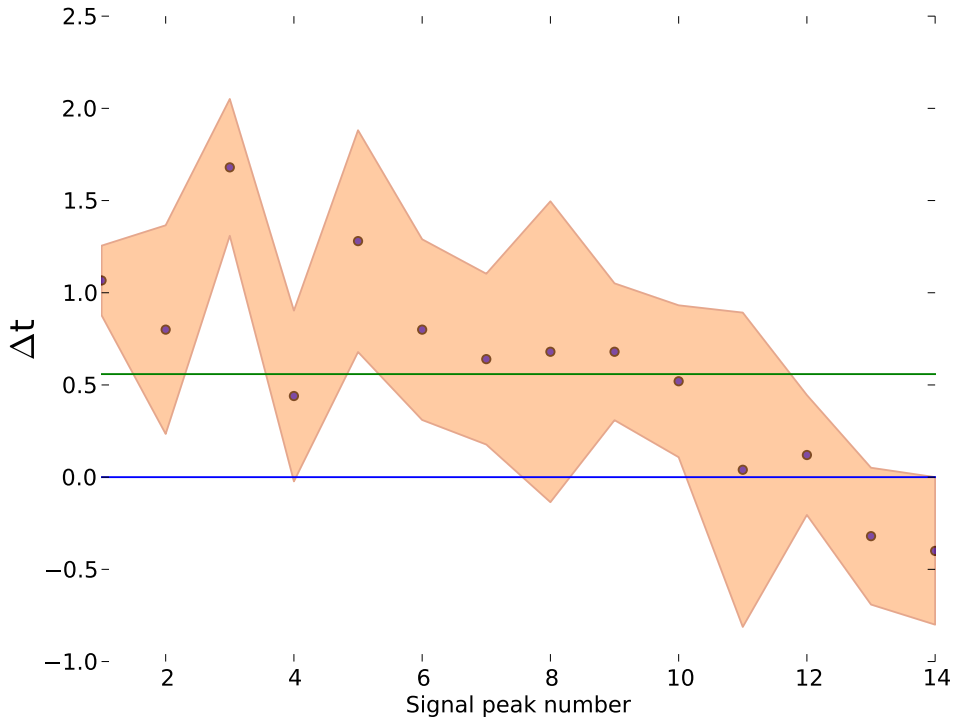

Figure 96: Oil: DE, Temperature: 50 °C.

Marcol

The results for both temperatures show an observable positive phase shift for Marcol. Both temperatures show a similar result. Since Marcol at 50 °C was by far the least viscous of the oils tested, it was difficult keeping the droplet in frame for several deformations. This is why all but one of the experiments only captured four deformations. This makes these results the weakest of the oils. Not much can be said about the different behavior of Marcol at low and high temperatures. These results can however be used as a benchmark for comparison with the other oils tested. The phase shifts were 0.35 ms and 0.56 ms for respectively 21.5 °C and 50 °C. The results can be seen in Figure 87 and Figure 88.

Oil A

The results for oil A are the only ones that gave averages below 0, and the phase shift at 21.5 °C is the only result that achieved a negative total average. The average is however very close to 0. If more experiments were conducted the average would likely move over to a slightly positive value. This result shows that the phase shift for oil A at 21.5 °C is so small that within the precision of the experimental setup, drop deformation can be considered simultaneous with the electric field. For 50 °C there are fewer values below 0, and the total average is positive. This may indicate that the droplets at 50 °C resist deformation more than at 21.5 °C. This agrees with the stiffening seen in previous experiments with oil A. The phase shifts were −0.02 ms and 0.17 ms for respectively 21.5 °C and 50 °C. The results can be seen in Figure 89 and Figure 90.

Oil C

The results for oil C gave the largest phase shifts of all the oils. The phase shifts for 21.5 °C shows a very steady behavior. Since the frame rate of the films of oil C was so low, it takes a lot for a peak to be detected a different amount of frames behind the peak of voltage. When it does, however, the result is very different. This can be seen in the results of the experiments at 50 °C. Both experiments show a relatively large phase shift, with the phase shift for high temperature being the lowest. These results show two characteristics of oil C, that the substances in the oil have unpredictable effects, and that they overall have a softening effect on the droplets. The phase shifts were 3.30 ms and 2.47 ms for respectively 21.5 °C and 50 °C. The results can be seen in Figure 91 and Figure 92.

Oil D

The results for oil D show a decrease in phase shift for higher temperatures. This is consistent with other results for oil D, as it indicates a softening for higher temperatures. The phase shifts were 1.90 ms and 1.07 ms for

respectively 21.5 °C and 50 °C. The results can be seen in Figure 93 and Figure 94.

Oil D with demulsifier

There seems to be a decrease in phase shift going from 21.5 °C to 50 °C. The phase shift decreases to less than 30% when heating the oil. This is the most drastic change observed in all the oils tested. The phase shift for Oil D with demulsifier also shows signs of decreasing as the experiment is conducted on a single droplet. Other oils may show hints of this, but no other oils have as many deformations consistently showing this result. The experiments with oil D with emulsifier seem to be a strong indication of the effect of diffusion and adsorption of the demulsifier, and of previous deformations. The phase shifts were 1.96 ms and 0.56 ms for respectively 21.5 °C and 50 °C. The results can be seen in Figure 95 and Figure 96.

7 Conclusion

7.1 Stable deformations

The stable deformation behavior of water droplets was the studied parameter that most clearly showed an effect of previous deformations. The experiments on constant square waves showed quite clearly that in the time span of one second, dramatic changes in drop behavior could be found. This was most evident in oil D with added demulsifier. At 1000ppm, this concentration is quite high compared to industrial applications of demulsifiers ($\sim$100ppm), but it proves an important point. The effect of previous deformations can not be neglected. Depending on the oil, previous deformations can weaken or strengthen the drop. This is seen in the results respectively as an increase or decrease in stable and maximal AR between two consecutive deformations.

The effects of increasing vs decreasing square waves are not as apparent, and the temperature of the oil seems to have a bigger effect on the effective surface tension, than the signal form. The same effect on effective surface tension by temperature is seen for all oils, except oil C. This is also the only oil where there is a drastic difference between increasing and decreasing square waves. This seems to suggest that the more impure oils receive the largest effect of decreasing or increasing deformations. It is worth noting that oil C often showed seemingly random and irreproducible behavior, and that this result could be an example of this.

What do these results imply? The fact that previous deformations affect the deformation and stability of the droplets could explain why electrocoalescers break down or are ineffective. Ideally the electrocoalescer should take into consideration not only the chemical properties of the oil/water mixture, but also for how long the two phases have been mixed. Properly controlling the amount of time before the oil/water mixture is sent into the electrocoalescer, and the amount of time it spends inside, might be crucial to the effectiveness of the machine.

7.2 Oscillation frequencies

Droplet oscillation frequency was the parameter that showed the least change depending on number of previous deformations. There were no experiments that could, with much confidence, be said to demonstrate a changing oscillation frequency. All square wave experiments concluded with similar frequencies, yet again showing the frequency's relative indifference to previous deformations. The fact that these values are so similar could mean excitation by square waves is an effective way of determining the actual resonance frequency of an excited droplet. Since the values for surface tension and density were not available, the found values could not be compared to theoretical resonance frequencies from Eq. (58).

7.3 Damping coefficients

All damping coefficients have shown an increase with temperature. This is a sign that treating an electrically excited water drop as a damped harmonic oscillator is oversimplifying the problem. If this was the case the results would imply that all the oils tested have increased viscosity at increased temperatures, which is not the case. Looking not only at the values of damping coefficients, but also at the qualitative behavior of the droplets at different temperatures it is clear that the viscosities are lower at higher temperatures. This is seen both by an observable increase in settling speed, and the nature of the oscillations' damping. Only at 50 °C were oscillations observed for the crude oils. The behavior for 50 °C looks like oscillations where the amplitude ratio of consecutive oscillations is not constant, as would be expected by underdamped oscillations, but largest between the two first oscillations. This implies that the oscillations do not act as an underdamped oscillation. The contractive forces from surface tension come from the drops resistance against increases in surface area. From Eq. (40), it is apparent that the relation between surface area, S and aspect ratio $\frac{a}{b}$ is not easily compared to an ideal mass-spring system. Before any real conclusions can be made about the damping coefficients of drop oscillation, a better model for contractive forces rising from surface tension must be used.

7.4 Phase shift

It would seem logical to assume that the phase shift of drop deformation would decrease with viscosity. The theory of harmonic oscillators Eq. (24) suggests this. Oils C, D and D with demulsifier show this, and with more experiments Marcol is expected to do the same. Oil A is the only oil showing an increase in phase shift with temperature. This is not the only experiment where oil A deviated from the other crude oils. It seems that not only the oil viscosity, but also the adsorption of substances on the drop surface has an effect on the phase shift. The phase shift of deformation is linked with energy loss in the droplets. These results imply that if drop heating by energy loss in deformation is an issue, the effect of surface active components in the oil must also be considered.

8 Further work

8.1 Sine sweep

The sine wave experiments turned out not to be very good at determining the resonance frequency as it was conducted in this study. Since many different droplets were tested, the different results could not be confidently compared. For a continuation of this experiment it could be wise to subject the droplet to a frequency sweep. This will ensure the different frequencies are tested with the exact same drop. In a similar fashion as with the experiments with increasing or decreasing square waves voltages, this will

give a better justification for comparison, as well as giving more results from fewer experiments.

8.2 Improvement of oscillation model

The harmonic oscillator seems to have been an oversimplification of the oscillating motion of the droplets' aspect ratio around the stable value. If something is going to be confidently said about a damping coefficient of any nature, this model must be improved. This is a suitable project for simulation work on the electrical excitation of water drops in oil.

8.3 Automation of experimental procedure

Controlling the movement speed of the test cell, and triggering of the voltage signal was done manually. For the most viscous oils this was done quite easily, not as easily for the less viscous oils, and it was not possible at all for oils B and E. These two oils might have given great results if they could be tested. If the camera, the linear stage and a computer could track the droplet, and match its speed automatically, and trigger the voltage signal itself, the experiments on less viscous oils, such as oils B and E, could be conducted. This was discussed, but was not deemed feasible within the time constraints of the project.

8.4 Value determination for simulation comparison

If the results of all these experiments should be properly compared with simulations or theory, their chemical and physical properties need to be known. Very few values could be given, or tested, and the possible thoroughness of discussion was therefore limited. With more time, and proper equipment these values could have been determined.

8.5 Isolating effect of aging

All oils tested were aged for one minute. For a continuation of this work it could be interesting to isolate the effect of aging on the drops' behavior. The same experiments could be conducted, but instead testing different oils, different aging times could be tested. One major obstacle for this idea is time consumption. A failed experiment with an aging time of one minute is not a problem. If the droplets however age for e.g. an hour, failed experiments are a problem. Experiences during this project with extended aging suggests that older droplets behave unpredictably and therefore increase the number of failed experiments. For this idea to be carried out, automation of the experimental procedure is recommended.

References

[1] Å. Ervik, T.E. Penne, S.M. Hellesø, S.T. Munkejord, and B Müller. Influence of surfactants on the electrohydrodynamic stretching of water drops in oil. *Journal of Fluid Mechanics*, 2015. Unpublished.

[2] E. Tzimas, A. Georgakaki, and C. Garcia-Cortes. Enhanced oil recovery using carbon dioxide in the european energy system. *European Comission*, 2005.

[3] P. G. Saffman and Geoffrey Taylor. The penetration of a fluid into a porous medium or hele-shaw cell containing a more viscous liquid. *Proceedings of the Royal Society of London A: Mathematical, Physical and Engineering Sciences*, 245(1242):312–329, 1958.

[4] M.-H. Ese, X. Yang, and J. Sjöblom. Film forming properties of asphaltenes and resins. a comparative langmuir– blodgett study of crude oils from north sea, european continent and venezuela. *Colloid and Polymer Science*, 276(9):800–809, 1998.

[5] C. T. R. Wilson and G. I. Taylor. The bursting of soap-bubbles in a uniform electric field. *Mathematical Proceedings of the Cambridge Philosophical Society*, 22:728–730, 7 1925.

[6] Frank M. White. *Viscous fluid flow, Third edition.* McGraw-Hill, 2006.

[7] Geoffrey Taylor. Disintegration of water drops in an electric field. *Proceedings of the Royal Society of London A: Mathematical, Physical and Engineering Sciences*, 280(1382):383–397, 1964.

[8] C. G. Garton and Z. Krasucki. Bubbles in insulating liquids: Stability in an electric field. *Proceedings of the Royal Society of London A: Mathematical, Physical and Engineering Sciences*, 280(1381):211–226, 1964.

[9] A. Ervik, S.M. Helleso, S.T. Munkejord, and B. Muller. Experimental and computational studies of water drops falling through model oil with surfactant and subjected to an electric field. In *Dielectric Liquids (ICDL), 2014 IEEE 18th International Conference on*, pages 1–6, June 2014.

[10] Å. Ervik. The local level-set extraction method for robust calculation of geometric quantities in the level-set method. *Master's thesis, Norwegian University of Science and Technology*, 2012.

[11] P.J.Bailes and S.K.L.Larkai. An experimental investigation into the use of high voltage d.c. fields for liquid phase separation. *Chemical Engineering Research and Design*, 59a:229–237, 1981.

[12] P.J. Bailes and S.K.L. Larkai. Liquid phase separation in pulsed d.c fields. *Chemical Engineering Research and Design*, 60a:115–121, 1982.

[13] P. Atten. Electrocoalescence of water droplets in an insulating liquid. *Journal of Electrostatics*, 30:259–269, 1993.

[14] G. Berg, L.E. Lundgaard, M. Becidan, and R.S. Sigrnond. Instability of electrically stressed water droplets in oil. In *Dielectric Liquids, 2002. ICDL 2002. Proceedings of 2002 IEEE 14th International Conference on*, pages 220–224, 2002.

[15] G. Berg, L. Lundgaard, and F.K. Hansen. Elongation of water drops in oil during transient electric fields. In *Dielectric Liquids, 2005. ICDL 2005. 2005 IEEE International Conference on*, pages 189–192, June 2005.

[16] Robert Klimek and Ted Wright. *Spotlight-8 Image Analysis Software*. NASA, 2005. http://hdl.handle.net/2060/20060011194.

[17] Eli Billauer. *peakdetect.m*, 2012. http://billauer.co.il/peakdet.html.

[18] Steven B. Sample, Bollini Raghupathy, and Charles D. Hendricks. Quiescent distortion and resonant oscillations of a liquid drop in an electric field. *International Journal of Engineering Science*, 8(1):97 – 109, 1970.

[19] Erik B. Hansen. Numerical simulation of droplet dynamics in the presence of an electric field. *Thesis for the dr.ing. degree, Norwegian University of Science and Technology*, 2005.

Appendix

Results from transient oscillations experiment using increasing or decreasing voltage amplitude for Span-80 concentrations of 0.001 wt% and 0.016 wt%. These results, together with the results from 0.005 wt% will be used in a not yet published joint SINTEF-NTNU publication.[1]

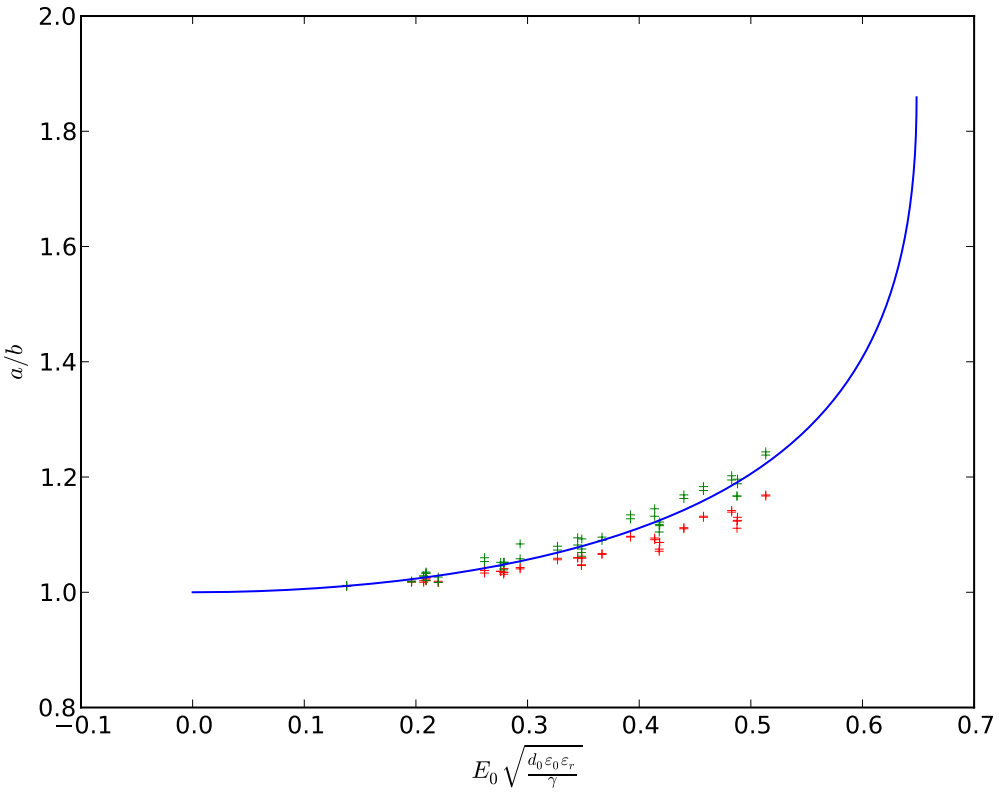

Figure 97: Oil: Marcol (0.001 wt% Span 80), Temperature: 21.5 °C.

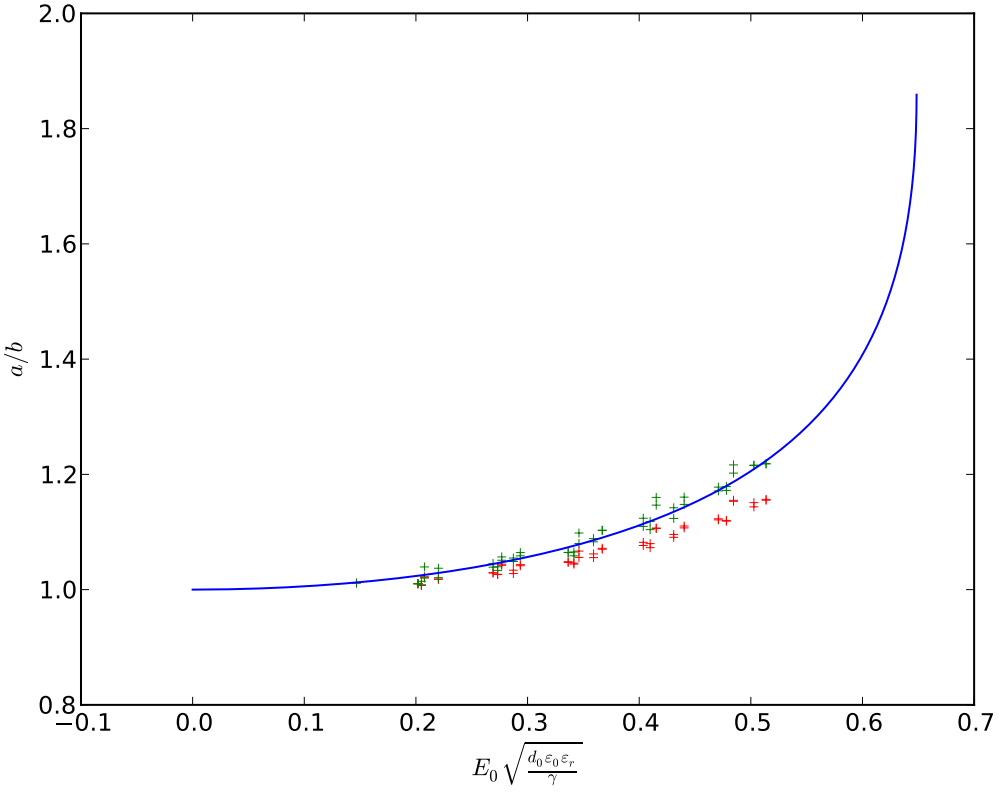

Figure 98: Oil: Marcol (0.001 wt% Span 80), Temperature: 21.5 °C.

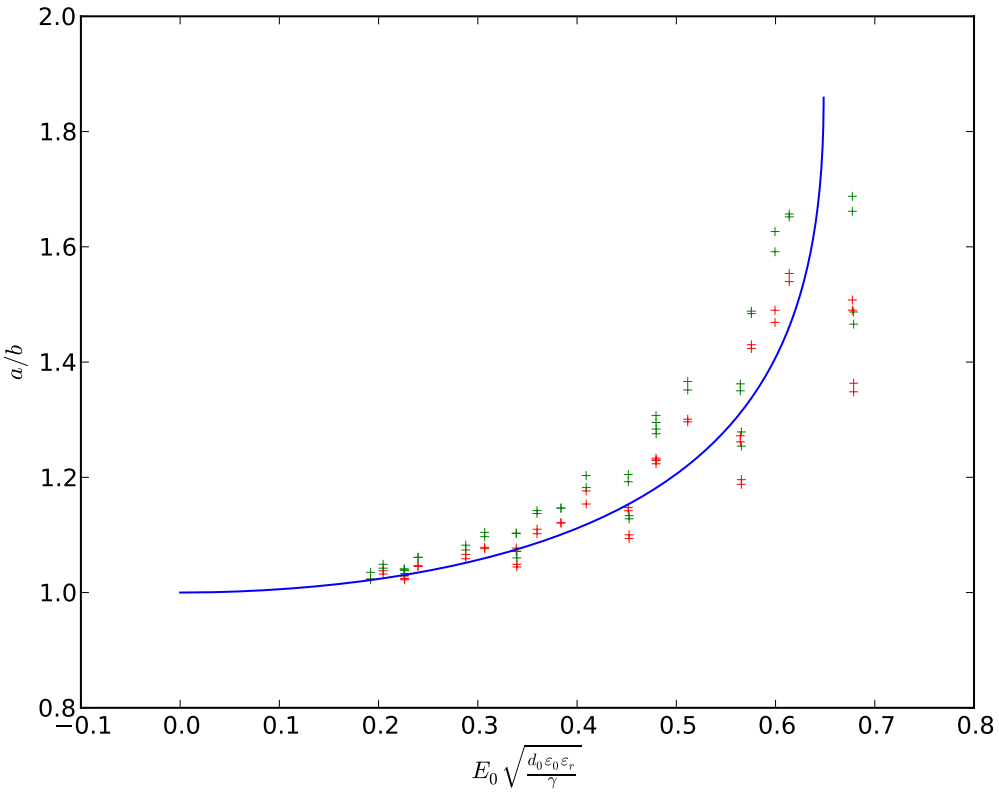

Figure 99: Oil: Marcol (0.016 wt% Span 80), Temperature: 21.5 °C.

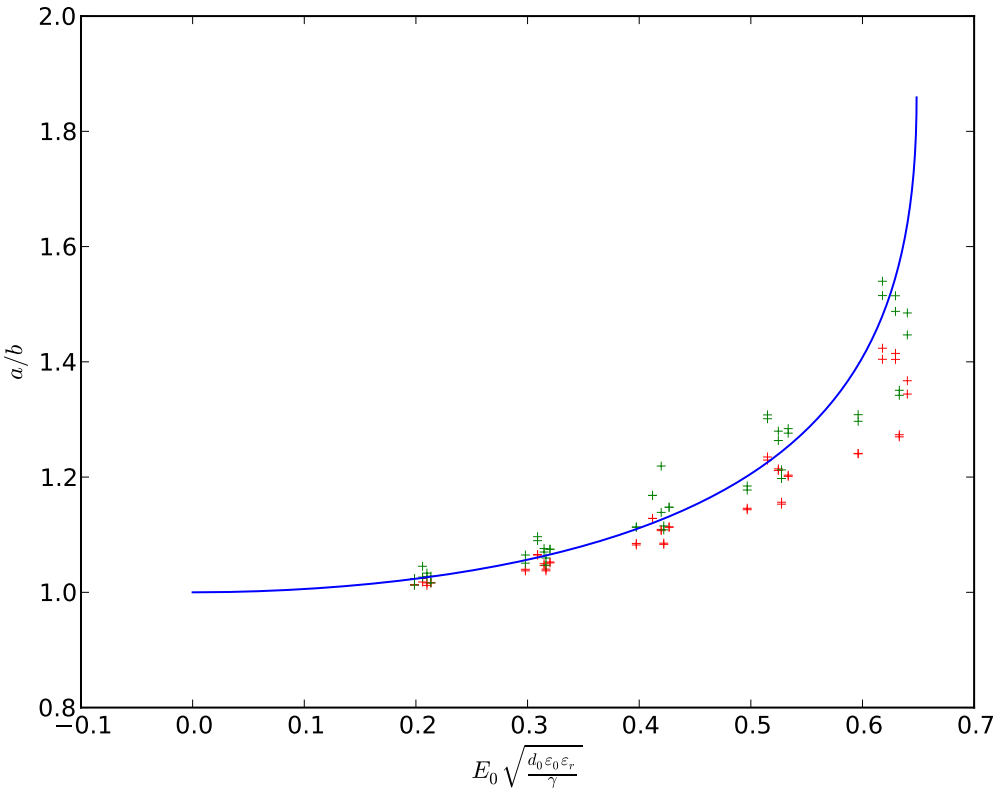

Figure 100: Oil: Marcol (0.016 wt% Span 80), Temperature: 21.5 °C.